ADVANCES IN LOW-K AND TRANSIENT POLYMERS

A Dissertation
Presented to
The Academic Faculty

by

Jared M. Schwartz

In Partial Fulfillment
of the Requirements for the Degree
Doctorate of Philosophy in the
School of Chemical and Biomolecular Engineering

Georgia Institute of Technology
August 2017

ADVANCES IN LOW-K AND TRANSIENT POLYMERS

Approved by:

Dr. Paul A. Kohl, Advisor
School of Chemical and Biomolecular Engineering
Georgia Institute of Technology

Dr. Elsa Reichmanis
School of Chemical and Biomolecular Engineering
Georgia Institute of Technology

Dr. Ryan Lively
School of Chemical and Biomolecular Engineering
Georgia Institute of Technology

Dr. Valdimir Tsukruk
School of Materials Science and Engineering
Georgia Institute of Technology

Dr. Peter J. Ludovice
School of Chemical and Biomolecular Engineering
Georgia Institute of Technology

Date Approved: April 25, 2017

ACKNOWLEDGEMENTS

First, I have to thank my entire family for their patience while I have pursued my PhD. I especially owe a lot to my immediate family for keeping me sane and visiting as often as they can. Thanks Mom, Dad, and Christine (aka Crusty). Thanks to my GT family, the graduate students in ChBE who started in the fall of 2012 – lots of wonderful memories.

Thank you, Dr. Kohl, for the guidance and healthy arguments about all of the research compiled here. Thanks to the Kohl lab group for everything from help with NMR to taking Dami's money. In the order of me remembering the graduate students who have been here during my tenure, thank you: Johanna (aka Yo Yo) Stark Goodman, Sarah Kim, Brennen Mueller, Erdal Uzunlar, Oluwadamilola Phillips, John (aka Ginger) Ahlfield, Anthony Engler, Lisha Liu, Jisu Jiang, and Garrett Huang. Special thanks to Dr. Mueller (aka Brendon), who mentored me through the beginning months. I have immense respect for Brennen, Oluwadamilola (aka Dami, Dambi, Steve, Oluwastevelola, Damn-ee), and Anthony (aka I can't believe you don't have a nickname by now). The three of us suffered through the tough times together.

There are a lot of people involved in every PhD thesis. From technicians to undergraduates, I have received an immense amount of help, without which I would be looking forward to a few more years of work. I would like to extend a special thanks to Dr. Leslie Gelbaum of the Georgia Tech NMR Center. By helping me do scary things with the NMR tools (cooling well below room temperature), I was able to figure out a lot about how these polyaldehydes form. The undergraduates that have worked with me

have also immensely helped with accomplishing a lot of this thesis. In chronological order, I would like to thank Helen Li, Ben Schmidt, Zach Pritchard, Jane Erickson, Jonathan Tuck, Mary Alsobrooks, Alexis Sutlief, Jihyun (Maria) Lee, and Niya Abdulkadir. I especially would like to thank the last three, Alexis, Maria (aka Ma-ri-ri, Mar Mar), and Niya for taking the dive into the unknown with the polyaldehydes. I wish you all the best in whatever direction your careers take you.

Last, but certainly not least, I must thank the companies and individuals involved with the funding of this thesis. Drs. Ed Elce and Andrew Bell at Promerus, LLC funded and intellectually furthered the polynorbornene work. Drs. Diane Hymes, Ratchana Limary, and Steven Sirard supported the high aspect ratio pillars work. Thanks to DARPA for funding of the VAPR program and the ongoing work with transient polymers in ICARUS.

TABLE OF CONTENTS

LIST OF TABLES

LIST OF FIGURES

LIST OF ABBREVIATIONS

Rhodorsil FABA	tetrakis(pentafluorophenyl)borate-4-methylphenyl[4-(1-methylethyl)phenyl]iodonium
PAG	Photoacid generator
p(PHA-co-T2M2B)	Poly(phthalaldehyde-co-trans-2-methyl-2-butenal)
P_1-t-Bu	tert-Butylimino-tris(dimethylamino)phosphorane
P_2-t-Bu	1-tert-Butyl-2,2,4,4,4-pentakis(dimethylamino)-2λ5,4λ5-catenadi(phosphazene)
1-PB	1-pyrenebutanol
2-NB	2-nitrobenzyl alcohol, ortho-nitrobenzyl alcohol
3-APTES	3-aminopropyl triethoxysilane
4-NPC	4-nitrophenyl chloroformate
4-TBA	4-tosyloxybutyraldehyde
AA	Acetic anhydride
Ac	Acetaldehyde
AC	Allyl chloroformate
$AlEt_3$	Triethylaluminum
BA	Butyraldehyde
BBr_3	Boron tribromide
BCl_3	Boron trichloride
BF_3-OEt_2	Boron trifluoride etherate
BZA	Benzaldehyde
DCM	Dichloromethane, methylene dichloride
DCM-d_2	Deuterated dichloromethane

DNQ	Diazonaphthoquinone
FTIR	Fourier transform infrared spectroscopy
GPC	Gel permeation chromatography
HAR	High aspect ratio
HATR	Heated attenuated total reflectance
MC	Methyl chloroformate
n-HOS	n-hydroxysuccinimide
NMR	Nuclear magnetic resonance
OEt_2	Diethyl ether
P(PHA-co-BA)	Poly(phthalaldehyde-co-butyraldehyde)
P(γBL)	Poly(γ-butyrolactone)
P_4-t-Bu	1-tert-Butyl-4,4,4-tris(dimethylamino)-2,2-bis[tris(dimethylamino)-phosphoranylidenamino]-2λ^5,4λ^5-catenadi(phosphazene)
PA	Propionaldehyde
PAC	Photoactive compound
PGMEA	Propylene glycol monomethyl ether acetate
PHA	Phthalaldehyde
PNB	Poly(norbornene)
PPHA	Poly(phthalaldehyde)
pphr	Parts per hundred parts resin
PVA	Pivalaldehyde
QCM	Quartz crystal microbalance
RTA	Rapid thermal annealer
SEM	Scanning electron microscope
T2M2B	Trans-2-methyl-2-butenal

t-BDMS	*tert*-butyldimethylsilanol
TEA	Triethylamine
THF	Tetrahydrofuran
THF-d_8	Deuterated tetrahydrofuran
$TiCl_4$	Titanium (IV) tetrachloride
TiF_4	Titanium (IV) tetrafluoride
TMBZA	3,4,5-trimethoxybenzaldehyde
TMPTGE	Trimethylolpropane triglycidyl ether
VA	Valeraldehyde
VC	Vinyl chloroformate
$ZnCl_2$	Zinc (II) chloride
γBL	γ-butyrolactone
PCB	Printed circuit board

LIST OF SYMBOLS

μ_q	Sheer modulus of quartz
A	Projected area of nanoindentation, area of top electrode
A_q	Active area between gold electrodes on quartz crystal
C	Capacitance
$Đ$	Polydispersity index
E_r	Reduced modulus
f_o	Resonant frequency of unloaded quartz crystal
h_c	Contact depth of indentation
h_{max}	Maximum displacement of indentation
m_i	Mass of polymer at i^{th} time interval
m_o	Initial mass of polymer
P_{max}	Maximum load of indentation
S	Stiffness
T	Thickness of polymer
β	Geometric constant for nanoindentation
Δf	Resonant frequency change
ϵ	Geometric constant of indentation tip
ε_o	Permittivity of free space
ε_r	Relative dielectric constant
ρ_q	Density of quartz

SUMMARY

Photo-definable dielectrics are necessary for fabricating microelectronic devices in order to separate conducting phases and form mechanical structures. Ever smaller features require superior lithographic, electrical, and mechanical properties. In this work, improvements were made in two types of positive tone dielectrics. One uses a bis(diazonaphthoquinone) (DNQ)-based lithography in a polynorbornene (PNB) film to achieve the electrical insulation for an inter-layer dielectric. The other uses polyaldehydes to electrically insulate layers in a printed circuit board. The polyaldehyde work focuses on the synthesis and characterization of these unique polymers. The polyaldehydes were also used in the bracing of high aspect ratio features due to their ability to directly evaporate.

The processing and properties of a positive-tone, aqueous develop, epoxy crosslinked permanent dielectric based on a PNB backbone and DNQ photosensitive compound were investigated. The developing and cure properties of the films were studied as a function of cure temperature, epoxy crosslinker loading and DNQ loading. Reduced modulus measurements showed that crosslinking of the polymer film occurred via reaction of the polymer with DNQ. The final modulus of the DNQ-crosslinked film was 4.0 GPa. Swelling measurements for a UV exposed film showed material leaching from the film. Residual solvent from swelling measurements was analyzed by gel permeation chromatography which showed the indene carboxylic acid form of DNQ leached out of the polymer film. The unexposed film did not exhibit material loss through leaching. When developed, films showed a decline in modulus to 2.6 GPa, likely

due to the reaction of DNQ with the aqueous base developer forming nonreactive byproducts that did not contribute to crosslinking. An epoxy crosslinker was added to the formulation which helped crosslink the polymer film by inhibiting uptake of the aqueous base during developing. The epoxy inhibition of the base uptake was confirmed by quartz crystal microbalance, where an increase in epoxy loading led to a decrease in base uptake of the film during developing. ^{19}F-NMR results support the DNQ-PNB crosslinking through esterification. Electrical characterization of the cured PNB films showed a relative dielectric constant of 3.65 for a DNQ and epoxy containing film after curing at 220°C. Less than 10% volume change upon cure was observed.

Transient materials can be used as temporary protective layers in device fabrication and devices which are intended to have short mission lifetime. Low ceiling temperature, thermodynamically unstable polymers have been troublesome to synthesize and keep stable during storage. Stable poly(phthalaldehyde) was synthesized with BF_3-OEt_2 catalyst. The role of BF_3 in the polymerization is described. The interaction of BF_3 with the monomer is described and used to maximize the yield and molecular weight of poly(phthalaldehyde). Various Lewis acids were used to investigate the effect of catalyst acidity on poly(phthalaldehyde) chain growth. In-situ NMR was used to identify possible interactions formed between BF_3 and phthalaldehyde monomer and polymer. The molecular weight of the polymer tracks with polymerization yield. The ambient temperature stability of poly(phthalaldehyde) was investigated and the storage life of the polymer has been improved.

Knowledge of the ceiling temperature and thermodynamic variables for low ceiling temperature polymers is critical to understanding the material's synthesis and use.

Synthesis of the polymer below its ceiling temperature is the routine polymerization route. In-situ ^{1}H NMR of the equilibrium polymerization reaction can provide critical information for determining the enthalpy and entropy of polymer formation. Three polyaldehydes were synthesized with in-situ ^{1}H NMR, and their energies of formation were determined for the linear region of ceiling temperature. Insights into the mechanism of polymerization were also found using this method. A fourth low ceiling temperature polymer, poly(γ-butyrolactone), was unsuccessful for the in-situ ^{1}H NMR due to the minor differences between polymer and monomer proton peaks.

The copolymerization of low ceiling temperature aldehydes is of interest as a means of investigating the reaction mechanism and creating materials with different properties. In particular, changing the vapor pressure of the depolymerized monomer would assist in evaporation rate. Fast depolymerization rates have been achieved with aldehyde-based polymers, however, the rate of monomer evaporation after depolymerization presents a challenge to material volatilization. Polyaldehyde copolymers can overcome the vaporization limitation by incorporating more volatile aldehyde monomers in the copolymer. High vapor pressure aliphatic aldehydes have been copolymerized with low vapor pressure and high reactivity phthalaldehyde to create high molecular weight polymers with high vapor pressure. The best performing copolymer for the transient electronics application is the copolymer with phthalaldehyde and butyraldehyde. Molecular weights up to 120 kDa were achieved with butyraldehyde incorporation up to 20 mol%. A method for measuring the depolymerization time of polyaldehydes by quartz crystal microbalance has been developed. The copolymer of

phthalaldehyde and butyraldehyde improves the evaporation time for the polymer by a factor of 11.

The sacrificial bracing of high aspect ratio structures by polyaldehydes with little or no residue is of interest as a means to temporarily support fragile structures during device fabrication. Low ceiling temperature polyaldehydes have properties applicable to these applications. When polyaldehydes depolymerize, they return to monomer that can be directly volatilized prior to forming a liquid state. Avoiding this liquid state allows the bracing of these high aspect ratio structures without causing any collapse due to surface tension. Features with an aspect ratio of 9.86:1 were successfully braced by a copolymer of phthalaldehyde and butyraldehyde. This copolymer was removed without causing collapse by a rapid thermal anneal-type process (e.g. infrared lamps) that used a fast heating rate, 75°C/min, to a peak temperature of 425°C and low pressures, < 0.5 mTorr.

This work produced two positive tone dielectrics for electrical insulation between printed circuitry. The unique cross-linking of a PNB and DNQ-based dielectric was shown to improve mechanical properties for a low volume change cross-linking mechanism. For transient electronics, synthetic routes to stable, high-molecular-weight polyaldehydes were found. The copolymerization of aldehydes with phthalaldehyde improved the evaporation of these transient materials.

CHAPTER 1. INTRODUCTION

Polymers have had an important role in microelectronic device fabrication and device operation.[1] Integrated circuits (ICs) rely on polymeric material to separate electric lines or individual die. Functional devices rely on a printed circuit board (PCB), often made out of polymers, to connect individual ICs. These polymers are an important part to the packaging of microelectronics.

Microelectronics packaging faces a continuing challenge to accommodate scaling of electronic components to smaller size and higher performance. A higher density of electronic components requires superior dielectrics, such as in the form of photo-definable dielectrics to insulate the components electrically and mechanically support them.[2] Closer features requires a lower dielectric constant to properly isolate the electrical connections. Two areas that rely on the use of organic-based insulation are the PCB and inter-layer dielectrics. PCB dielectrics are typically composed of woven glass fiber sheets with a thermoset polymer matrix binding the woven glass together.[3] PCB polymers typically are present for high mechanical strength. Inter-layer dielectrics are typically lower dielectric constant materials with photo-definable chemistries.

1.1 Low Dielectric Polymers in Microelectronics

Epoxies are often used as the polymeric material used for microelectronic devices. Most PCBs are formed by combining woven glass fiber and epoxy-based chemistries. The use of purely epoxy-based polymers is limited to applications where a permittivity of 4.2 or higher is acceptable.[4] Epoxies also are used for the cross-linking of inter-layer

dielectrics, which can take advantage of lower dielectric constants for the bulk polymeric material.[5–7]

Polyimides are often used as photo-definable dielectric due to their mechanical and electrical properties, especially their relatively low dielectric constant.[8] Many advances in polyimides have been made.[9–13] The continual pursuit of better lithographic and dielectric properties has led to attempts to replace polyimides.

Polynorbornene (PNB) has shown promise for use as a dielectric material because of its low dielectric constant and good mechanical properties.[5] Numerous polymers of functional PNB have been utilized for this purpose.[14–18] The functionalization of PNB increases the dielectric constant of the polymer, however, marked improvements can be made by efforts to cross-link these pendant groups, reducing the polarizability of these groups.

1.1.1 Photo-definable Polymers

Photo-defined polymers allows the use of short wavelength light to directly pattern the dielectric. This is desirable to minimize the number of processing steps necessary to achieve the small feature sizes necessary. The photo-definability can be achieved with a negative tone or positive tone chemistry. Negative tone materials become less soluble in a developer when exposed to UV radiation, whereas positive tone materials become more soluble in a developer when exposed to UV irradiation. This is shown in cartoon form in Figure 1.1. Negative tone dielectrics have been well studied.[14,16,19–21]

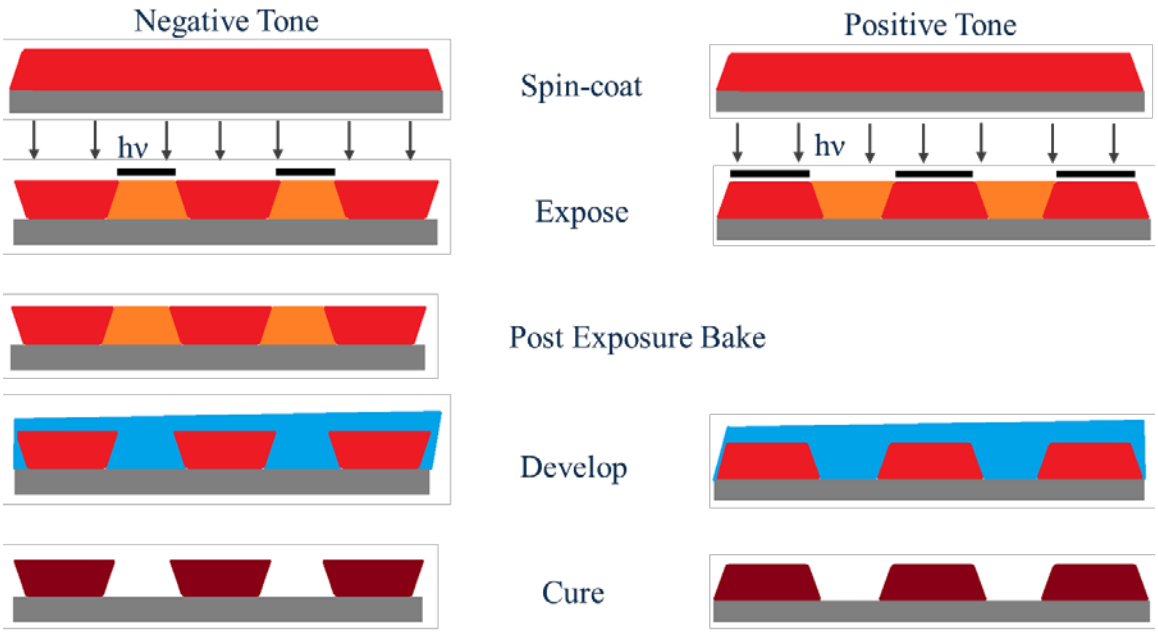

Figure 1.1. Negative tone (left) and positive tone (right) typical processing conditions.

A positive tone chemistry is desirable for packaging applications, because the film is less sensitive to mask defects or particulates during exposure due to the light field mask. Evaluation of the performance of photo-definable dielectrics is achieved through a contrast curve. A photo-sensitive film is exposed to UV irradiation at specific doses and thickness change after develop is recorded. Figure 1.2 shows an example of a contrast curve with normalized thickness plotted against the log of exposure dose. A linear regression through these points is defined as the contrast. For a positive tone material, the intersection of the contrast line and a normalized thickness of 1 is the D_0, or maximum dose before any solubility switch, and the intersection of the contrast line and the x-axis is the sensitivity (D_{100}), or minimum dose to make an area completely soluble in a developer. Contrast (γ) is the slope of the line through the D_0 and D_{100}. In Figure 1.2, the D_0 is 138 mJ/cm^2, the D_{100} is 618 mJ/cm^2, and γ is 1.5.

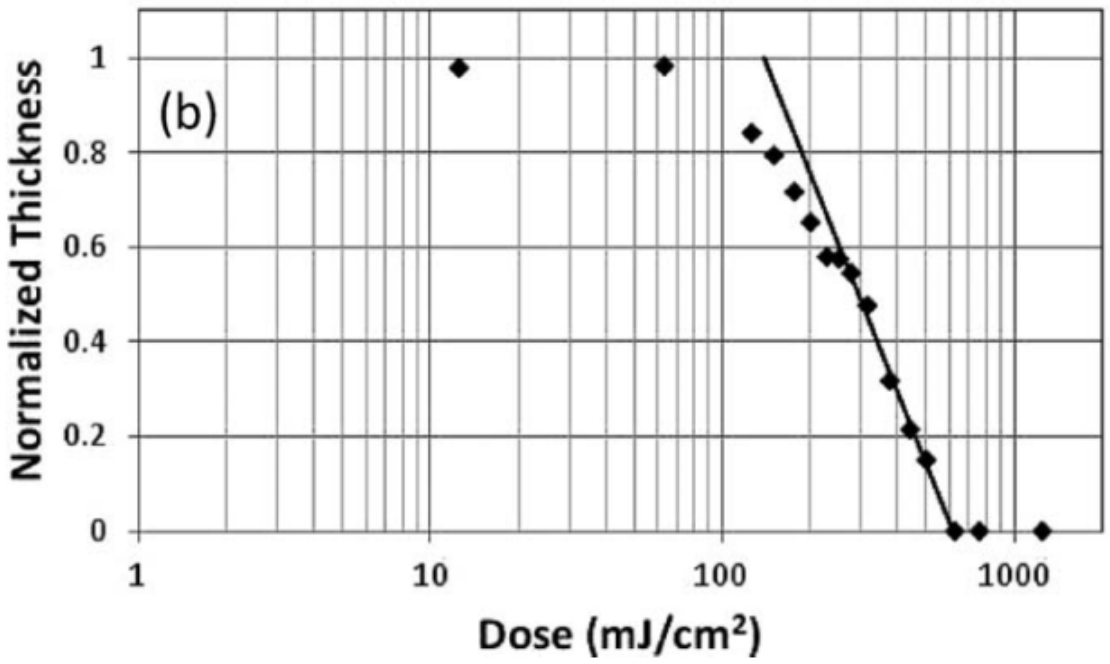

Figure 1.2. Contrast curve of a positive tone dielectric. ***Adapted from Mueller, et al.***[17]

The most common positive tone chemistry utilizes diazonaphthoquinone (DNQ) to inhibit the dissolution of a hydroxyl functionalized polymer. The DNQ additive in the polymer film inhibits dissolution by formation of a hydrogen bonded complex. Ultraviolet exposure causes the DNQ to undergo the Wolff rearrangement to form an indene carboxylic acid. Unlike DNQ, the indene carboxylic acid does not extensively hydrogen bond to the polymer, leading to the solubility switch of the polymer in aqueous base.[22] DNQ-based photochemistry is compatible with an aqueous developer which is more environmentally friendly than solvent-based developers.

Positive tone chemistries are not limited to DNQ-based inhibition reactions. Similar solubility switches can be achieved through the use of what is known as chemically amplified responses. These include removal of protecting groups that

regenerate the catalyst used to deprotect the more soluble moiety. The two most common moieties for this solubility switch are t-butyl esters and t-butoxycarbonates, which reveal carboxylic acids and alcohols, respectively, when removed by an acid.[23] Similarly, entire polymer chains can be made sensitive to a light trigger and depolymerize into molecules that become soluble in a developer.[24]

1.1.2 Permanent Low Dielectric Polymers

Curing mechanisms for permanent dielectrics can vary wildly depending on the application. Generically, the curing mechanisms must avoid any photo-definable reactions. For example, in the case of the positive tone t-butyl ester chemistry, the reaction for photo-definability requires an acid. Epoxies have to be avoided due to the catalytic ring-opening with acid. Instead, reactions with much longer time-scales or compatible chemistries can be used for the curing mechanism. Fischer esterification is an example of long time-scale reactions that can achieve the curing necessary. Vinyl-vinyl cross-linking could also be used, which avoids a reaction with the strong acid necessary for t-butyl ester photo-definability.

Cross-linking reactions with DNQ-based photochemistries are somewhat less restrictive. Curing mechanisms that rely on purely heat can be achieved in DNQ-based dielectrics. This allows the use of epoxies, which are well-studied reactions, to achieve the necessary cross-linking.[14,15]

1.1.3 Properties of Low Dielectric Polymers

Low dielectric, positive tone polymers can be summarized by a few basic material properties. Realistic targets for all of these material properties can be taken from the properties of polyimides and bezocyclobutene, which collectively dominate the market for photo-definable dielectrics. Table I summarizes these values for polyimide and BCB.

Table I. Summary of important polyimide and BCB material properties.

Dielectric	Volume Change During Cure	ε_r	tanδ	D_{100} (mJ/cm^2)	γ
Polyimide[25]	~32%	2.94	0.0089	350	1.2
Benzocyclobutene[26]	~25%	2.65	0.0008	810	1.02

Both the ideal (ε_r) and imaginary (loss tangent) portions of the dielectric should be minimized. The volume change upon cure should be minimized. A higher sensitivity is desired (lower value), as well as a higher contrast. Although not shown in the table, the mechanical modulus should be higher than 1 GPa.[5]

1.2 Self-immolative Polymers – Extreme Chemical Amplification

Thermodynamically unstable polymers have emerged in applications where a catalytic response to a small trigger is necessary or environmental degradation is desired.[27–30] The amplified degradation in macro-scale plastics offers a solution to a variety of problems including drug delivery, dry-developing photoresists, and transient electronics.[24,30–36] The catalytic response to a stimulus allows the polymer to decompose into its original monomer or other small molecule products. These catalytically depolymerizing plastics are known as self-immolative polymers (SIPs).

SIPs have recently made a resurgence in literature for drug delivery applications.[37,38] Encapsulation of drugs for the targeted release of material can be

achieved through SIPs, especially for a trigger sensitive to a specific location. A catalytic response ensues and allows the release of drugs. Polymers for drug delivery are targeted to have moderate depolymerization time scales in aqueous solutions and use chemicals that can be biologically expelled.[38,39]

Some SIPs have been used to amplify an otherwise small signal.[40] A fluorescent dye was attached to a SIP that was triggered by a free version of the dye. As the polymer depolymerized, it resulted in an exponential increase in the fluorescence. By taking advantage of the catalytic depolymerization of the SIP, researchers were able to visualize otherwise difficult-to-see responses.

1.2.1 Modes of Depolymerization

The most important consideration for selecting a SIP is the mode of depolymerization, which can be separated into two generic groups: end-group removal and random chain scission. End-group removal is the removal of a sensitive protecting group on the end of a polymer chain. Once the end is removed, the polymer rapidly depolymerizes in an unzipping-type reaction. Random chain scission is the non-specific attack of any bond on the backbone that results in the polymer unzipping in two directions from the initial point of attack. Another way to view the two modes is the end-group removal is an end-to-end depolymerization similar to a zipper, whereas the random chain scission is an inside-out depolymerization.

Each SIP has specific decomposition products which may be different for each type of decomposition. This must be taken into account when considering the polymer

of choice for each application. In any application, the byproducts of decomposition must allow fast dissolution and not disrupt the catalytic nature of the SIP depolymerization.

1.2.2 Depolymerization Time-scales

Each SIP mode of depolymerization lends itself to a specific time-scale. In applications for drug delivery, the time scale may be on the order of weeks due to the sensitivity of the trigger present. Typically the slow time scales rely on end-group triggers to limit the number of susceptible sites for attack. One example is the polymer that reignited interest in SIPs, a polycarbamate shown in Figure 1.3.[40] The polycarbamate had an end cap that, once removed, would allow the slow depolymerization over the course of 10 h. A similar polycarbamate had a depolymerization time of up to 80 days.[41]

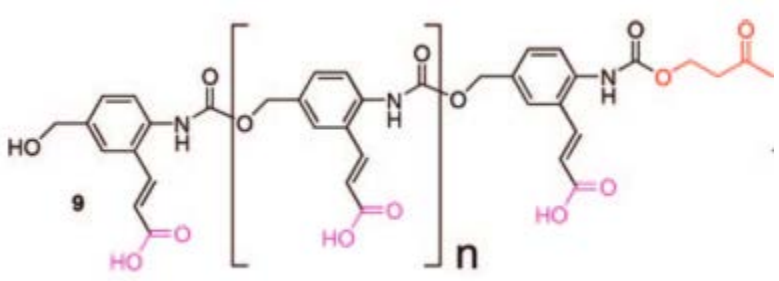

Figure 1.3. Polycarbamate with end-cap removal mechanism of depolymerization. Adapted from Sagi, et al.[40]

A fast depolymerization is achievable through the attack of many intra-chain locations. Ma, et al. used a polycarbamate structure that contained a photo-labile trigger on each repeat unit.[42] The removal of any of the labile triggers initiated an elimination reaction that depolymerized a polymer matrix within 200 s.

1.2.3 Transient Electronics

One application of depolymerizing polymers is in the field of transient electronics. Transient electronics approach functional microelectronic devices from a different point of view, where, instead of indefinitely defined function, there is a targeted lifetime.[33,43–47] Once the lifetime has been reached, a trigger will cause the device to effectively vanish. Current transient materials rely on the aqueous dissolution of monomers on large time scales up to weeks.[47] Polymers that evaporate are more desirable for shorter transience times. This requires the use of SIPs whose decomposition products yield high vapor pressure materials. These polymers are also described as dry-developing polymers.[24,48]

1.2.3.1 Dry-developing Polymers

Previously, dry-developing polymers were used in the microelectronics industry for the chemical amplification they offer for high sensitivity photoresists.[24,48] Small doses of radiation allows the depolymerization of polymer chains to high vapor pressure material. Poly(olefin sulfones), polycarbonates, and polyaldehydes have all been used as dry-developing resists.[49] All of these polymers take advantage of their relatively low ceiling temperatures.[50] A ceiling temperature is an equilibrium temperature for the polymerization and depolymerization reactions for a polymer. Above the ceiling temperature, monomer is favored. Below the ceiling temperature, polymer is favored. Stable polymer can be formed well below the ceiling temperature and kinetically trapped in this state. Once kinetically stabilized, the polymer can be brought to temperatures above the ceiling temperature and utilized in any application. Any stimulus for

depolymerization above the ceiling temperature will cause the polymer to fall apart into monomer units. These monomer units can then evaporate away.

Poly(olefin sulfone)s are the reaction product of SO_2 and olefins. They can be depolymerized by heat or irradiation back to the SO_2 and olefin. Poly(olefin sulfone)s have some limitations in their dry-developing behavior. The decomposition requires two mechanisms for the removal of the vinyl portion and the sulfone. Quite often, the highly reactive vinyl site during depropagation will react with a byproduct of the depolymerization reaction or will react with a neighboring depropagating vinyl.[35,51,52] This leads to a bimodal thermal decomposition profile. Figure 1.4 shows a dynamic thermal gravimetric analysis profile for four poly(vinyl sulfone)s.

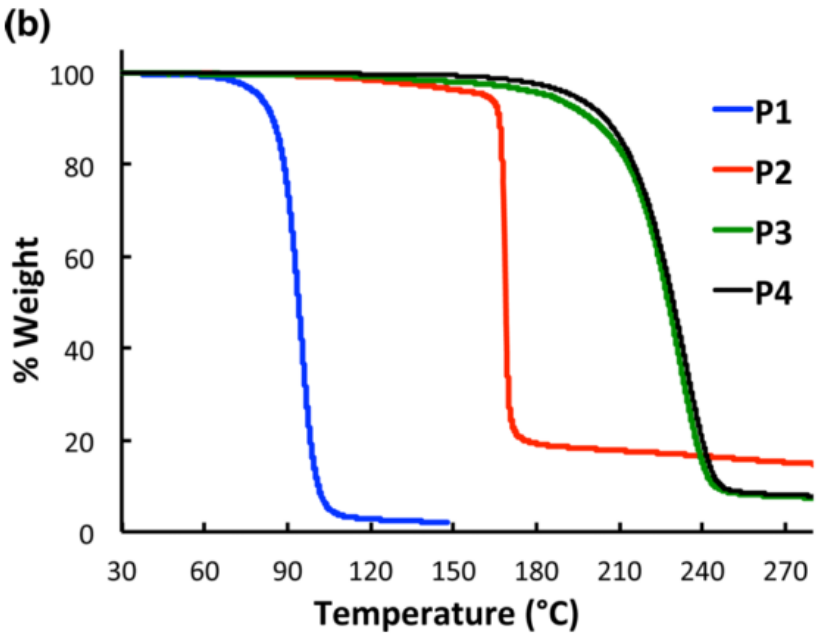

Figure 1.4. Dynamic TGA traces (5°C/min) of four different poly(vinyl sulfone)s. ***Adapted from Lee, et al.***[53]

There are two distinct decomposition modes for each polymer. The initial mass loss is due to the desired depolymerization reaction, and the second, prolonged mass loss is due to the increased thermal energy required to break the byproduct bonds. In the case of P1, the second decomposition mode comprises only a small percentage of the mass, but this is stable to higher temperature. The complete removal of poly(olefin sulfone)s, therefore relies on substantial heat, which is undesirable.

Polycarbonates share similar characteristics to poly(olefin sulfone)s for dry developing. One such polycarbonate, poly(propylene carbonate) (PPC), is especially useful for dry developing applications. When exposed to a strong base, PPC will decompose through an unzipping reaction where the polymer backbites onto itself and forms propylene carbonate. When exposed to strong acid, PPC will cleave in a random chain scission mode into largely unpredictable products.[54] The two decomposition modes are shown in Figure 1.5. In both cases, the byproducts are highly volatile and can be used for a dry-developing material.

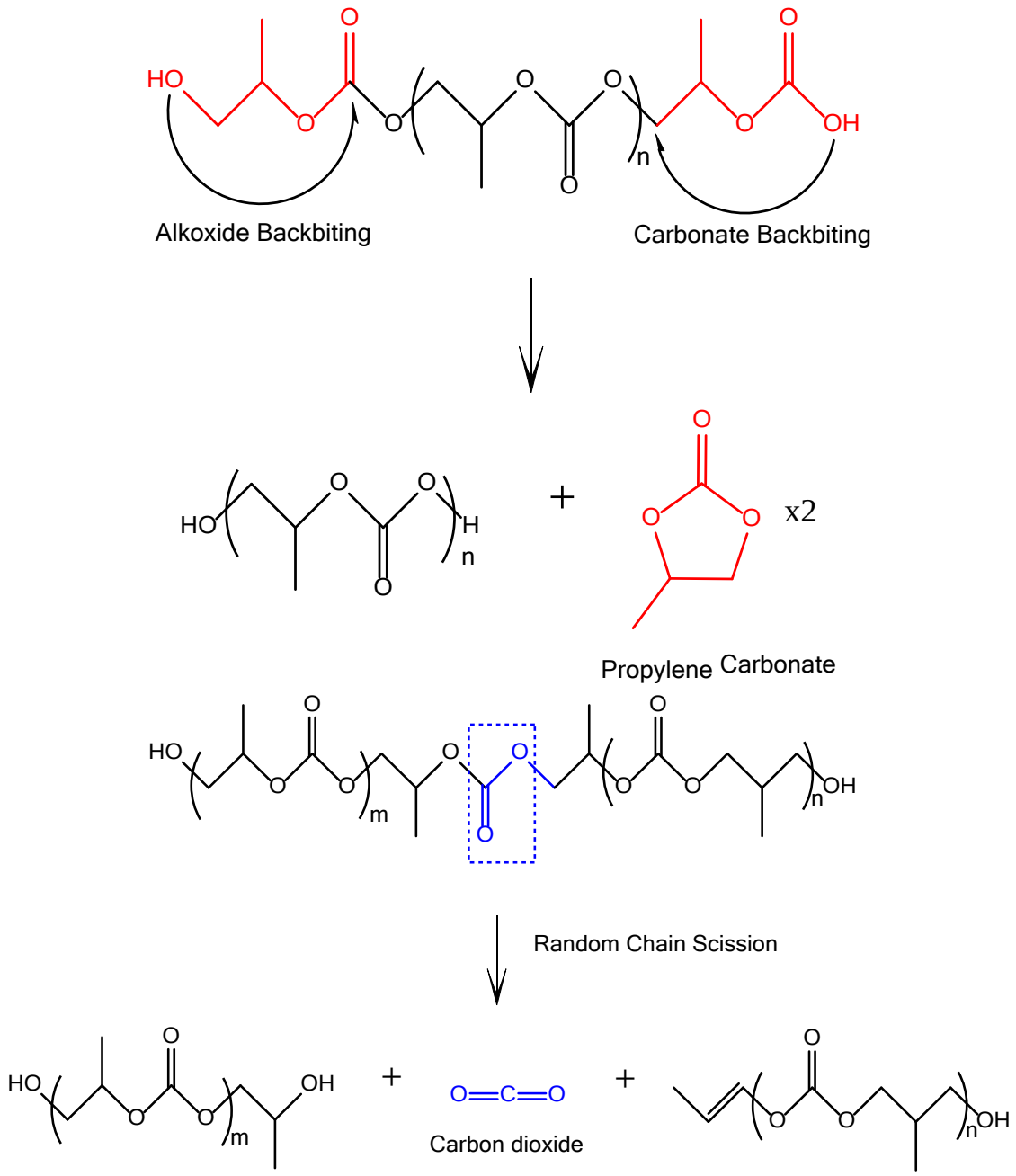

Figure 1.5. Two decomposition modes of PPC. The backbiting reaction (above) is catalyzed by a strong base. The random chain scission reaction (below) is catalyzed by a strong acid. *Adapted from Phillips, et al.*[54]

The amount of residue from the decomposition of a polycarbonate depends on the ether content.[54] An ether linkage will interrupt the carbonate backbiting reaction, inhibiting the unzipping reaction. Similarly, an ether linkage will inhibit the random

chain scission by consuming the acid, thus removing the catalytic nature of the depolymerization. While ether contents of <0.1 mol% have been achieved, this can still generate a substantial quantity of undesirable residue. The decomposition of polycarbonates also relies on some heat to overcome the required energy for depolymerization.

Polyaldehydes avoid the problems of residue and temperature due to the polyether structure. Polyaldehydes of different chemical structures have been synthesized. Polyaldehydes, other than polyformaldehyde, take advantage of the thermodynamic stability imparted by their very low ceiling temperatures, <-40°C.

Short chain aliphatic monomers, like acetaldehyde, were synthesized early in the understanding of low ceiling temperature polymers.[55–59] Unfortunately, the crystallinity of the polymer they formed tended to create highly insoluble polymer with no beneficial application.[57] Poly(phthalaldehyde) (PPHA) is highly sensitive to acid and has been shown to rapidly depolymerize when deprotected either by end-group removal or direct chain attack.[60,61] The polymerization of phthalaldehyde can proceed by either an anionic or cationic mechanism.[24,60,62,63] The anionic mechanism allows control over the end-groups of the polymer chain (i.e. potential trigger sites), while the cationic mechanism provides a more thermally stable polymer.[60,63] PPHA offered a soluble polyaldehyde that reinvigorated interest in the polymers.

1.2.3.2 On-command Disappearance of a PCB

Previous approaches to transient PCBs rely on the use of solvent either carried with a package or occurring naturally (i.e. dew or rain).[43,45,64] This solvent either adds

significant weight to a package or relies on something inherently unreliable. A PCB that can disappear on command or with a reliable, naturally occurring trigger (i.e. light) is desirable.

Environmentally friendly by-products of PCB depolymerization are necessary. Fortunately, the depolymerization reactions of SIPs result in consistently predictable products – monomer. The monomer in a SIP can be carefully selected to cause little to no harm to the environment. At the volumes necessary to create plastic supports for microelectronics, aldehydes, other than formaldehyde, can be used with minimal consequence to the environment.

The work presented here uses the concept of SIPs to create polymer support in a PCB that can evaporate on command. Once a stimulus is applied to a polymer film, the polymer will rapidly depolymerize back to monomer and evaporate. Polyaldehydes offer the best approach for the creation of a polymer film with minimal residue. Polymers of phthalaldehyde and butyraldehyde are the focus of these studies after screening of numerous aldehydes. The polyaldehydes are sensitized to UV light by addition of a photo acid generator. Through this PAG, decompositions of PCBs can be triggered by exposure to light absorbed by the acid generator or through visible light sensitizers that transfer the light energy to the PAG.

CHAPTER 2. MATERIALS, PROCEDURES, AND METHODS

2.1 Materials

The PNB polymers were a random copolymer of a norbornene fluoroalcohol (75%) and norbornene carboxylic acid (25%) and a homopolymer of norbornene fluoroalcohol (Promerus LLC, Brecksville, OH). Monofunctional and difunctional DNQs were obtained from Promerus LLC. Propylene glycol monomethyl ether acetate (PGMEA), deuterated chloroform, TMPTGE and 3-aminopropyl triethoxysilane (3-APTES) (Sigma-Aldrich) were used as-received. Microposit Developer MF-319, 0.26 N tetramethylammonium hydroxide, was obtained from Doe and Ingalls (Durham, NC). 100 mm diameter, <100> p-doped silicon wafers were used as the substrate for the experiments. Mixtures of PNB, PGMEA, photoactive compound (PAC) and crosslinker were made and allowed to ball-roll for at least 24 h before use. Table II shows the formulations used in this study with additive concentrations given in parts per hundred parts PNB mass (pphr).

Table II. Formulation List. Concentrations are given in parts of chemical per hundred parts PNB mass.

Formulation ID	PAC (concentration)	Additive (concentration)
PNB	None	None
PNB – E	None	TMPTGE (10 pphr)
PNB – D	bis-DNQ (20 pphr)	None
PNB – D & E	bis-DNQ (20 pphr)	TMPTGE (10 pphr)

For anionic syntheses, PHA was obtained from Alfa Aesar (98% purity) and used as-received, purified by recrystallization according to Dilauro, et al., sublimated at 50°C, or dried by azeotropic distillation in toluene.[60] THF was purchased from BDH and used

as-received, dried over molecular sieves, or distilled. DCM was purchased from BDH and used as-received, dried over molecular sieves, or distilled. P_2-t-Bu was used as-received. Butyraldehyde was purchased from Acros Organics and used as-received.

For cationic syntheses of poly(phthalaldehyde), PHA was obtained from Alfa Aesar (98% purity) and purified by sublimation in a nitrogen rich atmosphere at 45°C. BF_3-OEt_2 (ca. 48% BF_3) and titanium (IV) tetrafluoride (TiF_4) were purchased from Acros Organics and used as-received. ACS Reagent-grade hexane, tetrahydrofuran (THF), and methanol were purchased from BDH and used as-received. ACS Reagent-grade dichloromethane (DCM) and diethyl ether were purchased from BDH and dried over 3 Å molecular sieves. Deuterated DCM (CD_2Cl_2), boron trichloride (BCl_3), and boron tribromide (BBr_3) were purchased from Sigma-Aldrich and used as-received. Titanium (IV) tetrachloride ($TiCl_4$) and triethylaluminum ($AlEt_3$) were purchased from Alfa Aesar. Triethylamine (TEA) was purchased from AMRESCO and used as-received. Zinc (II) chloride was purchased from J.T. Baker and treated with thionyl chloride to remove water. Hexafluorobenzene (99% purity) was purchased from TCI America and used as-received.

For copolymerizations, BA was purchased from Acros Organics and purified by mixing with CaH_2 over night and distilling over molecular sieves. Propionaldehyde (PA) and valderaldehyde (VA) were purchased from Acros Organics and used as-received. Benzaldehyde (BZA), acetaldehyde (Ac), pivalaldehyde, furfural, trans-2-methyl-2-butenal (T2M2B), and 2-ethyl butyraldehyde (2-EB) were purchased from Alfa Aesar and used as-received.

Special thanks to Anthony Engler for the synthesis of this aldehyde. 4-tosyloxybutyraldehyde (4-TBA) was synthesized by the reaction of butane diol with p-toluene sulfonyl chloride and the subsequent oxidation (via Swern oxidation) of the unreacted alcohol. Butane diol (252 mmol), 4-dimethylaminopyridine (2.1 mmol), pyridine (168 mmol) and DCM (70 mL) were added to a 500 mL, flame dried flask (filled with Ar) and cooled to 0°C in an ice bath. p-Toluene sulfonyl chloride (42 mmol) was added slowly over 40 min. The solution was stirred for 3 h and quenched with cold water (150 mL). The aqueous phase was washed three times with DCM (70 mL) and combined with the organic phase. The organics were washed with 2M HCl (80 mL), saturated $NaHCO_3$ (80 mL), and brine (80 mL), respectively. The organics were dried with Na_2SO_4, filtered, and concentrated to a clear oil. The product was purified by column chromatography using 1:1 ethyl acetate:hexanes as the eluent. Yield for this step was 57% based on p-toluene sulfonyl chloride use. For the oxidation, a 500 mL round bottom flask with an addition funnel was flame dried and filled with Ar. Oxalyl chloride (25.5 mmol) and DCM (78 mL) were added to the flask and cooled to -78°C. Dimethylsulfoxide (57 mmol) in DCM (26 mL) was added to the flask dropwise through the addition funnel and allowed to stir for 20 min. The purified 4-tosyloxybutanol (23.74 mmol) in DCM (48 mL) was added to the reaction dropwise through the addition funnel and allowed to stir for 40 min. Diisopropylethyl amine (166 mmol) was added dropwise through the addition funnel and allowed to stir for 10 min. The reaction was then warmed to room temperature and water (120 mL) was added. After 5 min, the aqueous phase was extracted with dichloromethane (50 mL). This extraction and the organic phase was combined and washed with water and brine. The organic phase was then dried

with Na_2SO_4, filtered, and concentrated to a yellow oil. The product was purified by column chromatography using DCM as the eluent.

For the in-situ NMR study, PHA was purchased and purified as above. DCM-d_2, THF-d_8, γBL, and P_4-t-Bu 0.8M solution in hexane were purchased from Sigma-Aldrich. DCM-d_2, 99.9 atom % D, THF-d_8, ≥99.5 atom % D, and P4-t-Bu were used as-received. ACS Reagent-grade hexane, THF, and methanol were purchased from BDH and used as-received. ACS Reagent-grade DCM was purchased from BDH and dried over 3Å molecular sieves. ACS grade benzyl alcohol, 99%+, was purchased from Alfa Aesar and used as-received. The γBL was prepared according to Hong, et al.[65] BA was purchased from Acros Organics and purified as above.

2.2 Methods

2.2.1 Poly(norbornene)Permanent Dielectrics

For PNB studies, the silicon wafers where pretreated with 3-APTES to improve adhesion. A 2 wt% solution of 3-APTES in acetone was puddled on the silicon wafer for 30 s. The wafer was then sprayed with acetone while spinning at a rotation speed of 2500 rpm for 60 s. The PNB mixtures were spin-cast onto silicon wafers using a CEE 100CB spinner at a rotation speed of 2500 rpm for 60 s. The films were soft baked on a hot plate for 2 min at 100°C. The film thickness was measured using a Veeco Dektak profilometer. Films were developed with MF-319 in an agitated puddle fashion. The films were cured in a nitrogen-purged furnace. The temperature of the furnace was ramped to the cure temperature over a period of 130 min, held at the peak temperature for 2 h, and allowed to cool slowly to ambient temperature.

2.2.1.1 Reduced Modulus

The reduced modulus of the spin-cast films was determined using a Hysitron Triboindenter in a quasistatic nanoindentation mode. A north star standard head diamond tip was used for a varying load of 150 to 550 μN. A constant load time of 20 s was used. Maximum indentation depth across all samples was less than 8% of the film thickness. To minimize variables from the stress of the film, the formulations were spin-coated onto 6.5 cm^2 area silicon substrates. The reduced modulus was determined using Equation 1.[66]

$$E_r = \frac{\sqrt{\pi}}{2\beta}\frac{dP/dh}{\sqrt{A}} \quad [1]$$

E_r is the reduced modulus of the material, β is a geometric constant on the order of unity, dP/dh is the slope of the linear portion of the unloading curve, and A is the projected area of the indentation. The projected area of indentation was estimated via Equation 2 by calibration to a polycarbonate standard.

$$A = C_o h^2 + C_1 h + C_2 h^{1/2} + C_3 h^{1/4} + \cdots + C_8 h^{1/128} \quad [2]$$

Curve-fitting was used by adjustment of the constants C_o to C_8, where C_o is by definition 2.598 for a north star tip. The contact depth from experiment, h_c, was obtained by Equation 3.

$$h_c = h_{max} - \epsilon\frac{P_{max}}{S} \quad [3]$$

P_{max} is the maximum load, h_{max} is the maximum displacement, ϵ is a geometric constant for the indenter tip, and S is the stiffness. Equations 2 and 3 are the method described by Oliver and Pharr.[67]

2.2.1.2 Chemical Characterization

^{19}F NMR spectroscopy was performed in a Varian Mercury Vx 400 MHz. All samples were dissolved in deuterated chloroform. HATR measurements were performed in a Nicolet Magna-IR 560 Spectrometer. The molecular weight measurements were made by GPC using a Waters 2690 separation module and a 2410 differential refractive index detector. These were connected to Waters Styragel columns (HP 1, HP 3, and HP 4), and THF was used as an eluent and solvent. The molecular weight was compared to polystyrene standards.

2.2.1.3 Film Development

QCM was performed on a Stanford Research Systems QCM 200. The Butterworth-van-Dyke model was used to describe the physical changes the quartz crystal experiences. Thin film samples were spin-coated onto a 2.54 cm QCM with 5 MHz unloaded resonant frequency and an active surface area of 0.4 cm^2.

For the dissolution experiments, the coated QCMs were developed with MF-319 in a 125 µL flow cell connected to a Thermo Scientific 800 µL min^{-1} peristaltic pump. A manual valve positioned 5 cm from the inlet of the flow cell was placed in the flow path to alternate between water and MF-319. The polymer-coated QCM samples were first equilibrated in water before developing to minimize sharp frequency and resistance changes that result from an immersion into a liquid from air. Equation 4 was used to determine the mass changes (Δm).

$$\Delta f = -\frac{2f_o^2}{A_q\sqrt{\rho_q \mu_q}}\Delta m \qquad [4]$$

Δf is the resonant frequency change, f_o is the resonant frequency of the unloaded quartz crystal, A_q is the active area between the gold electrodes, ρ_q is the density of quartz, and μ_q is the shear modulus of quartz. The thickness was calculated by taking the density of the polymer to be 1.3 g cm^{-3}, as obtained from measuring thickness and mass.

2.2.1.4 Qualitative Cross-linking

The swelling measurements were performed in PGMEA. Each polymer was submerged in PGMEA and a sample was removed from the PGMEA at 15 minute intervals. Each polymer type was measured multiple times and the trends were consistent. Since each individual sample was slightly different (e.g. mass) the values could not be averaged. One data set is shown along with its corresponding gel permeation chromatography (GPC) results. The mass of the polymer was taken after removing excess solvent from the surface. Equation 5 was used to calculate the swelling ratio, or the percent increase in mass of the polymer film.

$$Swelling\ Ratio = \frac{m_i - m_o}{m_o} \quad [5]$$

In Eq. 5, m_i is the mass of the polymer film at the i^{th} time interval and m_o is the initial mass of the polymer film prior to submersion in PGMEA.

2.2.1.5 Electrical Characterization

Dielectric measurements were conducted by fabrication of parallel-plate capacitors with a bottom electrode formed from evaporated aluminum metal with a thickness of 300 nm covering the full surface of an oxidized wafer. After spin-coating and curing the film onto the metal substrate, a second layer of metal was deposited

through a shadow mask to form the top electrode of the parallel plate capacitor. Contact to the top and bottom metal electrodes of the capacitor was made on a Karl Suss probe station. The capacitance and dielectric loss tangent were measured using a Gwinstek LCR-821 meter. The real part of the relative dielectric constant, $\varepsilon_{r,}$ was determined using Equation 6.

$$\varepsilon_r = C\frac{t}{A\varepsilon_o} \quad [6]$$

In Eq. 6, C is the capacitance, t is the thickness of the polymer, A is the area of the top electrode pad, and ε_o is the permittivity of free space, 8.854 x 10^{-12} F/m. ASTM standard D150 – 11 was used to correct the measurements for edge fringing.[68] There were 9 to 15 capacitors tested for each data point (average and standard deviation) presented in the results.

2.2.2 Low Ceiling Temperature Polymer Synthesis and Characterization

For the anionic polymerizations of phthalaldehyde, varying amounts of PHA were added in a nitrogen purged glovebox to a reaction flask with a specific amount of solvent. To this reaction vessel, an alcohol was added to act as the initiator. The flask was sealed and cooled to the desired temperature. After the solution reached the desired temperature, a phosphazene base was added and the reaction was allowed to proceed for a predetermined amount of time. The reaction was quenched by the addition of pyridine (5 pyridine to 1 alcohol) and a strong electrophile (2 electrophile to 1 alcohol). The solution was then allowed to react for 30 min at temperature. The quenched solution was

precipitated into methanol and filtered. The filtrate was washed by alternating hexane and methanol washes and dried to constant weight.

For the cationic homopolymerizations of phthalaldehyde, 2 g (15 mmol) of PHA monomer was dissolved in 20 mL DCM in a 100 mL round bottom flask in a nitrogen purged glovebox. To the monomer solution, a catalyst was added and the flask sealed with a septum. The flask was cooled to -78°C and allowed to react for the desired length of time. The reaction was quenched with 0.24 mL (3 mmol) pyridine. The subsequent solution was precipitated into methanol and filtered. The precipitate was redissolved in either THF or DCM; 0.05 mL (0.36 mmol) of TEA per gram of precipitate was added to some polymers to help remove residual catalyst. The polymer in either THF or DCM was precipitated into hexane, filtered, and allowed to dry until constant weight was achieved.

For the cationic copolymerizations of PHA and BA, the mixtures used in polymer synthesis were prepared in a nitrogen filled glove box. Purified PHA (15 mmol) and BA (7 mmol) were added to a 100 mL round bottom flask with 25 mL dried DCM. A specific amount of BF_3-OEt_2 was added, and the reaction vessel sealed. The vessel was then submerged in a cold bath at a specified temperature for a specific amount of time followed by the addition of pyridine (2 mmol) to quench the reaction. The polymer was precipitated from the reaction solvent into methanol. The precipitate was redissolved in THF with 0.05 mL TEA per gram of precipitate. This solution was precipitated into hexane. The resulting precipitate was again dissolved in THF with TEA, as described above, and precipitated into methanol. The polymer was dried until constant weight was achieved.

For the cationic copolymerization of PHA with other aldehydes, the mixtures were again prepared in a nitrogen filled glove box. Purified PHA and as-received coaldehyde were added to a flask with DCM to a final aldehyde concentration of 0.75M. A molar ratio of 4 PHA to 1 coaldehyde was used in each case. A specific amount of BF_3-OEt_2 was added, and the reaction treated as above.

2.2.2.1 NMR Characterization

^{1}H NMR was performed in a Bruker Avance III 400 MHz or Varian Mercury Vx 400 MHz tool. In-situ ^{1}H and ^{19}F NMR was performed in a Bruker Avance III 400 MHz tool. DCM-d_2 and THF-d_8 were used as the reaction solvents, with residual solvent peaks, 5.32 ppm, and 1.72 and 3.58 ppm, respectively, as the internal references. Temperature was calibrated by the relation of the chemical shift differences of a pure solution of methanol.[69] Each reaction was allowed to proceed at each temperature until no change was observed in the integrated peaks.

Determination of the thermodynamic properties of the polymerization is based on the equilibrium reaction. Equation 7 shows the equilibrium reaction

$$M + M_n \cdot \overset{K}{\leftrightarrow} M_{n+1} \cdot \qquad [7]$$

where M is monomer, $M_n\cdot$ is a propagating polymer chain of length n, K is the equilibrium constant for the reaction, and $M_{n+1}\cdot$ is a propagating chain of length n + 1. The reaction can be described thermodynamically by assuming equilibrium conditions with the propagating chain of length n ($M_n\cdot$) being approximately equal to the

propagating chain of length n + 1 ($M_{n+1}\cdot$). The resulting equation, shown as Equation 8, can be used to determine the change in enthalpy and entropy of polymerization.[70]

$$\frac{\Delta H^\circ}{RT} - \frac{\Delta S^\circ}{R} = \ln([M]) \quad [8]$$

where ΔH is the change in enthalpy of polymerization in J/mol, R is the ideal gas constant, T is the temperature in K, ΔS is the change in entropy of polymerization in J/mol-K, and [M] is the monomer concentration. The extrapolation of this line through the initial concentration, allows the calculation of T_c as shown in Equation 9.[71]

$$T_c = \frac{\Delta H^\circ}{\Delta S^\circ + R * \ln([M]_o)} \quad [9]$$

$[M]_o$ is the starting concentration of monomer. For addition polymerizations, ΔH is exothermic on the order of tens to hundreds of kJ/mol, and ΔS is exoentropic on the order of tens to hundreds of J/mol-K.[50,72]

2.2.2.2 Molecular Weight

Molecular weight and $Đ$ were determined by gel permeation chromatography (GPC) in a Shimadzu GPC tool equipped with an LC-20 AD HPLC pump and a refractive index detector (RID-10 A, 120 V). THF was used as the eluent with a flow rate of 1.0 mL/min at 35˚C. The molecular weight was measured by a calibration curve based on polystyrene standards.

2.2.2.3 Thermal Characterization

Accelerated aging was performed in a TA Instruments Thermal Gravimetric Analysis (TGA) Q50 with a ramp rate of 20°C/min to 10°C below desired isothermal temperature and a 1°C/min ramp over the remaining 10°C to the final temperature to avoid overshoot. A N_2 rich atmosphere with a flow rate of 40 mL/min was used. Further studies of the thermal stability of polymers were performed in the same TGA with a ramp rate of 2°C/min to 250°C.

2.2.2.4 Dry-development Rate

For the dry-developing rate experiments, polymer formulations were made with specific loadings of a PAG, Rhodorsil FABA. The film-coated QCM was exposed under a solar simulator lamp filtered to 248 nm light. The time was started as soon as exposure began. Each film was exposed to a dose of 1000 mJ/cm^2. The resulting frequency and resistance changes were monitored. The inductive changes correspond to the frequency response, or change in mass with developing time. Resistance corresponds to losses due to changes in viscosity of the fluid under which the quartz crystal oscillates. Figure 2.1 shows a typical frequency and resistance response. After initial exposure at t = 0 s, the resistance shows a sharp rise (I). This sharp rise is the liquification of the polyaldehyde film as a result of the exothermic, acid-catalyzed depolymerization reaction. As the film liquefies, the film decouples from the crystal, giving a false rise in the frequency. While the film is decoupled from the crystal, no frequency data is used. After reaching a peak resistance, the film slowly evaporates (II), withdrawing heat from the liquid. The liquid will eventually freeze due to the melting temperature of the majority monomer (55°C). As the monomer freezes, the resistance returns to the initial resistance as the solid has

coupled to the crystal oscillations. Frequency readings are then used to determine the evaporation of the remaining mass according to Equation 4 (III).

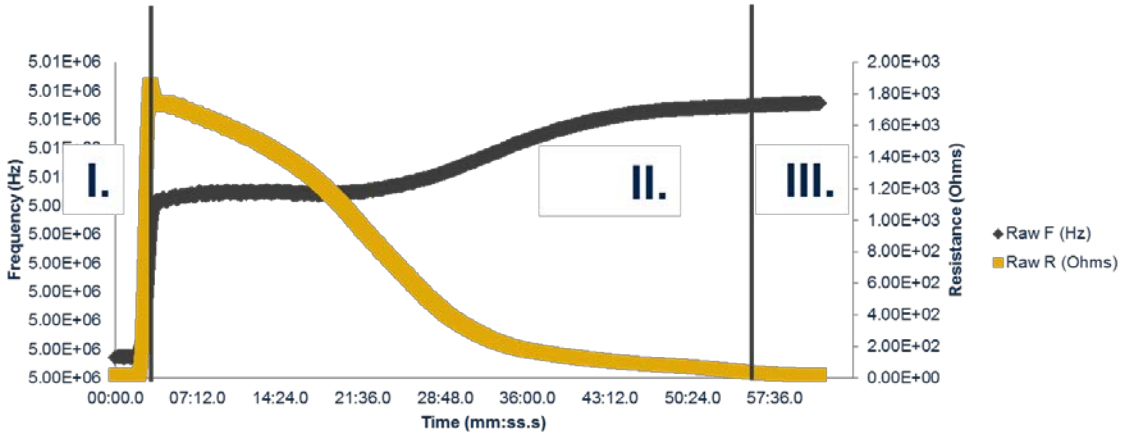

Figure 2.1. Frequency and resistance versus time for a representative QCM depolymerization of a polyaldehyde film. A rapid liquification (I) is followed by a region of slow evaporation and eventual freezing (II). A region of slow sublimation follows (III).

To compare depolymerization rates between samples, the resistance was normalized by dividing by the peak resistance for each respective depolymerization. The resulting data was plotted against time and used to create an exponential regression of the form $R_{norm} = e^{(b*(t-c))}$, where b is taken to be the rate of depolymerization and c is taken to be the delay from t = 0, or the initial exposure, to the start of depolymerization. An example is shown in Figure 2.2.

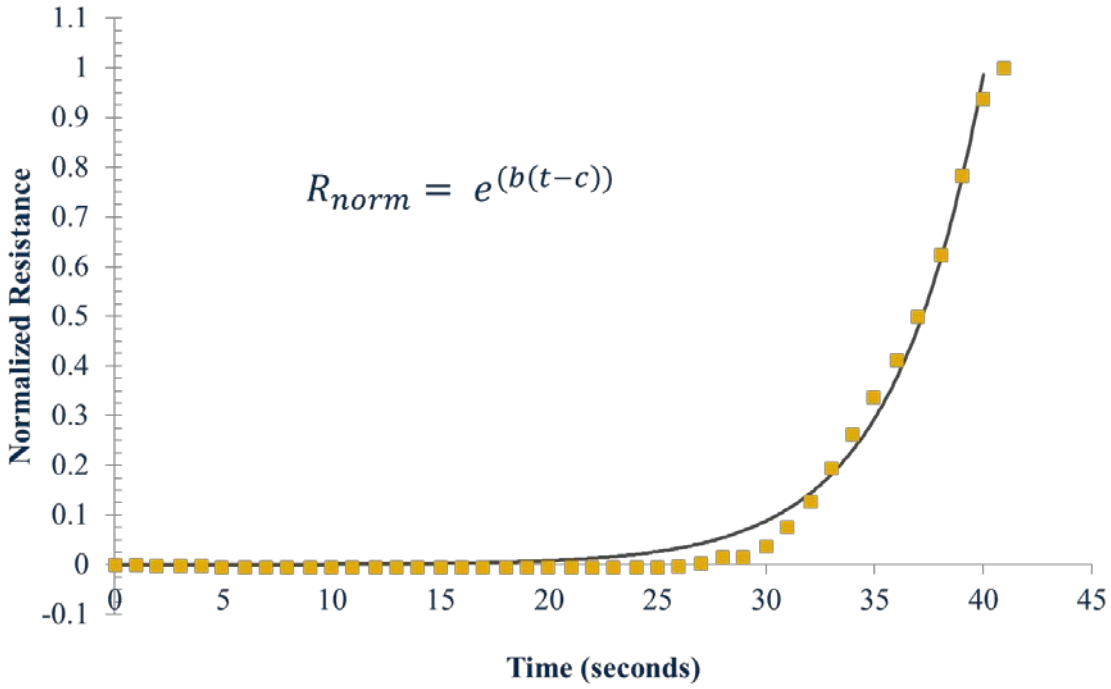

Figure 2.2. Representative resistance response versus time for a polyaldehyde film exposed to a photo acid generator. The yellow squares represent the raw data and the line through the data points is an exponential fit of the form shown.

CHAPTER 3. POSITIVE TONE, POLYNORBORNENE DIELECTRIC CROSSLINKING

Parts of this chapter were also presented in Dr. Brennen Mueller's PhD thesis.[73] This information is reproduced here to provide the complete story. The swelling ratio, HATR, and dissolution rate data and figures are reproduced from his work. Positive tone photo-definability has previously been demonstrated with a bis-DNQ added to a polynorbornene polymer.[17]

3.1 Motivation

Previously, crosslinking in a negative tone polynorbornene material was observed through acid-catalyzed ring-opening of an epoxy.[19] Efficient polymer patterning and crosslinking with a minimal amount of invasive additives is of interest. PNB patterning was achieved via UV exposure and developing of the DNQ additive. Figure 3.1 shows the UV irradiation induced Wolff rearrangement of DNQ that results in the indene carboxylic acid (III). UV radiation causes the loss of the diazo group and forces a rearrangement of the aromatic ring to form a ketene (II). The ketene is a very reactive species that will react with water to form the indene carboxylic acid (III).

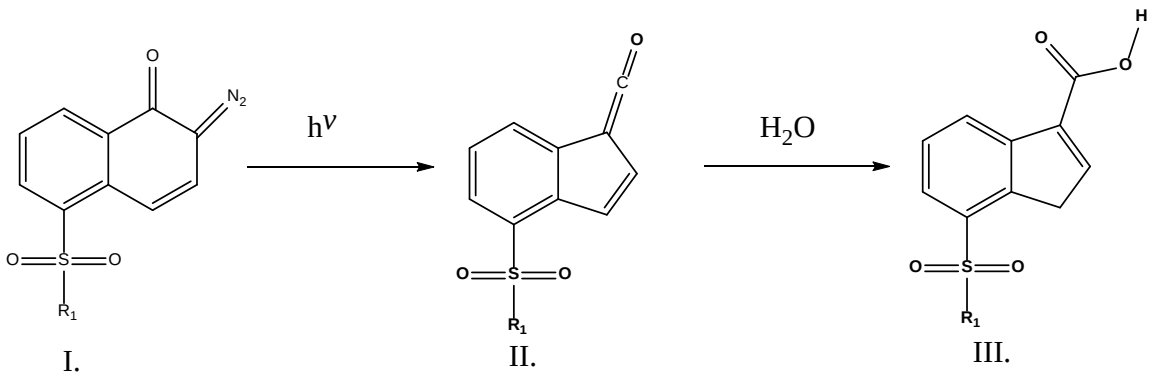

Figure 3.1. Wolff rearrangement of DNQ moiety (I) to ketene intermediate (II) and with the presence of water to indene carboxylic acid (III).

A permanent dielectric can be achieved with an epoxy-based crosslinking and DNQ-based photochemistry, similar to previous PNB films.[16,19] Trimethylolpropane triglycidyl ether (TMPTGE) was used as the crosslinking agent with a random PNB copolymer of a fluoroalcohol norbornene and carboxylic acid norbornene, shown in Figure 3.2. DNQ was used as the photo active compound. This study provides evidence for DNQ crosslinking in the positive tone PNB dielectric.

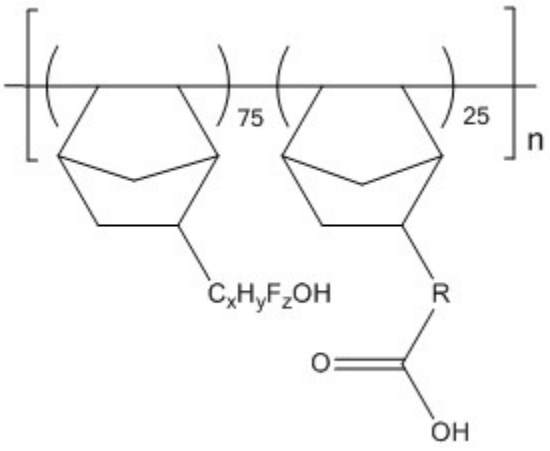

Figure 3.2. Random copolymer of polynorbornene with fluoroalcohol and carboxylic acid functionalities.

3.2 Results and Discussion

3.2.1 Swelling of Cured PNB Films

Polymer films with 20 pphr difunctional DNQ and varying loadings of the trifunctional epoxy, TMPTGE, were exposed to a UV dose of 2000 mJ/cm^2 and cured at 200°C for 2 hr. The exposure dose was sufficient to convert the DNQ to the indene carboxylic acid. The cured polymer films were soaked in PGMEA to evaluate the swelling of the polymer which gives an indication of the crosslinking density. Figure 3.3 shows the swelling ratio for the exposed and cured films expressed as percent mass increase.

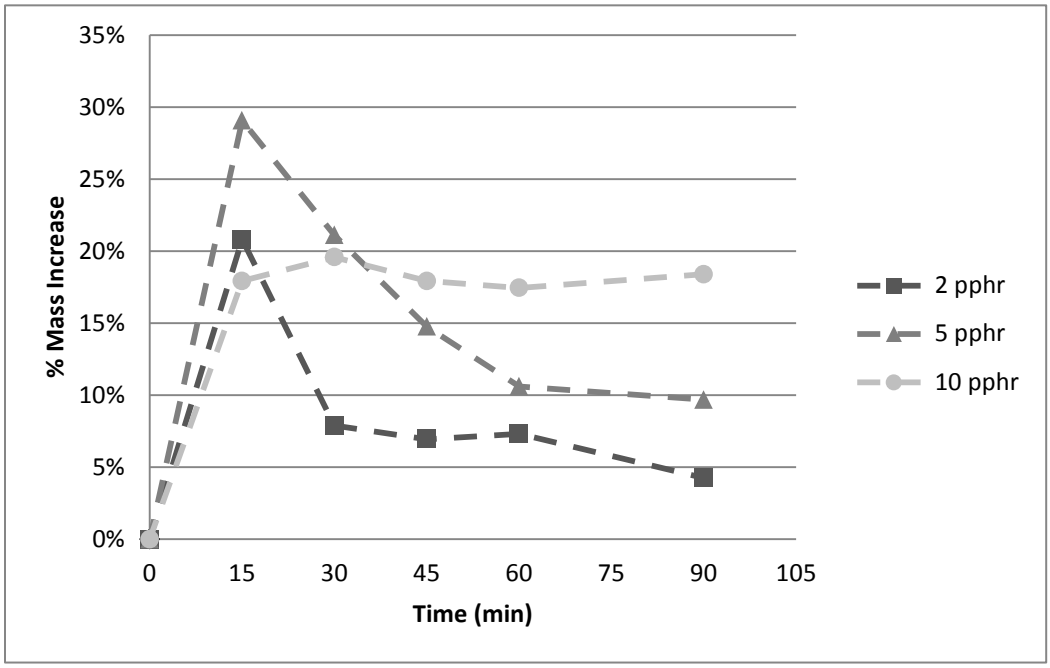

Figure 3.3. Swelling ratio versus soak time in PGMEA for various TMPTGE loadings (given in pphr) in an exposed, cured film.

The data shows that increasing the epoxy loading leads to higher apparent solvent uptake even though the films were fully cured. The film without epoxy (i.e. zero pphr

epoxy) is not shown because the film dissolved in the swelling solvent within the first 15 min. The 2 and 5 pphr epoxy films show a maxima in the solvent uptake after fifteen minutes followed by a decline in mass. The 10 pphr epoxy film maintained a constant swelling ratio of approximately 0.18 over all swelling times.

The behavior for the 10 pphr epoxy film was typical for a crosslinked epoxy-based polynorbornene film.[14] After 15 minutes in the swelling solvent, the film was saturated with solvent and the mass uptake of the polymer film did not increase with additional time in the solvent. The maximum uptake in solvent seen in the 2 and 5 pphr epoxy films (followed by a decline in mass with additional time) is uncommon and is the result of swelling and leaching of material from the film. The mass increase at the longest times in the solvent was lower with smaller epoxy loadings supporting the concept that the decrease is due to mass loss from leaching. Higher epoxy loading leads to a greater crosslink density and less material being leached from the film. Compounds that can be leached during swelling studies have the potential to act as mobile charge carriers in a dielectric, increasing the permittivity.

The solvent used in the swelling experiments was analyzed by GPC to investigate the leaching of additives from the film. Each solvent was analyzed after 90 min of exposure to the samples. A lower retention time corresponds to a higher molecular weight solute in the solvent.

There were two peaks of note in the GPC at retention times of 16 and 25 minutes. The 16 minute retention time corresponds to a material with a molecular weight of approximately 180,000 Da. The 25 minute retention time corresponds to a material with

a molecular weight of 880 Da. The polymer film with no TMPTGE, which at least partially dissolved in the solvent, had a broad peak at 16 min retention. This broad peak is consistent with the polymer prior to processing. At 25 min retention, the indene carboxylic acid form of the difunctional DNQ molecule is most apparent in samples containing 0 to 5 pphr TMPTGE. The indene carboxylic acid does not readily react with TMPTGE possibly due to the limited mobility and proximity of the indene carboxylic acid and epoxy.

A set of unexposed films with the same TMPTGE loadings were created to further understand the role of the epoxy. A typical swelling result for the unexposed PNB films is shown in Figure 3.4. Multiple samples were tested and all gave consistent results. GPC data was collected for the sample used to obtain the data displayed in Figure 3.4. All films remained after 90 min exposure to PGMEA. No significant difference was seen between films containing 2, 5, and 10 pphr TMPTGE loading. The 0 pphr TMPTGE film did not dissolve in the swelling solvent, as occurred with the UV exposed film. A comparison of the exposed and unexposed films of the same composition (TMPTGE loading) can be made. The fact that an unexposed film with no TMPTGE does not dissolve in the swelling solvent and the exposed film does, indicates that additional crosslinking occurred in the unexposed films compared to the exposed films. This additional crosslinking likely occurred via the DNQ, becasue its presence is the only difference between the formulations which dissolved (i.e. UV exposed) and did not dissolve (i.e. unexposed). The swelling behavior of the films containing different amounts of TMPTGE support this conclusion. Unexposed films do not drastically lose

mass in the same manner as exposed films, suggesting that the ICA is not an effective crosslinker in the final polymer structure.

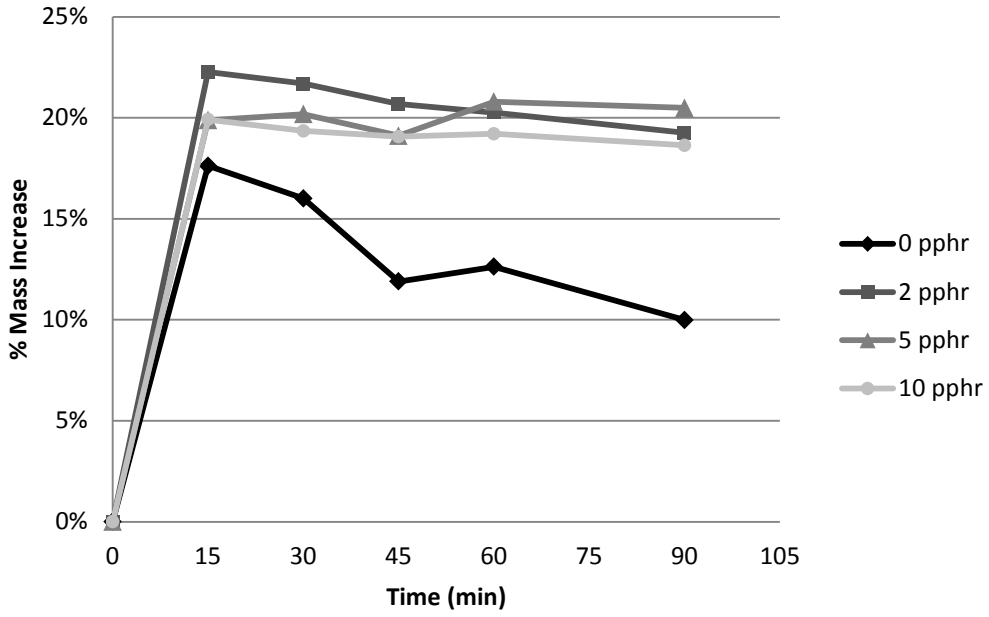

Figure 3.4. Swelling ratio versus soak time in PGMEA for various TMPTGE loadings (given in pphr) in an unexposed, cured film.

The products of the thermolysis of DNQ are likely similar to those formed from UV irradiation, however, when the films were not exposed to UV radiation, the DNQ reaction occurred at a high temperature in the absence of water. The diazo bonds are the least stable ones in the DNQ compound and are the most thermally labile. Without water, the reactive ketene intermediate of the Wolff rearrangement does not convert to a carboxylic acid but is instead available for crosslinking in the unexposed case.

3.2.2 HATR of DNQ-loaded PNB Films

Determining the thermal stability of the DNQ additive was found to be important to understanding the mechanism that likely occurs for DNQ crosslinking. HATR was

performed on a thin film of formulation PNB–D to investigate the disappearance of the DNQ diazo FTIR peak. A thin film of PNB-D was doctor bladed onto the ATR crystal. The thin film was heated to 130°C at a ramp rate of 3°C/min and the film was maintained at 130°C for 2 hr. Figure 3.5 shows the HATR curves at the cure temperature of 130°C as a function of time. The 2050-2175 cm^{-1} region corresponds to the diazo peaks[13]. As time increases, moving down the chart, the diazo peaks area decreased.

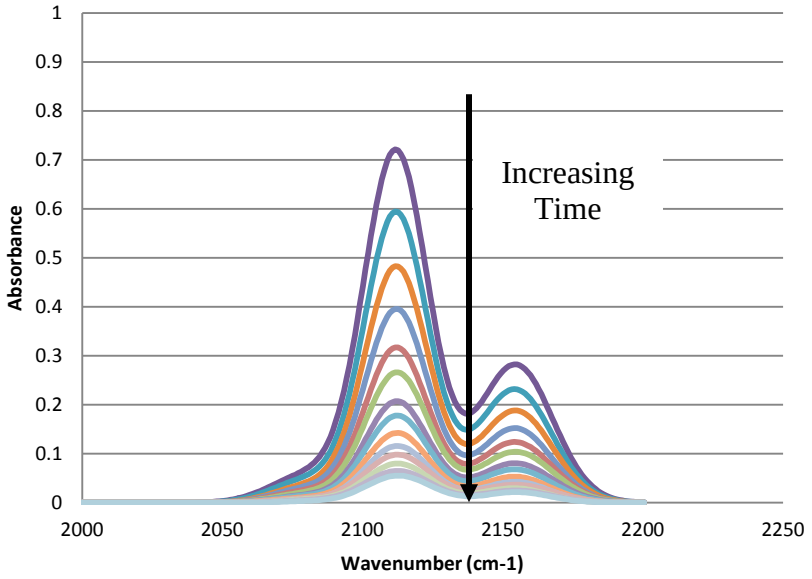

Figure 3.5. Attenuated total reflectance at 130°C for 2 hours of characteristic diazo peaks (2050-2175 cm^{-1}); absorbance units are arbitrary.

The HATR results show a thermal degradation of the diazo group of the DNQ. A thermal degradation of the diazo group leads to a ketene via the Wolff rearrangement. The 130°C cure for 2 hr was sufficient energy to remove 98% of the diazo group. Thus, the majority of the DNQ moieties have sufficient thermal energy to form the ketene at the cure temperatures used in this study.

3.2.3 Nano-indentation of Cured PNB Films

A chemical reaction between the epoxy and the reacted DNQ can occur during curing which likely affects the physical properties of the polymer film. To investigate the consequences of the DNQ crosslinking on the mechanical properties of the material, films were created with the four formulations in Table II, PNB, PNB–D, PNB–E, and PNB–D & E. The reduced modulus was used to compare the mechanical properties of the films. Figure 3.6 shows the reduced modulus for the four formulations at different cure temperatures. The cure temperature range shown should be high enough to thermally activate the DNQ.

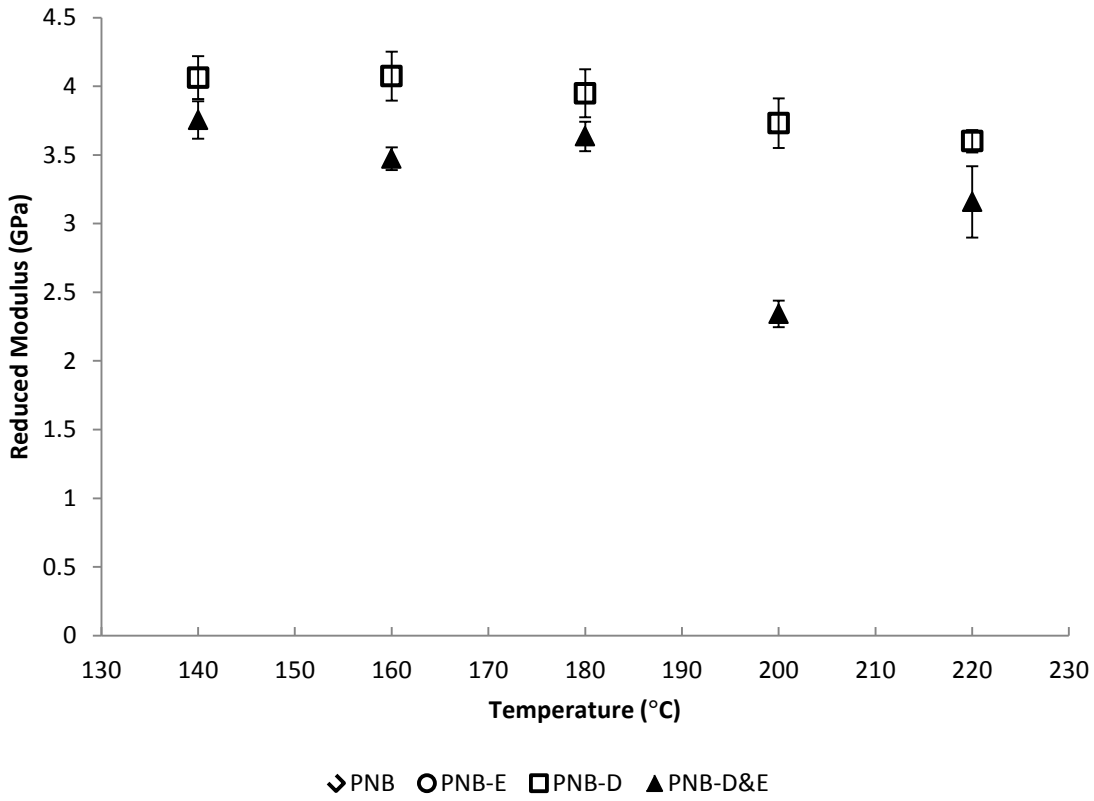

Figure 3.6. Reduced modulus vs. cure temperature for undeveloped PNB, PNB-E, PNB-D, and PNB-D & E.

The PNB modulus maintains a consistent value of 2.2 GPa across all temperatures, as expected. During the cure step, a polymer film without a crosslinker did not decrease in modulus as no reaction should be occurring. There was a decrease in modulus when the samples were cured at the highest temperatures, 220°C. It is known that the properties of epoxy-type materials are sensitive to exposure to temperatures above 200°C for long periods of time, such as the two hour cure performed here. Degradation of the crosslinking moieties and/or densification of the films is possible.[3,4] This data shows that curing and long term exposure to temperatures at or above 220°C should be avoided if changes in modulus are to be avoided. Indentation prior to the cure

step also showed a modulus of 2.2 GPa. Upon adding TMPTGE to the polymer, or PNB-E, the modulus increased slightly, but the modulus declined with increasing temperature.

Upon adding DNQ to the film, PNB-D, the modulus nearly doubled to 4 GPa. This result shows that DNQ participates in crosslinking. The rigid ballast molecule of DNQ contributes to the polymer structure, as reflected in the higher reduced modulus.

The effect of added, small molecule epoxy functionalities on the curing properties was also investigated. Adding TMPTGE to the formulation, PNB-D & E, causes the modulus to decrease slightly to 3.6 GPa. This decrease compared to the DNQ-only sample is likely a consequence of plasticization of the film by TMPTGE. The structure of TMPTGE would allow for more movement after crosslinking compared to the rigid DNQ structure.

Although the reduced modulus of the undeveloped films provides valuable information, a developing step would normally be used prior to curing the films. PNB–D and PNB–D & E were developed prior to curing. Figure 3.7 shows the reduced modulus of the developed films versus the cure temperature.

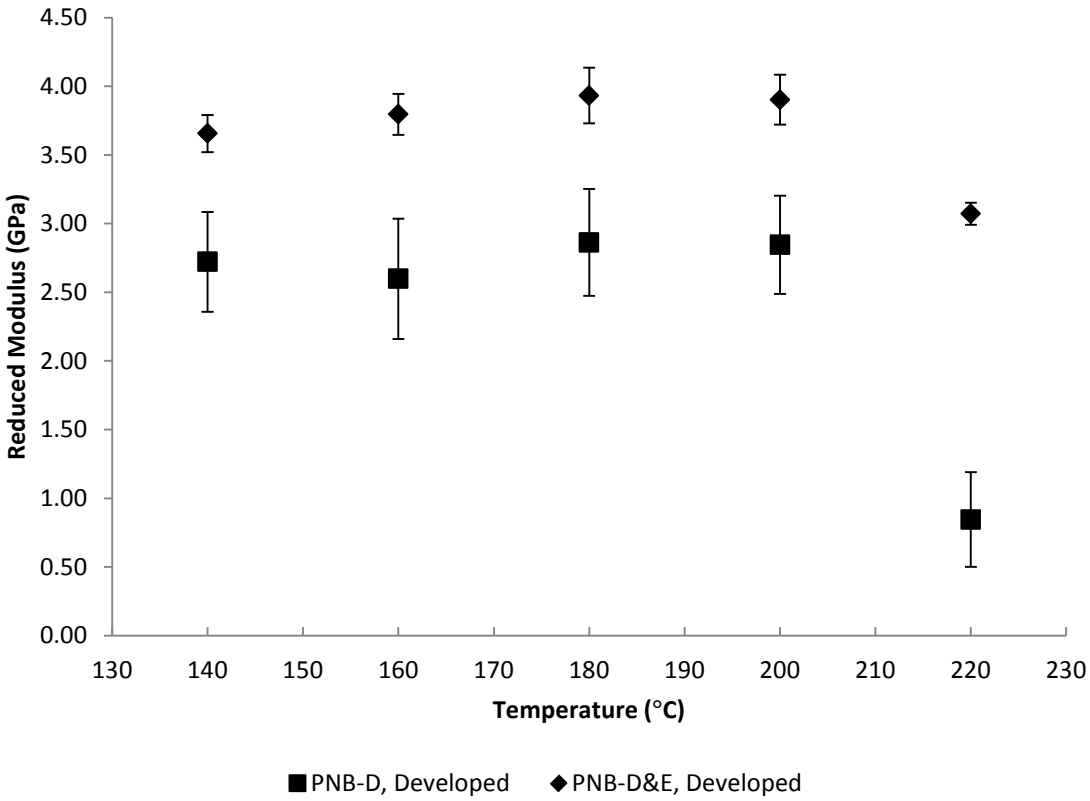

Figure 3.7. Reduced modulus versus cure temperature of developed PNB–D and PNB–D & E.

Although the modulus of PNB was 4 GPa after adding DNQ to the undeveloped film, a drop in modulus was observed when the DNQ-loaded film, PNB–D, was developed in aqueous base, MF-319, before curing. The modulus dropped to 2.7 GPa (standard deviation of 0.4 GPa) when cured after exposure to base. Adding TMPTGE to a developed film increased the modulus to the undeveloped value PNB–D, 4.0 GPa. TMPTGE either reduces base uptake in the film during developing or benefits the crosslinking in a similar manner to DNQ, which as previously shown is not likely. This is significant, because when creating features with a DNQ-based, photo-definable PNB dielectric, base will penetrate into the film.

3.2.4 Role of TMPTGE in Dissolution Rate

Exposure of DNQ to base has also been shown to lead to side-products[14]. Figure 3.8 shows two possible products of the base-catalyzed DNQ reaction. This reaction renders the DNQ unable to crosslink the polymer. DNQ crosslinking can also be inhibited by water-uptake during the base develop step through formation of the indene carboxylic acid. Since the intended use of the PNB dielectric material is a photo-definable, permanent dielectric, the aqueous develop step is unavoidable. Base uptake can inhibit the DNQ crosslinking significantly affecting the reduced modulus of the film.

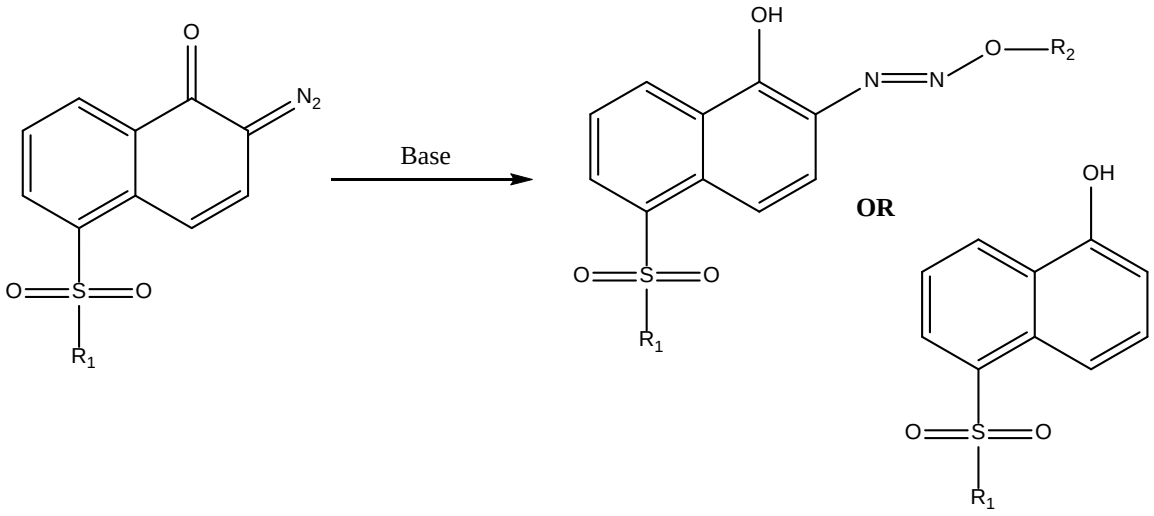

Figure 3.8. Base Catalyzed products of DNQ as described by Koshiba et al.[74]

Without an additive to reduce or prevent the aqueous base from swelling into the film, a significant drop in the modulus may occur as the DNQ crosslinking reaction is inhibited. Base uptake was likely minimized by the TMPTGE. The modulus of the TMPTGE-loaded polymer, PNB–E (shown in Figure 3.6), does not exhibit a modulus that is much different than the base polymer. The epoxy likely does not contribute

significantly to the modulus and more likely inhibits DNQ byproduct creation to allow this increase in reduced modulus.

QCM was used to investigate the amount of base uptake during the develop step for the DNQ inhibited films. A dissolution experiment was performed on seven polymer formulations of fluoroalcohol homopolymer with varying loadings of TMPTGE. The fluoroalcohol homopolymer was used because the 75/25 random copolymer of the fluoroalcohol and carboxylic acid decouples from the quartz crystal oscillation, and the measured response is the rate of decoupling rather than the dissolution rate. While the fluoroalcohol homopolymer films had no DNQ added to inhibit base dissolution, the dissolution rate of an uninhibited film is indicative of base uptake in an inhibited film. A similar trend would occur for base uptake in an inhibited film as observed for an uninhibited film, but on a smaller, possibly unmeasurable scale. Figure 3.9 shows the log of the dissolution rate at varying loadings of TMPTGE. With increasing TMPTGE concentration, there is a decrease in dissolution rate.

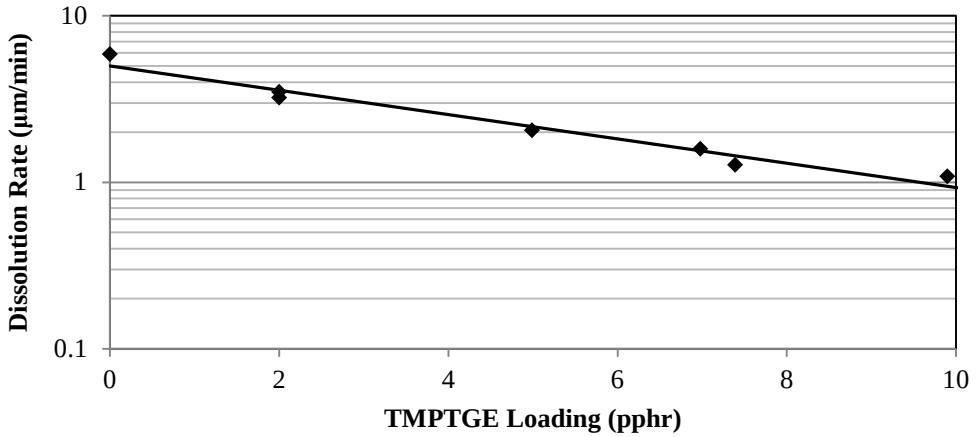

Figure 3.9. Dissolution rate of PNB film containing varied loadings of TMPTGE.

Including TMPTGE in the film will reduce the amount of aqueous base that could potentially react with DNQ. Any water that remains in the film during cure can react with the ketene intermediate and form the carboxylic acid, preventing any reaction of DNQ with the polymer. In additional, the base catalyzed DNQ degradation results in a product that can not undergo the Wolff rearrangement to form the reactive ketene[14,74]. The TMPTGE loading in the polymer films used in this study, 10 pphr, greatly reduces the dissolution rate, thereby allowing a developed DNQ loaded sample to form the potential crosslinking.

3.2.5 Model Reaction of DNQ and Norbornane

The modulus results show that DNQ contributes to the thermal crosslinking of the polymer dielectric during cure. To further understand the role of DNQ, a model reaction of norbornane fluoroalcohol with a monofunctional DNQ was used to examine the possible crosslinking mechanism between DNQ and the PNB copolymer. The monofunctional DNQ was dissolved in the norbornane fluoroalcohol at the same molar ratio as the previous formulations used in this study. The solution was continuously stirred and heated to 140°C for 40 min in an argon-filled glovebox. ^{19}F-NMR was used to look for a change in structure of the fluoroalcohol pendent group as a result of the reaction. Figure 3.10 shows the ^{19}F-NMR spectra for the reactants (top) and products (bottom). The insets highlight the difference between the spectra. The multiplets at -76.4, -76.8, -77.25, and -77.4 ppm are typical of the norbornane fluoroalcohol.

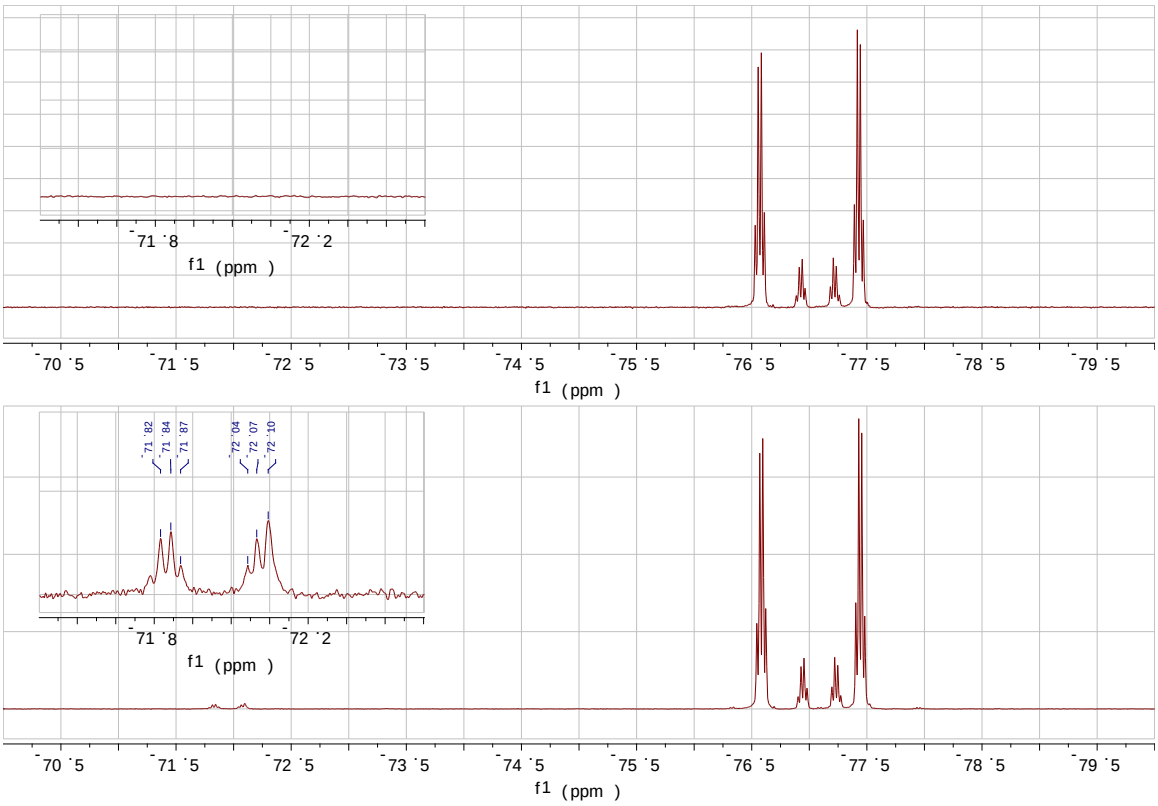

Figure 3.10. ^{19}F NMR of model reaction reactants (top) and products (bottom) with insets at -71 to -73 ppm.

While the bulk of the fluoroalcohol remained unchanged, a new downfield peak was observed. Koshiba, et al. described a reaction of a DNQ moiety with an alcohol, likely reacting with a thermally-derived ketene and forming an ester. Figure 3.11 shows the proposed DNQ and alcohol reaction for the model reaction in this study. The shift in the ^{19}F-NMR corresponds to an ester linkage formed at the alcohol oxygen in the fluoroalcohol, consistent with the reaction described by Koshiba, et al.[1474] In the polymer films described throughout this study, a similar reaction likely occurred, contributing to an increase in crosslinking.

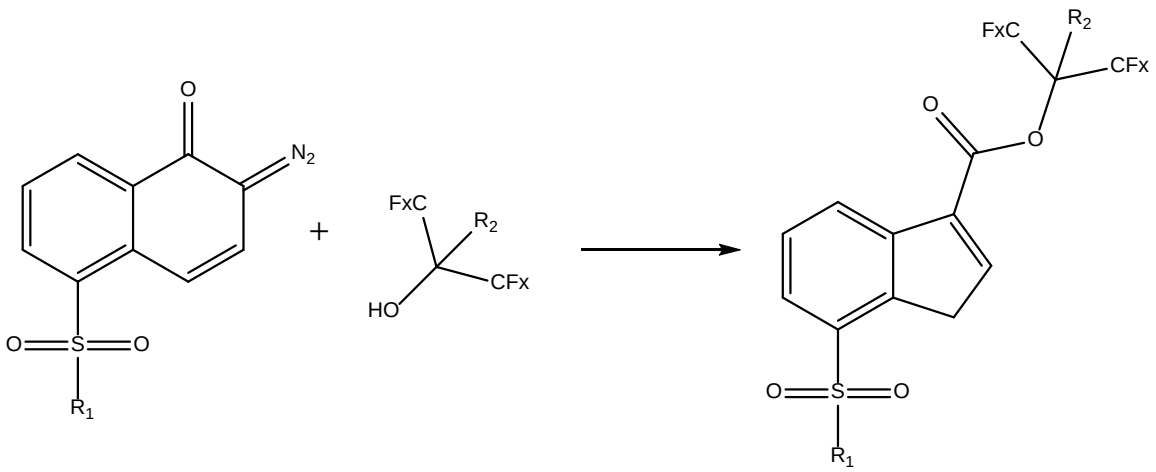

Figure 3.11. Proposed reaction of DNQ moiety with fluoroalcohol to form ester.

3.2.6 Dielectric Constant and Loss Tangent of PNB Films

The dielectric constant of the films was measured using a parallel plate capacitor configuration, as described in the Experimental Section. Capacitors were made from PNB–D and PNB–D & E formulations. The relative dielectric constant (i.e. real part of the permittivity) and loss tangent for samples made with PNB–D at different cure temperatures are shown in Figure 3.12. An increase in cure temperature causes a decrease in the dielectric constant and loss. Developing the PNB-D film prior to cure caused an increase in the dielectric constant compared to the undeveloped film likely due to inclusion of a small amount of aqueous developer.

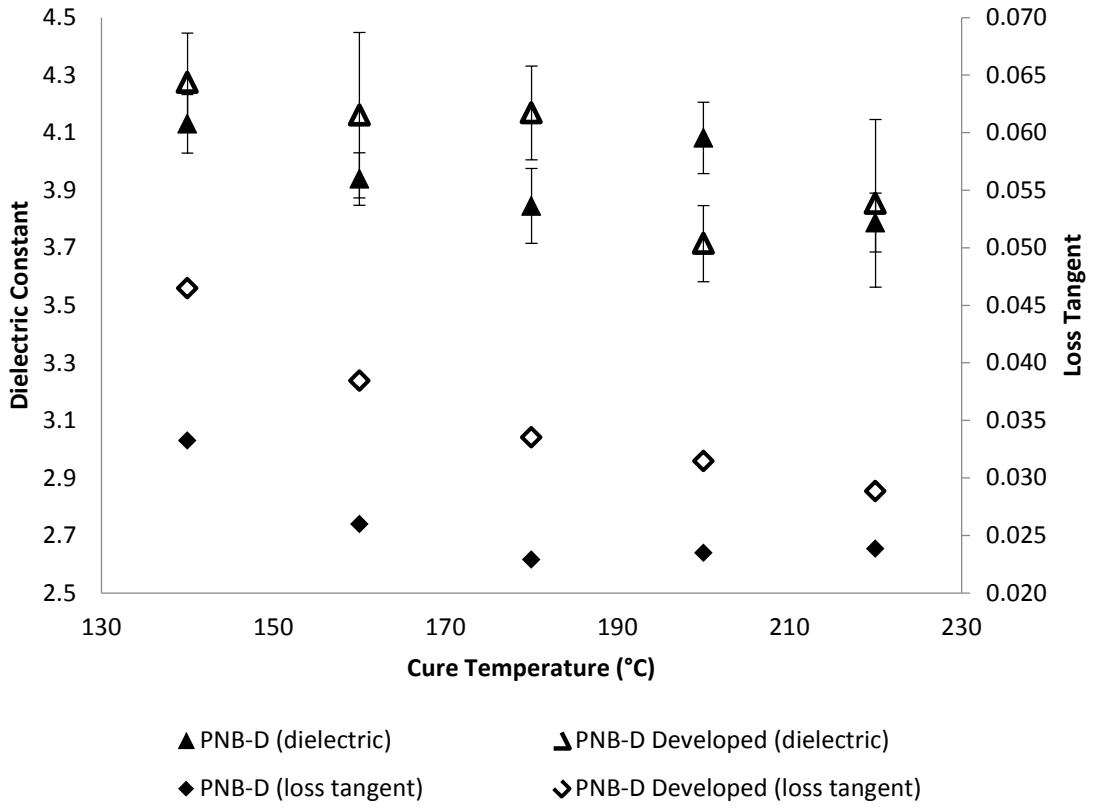

Figure 3.12. Relative dielectric constant and loss tangent versus cure temperature of positive tone films.

The loss tangent for the PNB-D samples exhibited a similar dependence on cure temperature to the dielectric constant. A decrease in loss tangent was observed with an increase in cure temperature. Developing the PNB-D samples raised the loss tangent compared to the undeveloped samples due to exposure to aqueous base.

The addition of the epoxy crosslinker lowered the relative dielectric constant compared to the DNQ-only PNB film. As seen in Figure 3.13, the PNB–D & E samples have a significantly lower dielectric constant compared to PNB–D at all cure temperatures. The dielectric constant declined with increasing cure temperature for all developed and undeveloped samples. Also of note is the lowest dielectric constant, 3.65,

across all sample processing conditions that occurred with a 220ºC cure of the developed epoxy and DNQ-loaded film. The addition of the epoxy crosslinker also changed the cure temperature dependence for the loss tangent compared to the DNQ-only PNB film. The PNB-D & E samples have a nearly constant loss tangent at all cure temperatures.

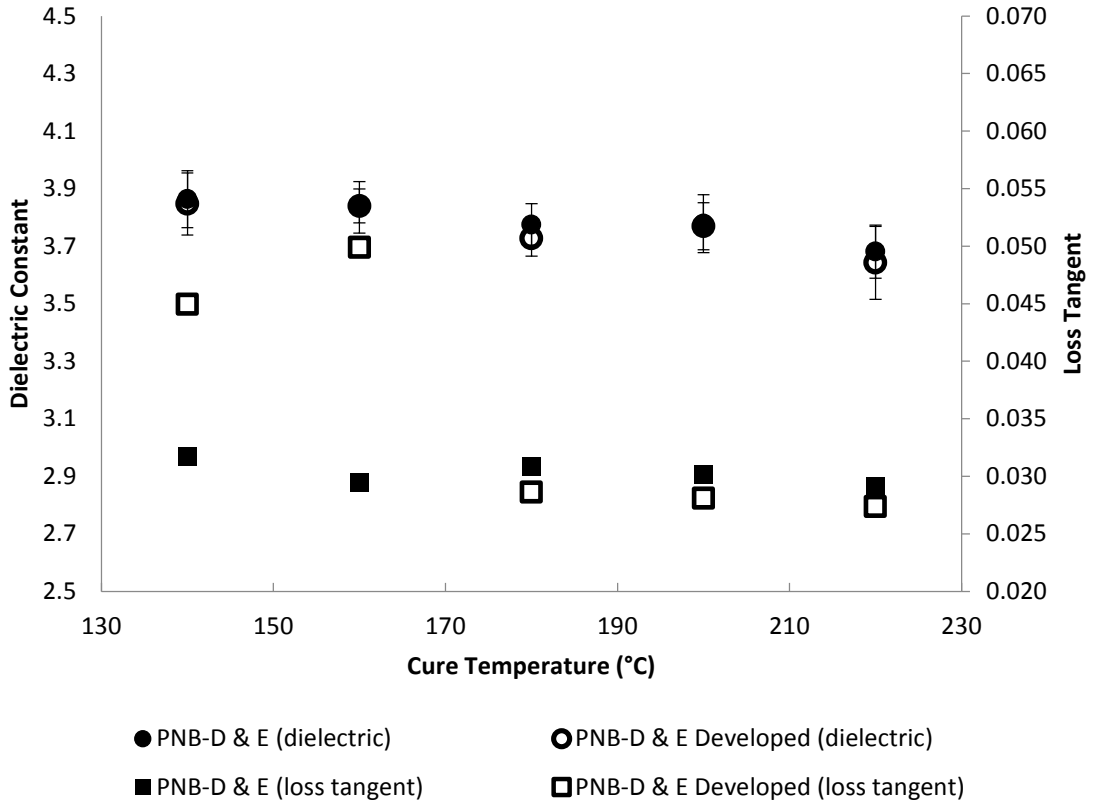

Figure 3.13. Relative dielectric constant and loss tangent versus cure temperature for positive tone films with TMPTGE.

The lower relative dielectric constant at each cure temperature indicates that the TMPTGE epoxy likely lowered the total polarizability of the film through crosslinking. This can be attributed to reducing the polarizability of present groups and possibly reducing the density of the film. Both developed and undeveloped films showed a steady decline in dielectric constant with cure temperature. At the higher cure temperatures, the

polymer would have higher mobility and rate of reaction, thereby increasing the likelihood of an epoxy or DNQ reaction and increasing the crosslink density and decreasing the number of polarizable groups. The difference in the loss tangent between films with and without epoxy can also be attributed to the epoxy lowering the total polarizability of the film.

3.3 Conclusions

The mechanical and electrical properties of a positive tone epoxy-based polymer dielectric were examined. The reduced modulus shows a dependence on the chemical crosslinking structure. Positive tone films with DNQ-based photochemistry are affected by the pH of the film due to aqueous base inhibiting DNQ crosslinking. Evidence for DNQ contributing to the crosslinking of a permanent dielectric film was shown for the first time. The addition of an epoxy crosslinker to the positive tone film inhibited base uptake, thereby allowing DNQ crosslinking to occur. This study provided a fundamental understanding of the effects of additives on the mechanical and electrical properties of the PNB film. Optimizing processing conditions and chemical additives can produce a dielectric material with tunable mechanical and electrical properties.

CHAPTER 4. HIGH MOLECULAR WEIGHT, LONG SHELF-LIFE POLYPHTHALALDEHYDE

Two issues have plagued the polymerization of phthalaldehyde, namely the reproducibility of the polymerization in achieving high molecular weight and the long term shelf-life of the polymer.[32,75] High molecular weight is desired for creating thick polymer films because chain entanglement provides mechanical strength.

One promising pathway for achieving high molecular weight is through the cationic synthesis route utilizing boron trifluoride etherate (BF_3-OEt_2) catalyst.[33,53,62,63,76] Kaitz, et al. found that the BF_3-OEt_2 catalyst forms a cyclic polymer with high thermal stability.[63] Previous studies with BF_3-OEt_2 catalyst support the concept that a cationic chain end is produced from a Lewis acid.[63,77] This cationic end is free to propagate the polymer chain. No evidence of the counter-ion produced to stabilize this propagating chain was provided.[63,72,77] Reported values of yield, molecular weight, and polydispersity index for PPHA suggest that cationic addition chain propagation is unlikely.

4.1 Motivation

This study sought to identify the role of BF_3-OEt_2 in the polymerization of phthalaldehyde, specifically in the interaction of BF_3 with the monomer. A possible mechanism is proposed to help explain the phenomenon observed in the experiments presented here as well as those previously reported. Strong evidence for a unique role of BF_3 in the polymerization of phthalaldehyde is presented.

Stability has also been called into question when working with polyaldehydes.[32] The general experience is that there is sudden depolymerization of the polymer even after weeks of what appears to be a stable material. In attempting to unravel the role of BF_3 in the polymerization of phthalaldehyde, a method for improving the polymer stability after polymerization was discovered. A procedure for increasing the shelf-life of PPHA is also reported.

4.2 Results and Discussion

4.2.1 Effect of Lewis Acidity on Phthalaldehyde Polymerization

To test the effect of Lewis acidity on poly(phthalaldehyde) chain growth, various Lewis acids were used as the catalyst in the polymerization.[78] Lewis acids were chosen to span a wide range of acidities. The same catalyst loading, 0.03 mmol, was used for all polymerizations. The acids, presented in increasing acidity, were $ZnCl_2$, $AlEt_3$, BF_3-OEt_2, TiF_4, $TiCl_4$, BCl_3, and BBr_3.[79–81] Table III shows polymer yields and relative acidities for the Lewis acids used.[79] Only two Lewis acids produced polymer under these conditions: BF_3-OEt_2 and $TiCl_4$.

Table III. List of Lewis acid catalysts for PPHA polymerization. Catalysts are listed in ascending order of acidity.

Lewis acid	Polymer Yield	Acidity[1]

$ZnCl_2$	-	1.70
$AlEt_3$	-	N/A[2]
BF_3-OEt_2	80.2%	2.76
TiF_4	-	2.78
$TiCl_4$	30.0%	2.93
BCl_3	-	4.08
BBr_3	-	4.33

1. Relative acidities from Hilt, et al.[79]
2. Relative acidity value of $AlEt_3$ not reported.

Interestingly, the only borohalide to produce polymer was BF_3-OEt_2. Other borohalides were used in an attempt to determine the effect of a decrease in hydrogen bonding to halide, in the order of F > Cl > Br.[82] In any condition where BF_3 was not used, no yield was obtained despite a color change being observed upon addition of the borohalide. BF_3 clearly has a unique interaction with the phthalaldehyde monomer. One explanation is that the conformational configuration of BF_3 supports a cationic propagating chain. The formyl proton interacts with a BF_3 fluorine forming a complex at closer than the summation of their van der Waals radii as shown in Figure 4.1 (A).[82] This BF_3-H complex shifts the cationic site from the boron-oxygen to the formyl carbon, Figure 4.1 (B). This allows cationic propagation through a cation-aldehyde interaction, Figure 4.1 (C).

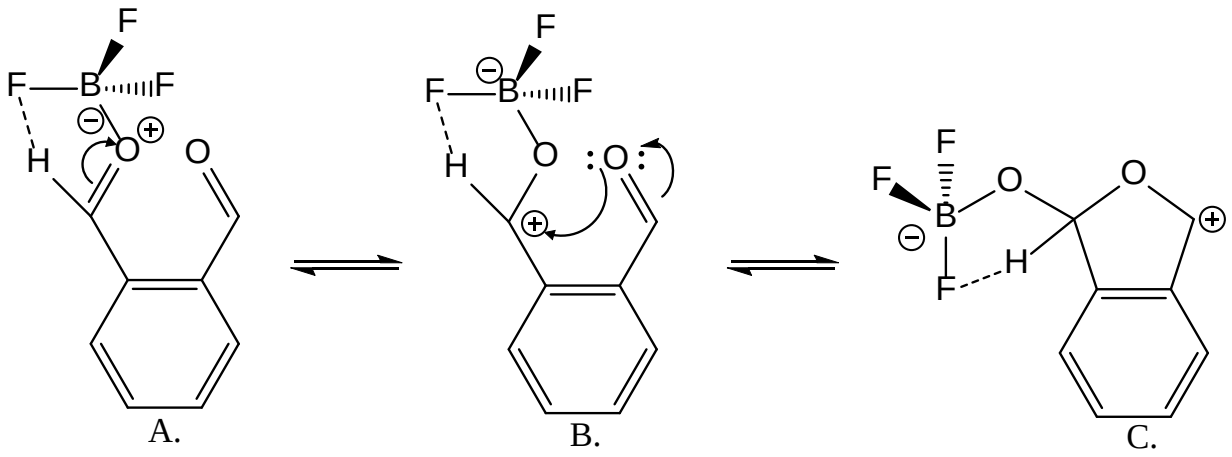

Figure 4.1. Proposed initiation mechanism of BF_3 and phthalaldehyde with the initial complexation (A), rearrangement of the cation to the formyl carbon (B), and the cyclized monomer cation (C).

Some papers suggest a co-initiator is necessary for borohalides, although these papers focus on the polymerization of olefins.[83,84] Diethyl ether was added to a solution of DCM and either BCl_3 or BBr_3 before adding to the monomer solution. The goal was to promote the complexation of the borohalide with ether, similar to that of BF_3-OEt_2. However, when adding ether to facilitate co-initiation of phthalaldehyde, the yield remained zero. The ether does not appear to be playing a role in the polymerization of phthalaldehyde, other than maintaining the solution concentration of the BF_3.

Metal halide and alkyl metal Lewis acids were used to test the catalysis of phthalaldehyde at different acid strengths. It is noted that $ZnCl_2$ was not soluble in the reaction solution, meaning that if any reaction were to take place, it would need to occur at the unfavorable solid-liquid interface. $AlEt_3$ is probably too weak of an acid to polymerize phthalaldehyde at such low loadings. Yield for the $TiCl_4$ polymerization was low (30 %) and the polymer was stable for less than 20 days at 0°C. TiF_4 did not yield

polymer even though its acidity is close to BF_3.[79] A possible explanation is that there is a difference in binding energy between the catalyst and the aldehyde. Lewis acidity does not appear to be the sole predictor for PPHA yield. BF_3 provides the best reaction conditions for stable, high molecular weight poly(phthalaldehyde).

4.2.2 In-situ NMR of Phthalaldehyde Polymerization with BF_3-OEt_2

To elucidate the structure of the intermediates during polymerization, in-situ ^1H NMR of the phthalaldehyde and BF_3-OEt_2 reaction was used. An NMR sample in 0.75 mL of CD_2Cl_2 was prepared with 5.6 mmol phthalaldehyde and 1.1 mmol BF_3-OEt_2. An NMR spectrum was obtained at each of five different temperatures, -80°C, -65°C, -50°C, -45°C, and -42°C. At each temperature, the spectrum was obtained after monomer-polymer equilibrium was obtained, defined as the time when no change in the peak integrals was observed, approximately 15 min at temperature. Figure 4.2 shows the ^1H NMR spectra for the five temperatures.

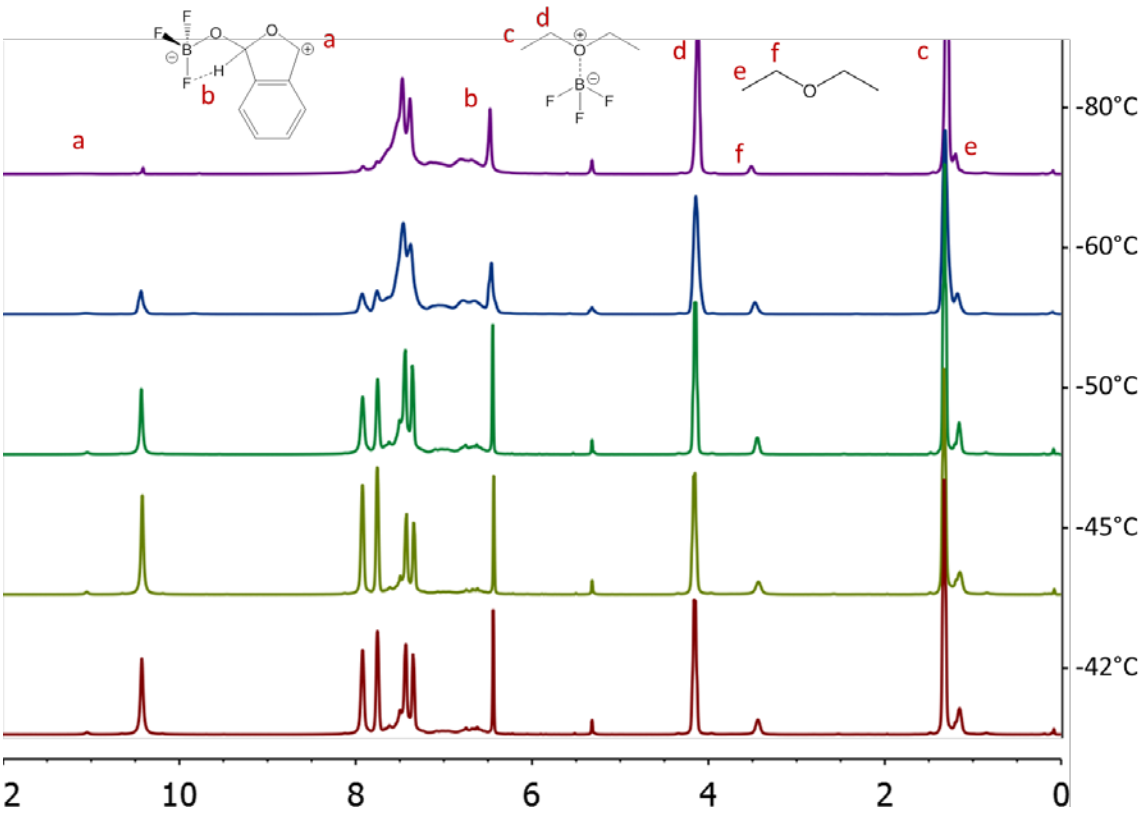

Figure 4.2. In-situ ^{1}H NMR spectra of phthalaldehyde polymerization in CD_2Cl_2 with BF_3-OEt_2 as the initiator.

Peaks that can be assigned to the catalyst, BF_3-OEt_2, are shown at 4.2 (d) and 1.35 (c) ppm for the -CH_2- and -CH_3 of the etherate, respectively. Ether (-CH_2-, f, 3.42 ppm and -CH_3, e, 1.13 ppm) that has become free from the influence of BF_3 is also shown. The inset focuses on a peak (a, 11.05 ppm) that is shifted further downfield than the monomer peak (aldehyde, 10.45 ppm). This peak is believed to be associated with the free propagating cation, as shown by the chemical structure. A large peak at 6.5 ppm is associated with a polyether proton closely influenced by BF_3. The large number of protons that are shifted to 6.5 ppm could show the influence of multiple BF_3 molecules complexing with the polyether backbone, as shown in Figure 4.3 (A). The ether protons

on either side of the oxygen bound to the boron could be influenced by the cationic oxygen.

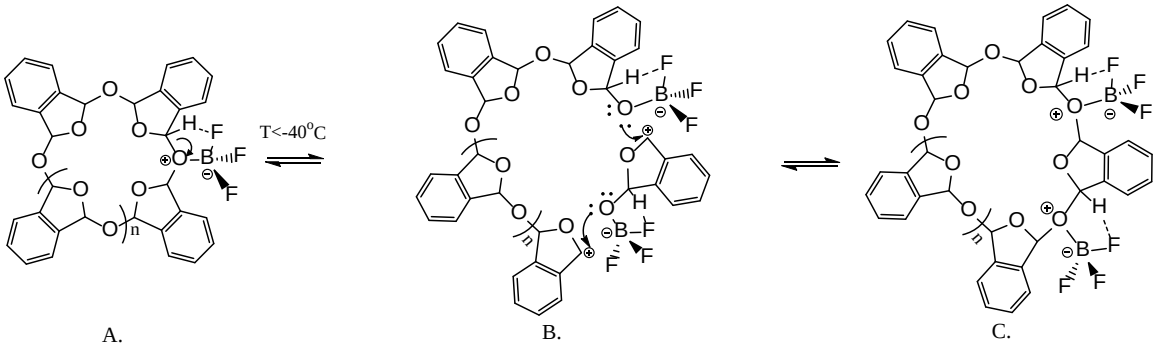

Figure 4.3. BF_3 complexes with existing polymer backbone (A). Rearrangement and opening of polymer chain (B) allows another monomer to insert itself. Both BF_3 complexes allow closing of polymer chain (C).

As the temperature decreased, the peak at 11.05 ppm decreased, showing a reduced number of cations and propagating chains. The consumption of complexed monomer during polymerization would cause a reduction of the 11.05 ppm peak. The peak at 6.5 ppm also decreased slightly, possibly from the smaller number of BF_3 complexed to the polymer. Once quenched, cleaned, and dried, the peaks at 11.05 and 6.5 ppm do not appear in a ^1H NMR spectrum of PPHA. The ^1H NMR provides confirmation of the structure that BF_3 and the aldehyde create when mixed at the reaction conditions necessary to create polymer (i.e. below the ceiling temperature).

There is also additional information concerning the interaction of BF_3 with monomer and polymer in the peak shifts of the free ether, OEt_2. At room temperature, the BF_3-OEt_2 structure is a pair of broad peaks at 4.2 and 1.35 ppm. At low temperature, the equilibration between different complexed structures is slowed so that separate NMR peaks are observed with and without BF_3 interaction.[85] The ether that is not actively

complexed with BF_3 will have peak positions more closely aligned to that of diethyl ether (-CH_2-, 3.43 ppm and -CH_3, 1.15 ppm). Complexation with ether is likely more favored than complexation with the polyether backbone.[86] As the BF_3 becomes less involved in the polymerization, it will preferentially return to complexation with OEt_2, slightly shifting the ether peaks downfield.[87] This is best seen at the peaks around 3.43 ppm in Figure 4.2. A decrease in temperature causes the -CH_2- peaks of the ether to shift downfield from 3.43 ppm (green) to 3.55 ppm (purple) as a consequence of BF_3 complexation.

^{19}F NMR was used to verify the interaction between BF_3 and the polymer backbone. This is best observed by the peak shifting between BF_3-OEt_2 and the complex formed at cold temperatures between BF_3 and phthalaldehyde. Two NMR samples were prepared in CD_2Cl_2, one with BF3-OEt2 and an internal standard of hexafluorobenzene, and another with the same concentration of monomer and catalyst as the ^1H NMR study and an internal standard of hexafluorobenzene. Figure 4.4 shows the ^{19}F NMR spectra at room temperature for BF_3-OEt_2 alone (top) and at -80°C for the monomer and BF_3-OEt_2 solution (bottom). The representative peak for BF_3-OEt_2 is -154.5 ppm. Adding phthalaldehyde and allowing the mixture to cool to -80°C, causes the peak to shift upfield to -156.5 ppm. The only explanation for the shift is a change in the BF_3 complexation equilibrium caused by polymerization. A small side peak also appears at -156.47 ppm that could correspond to BF_3 complexed with phthalaldehyde.

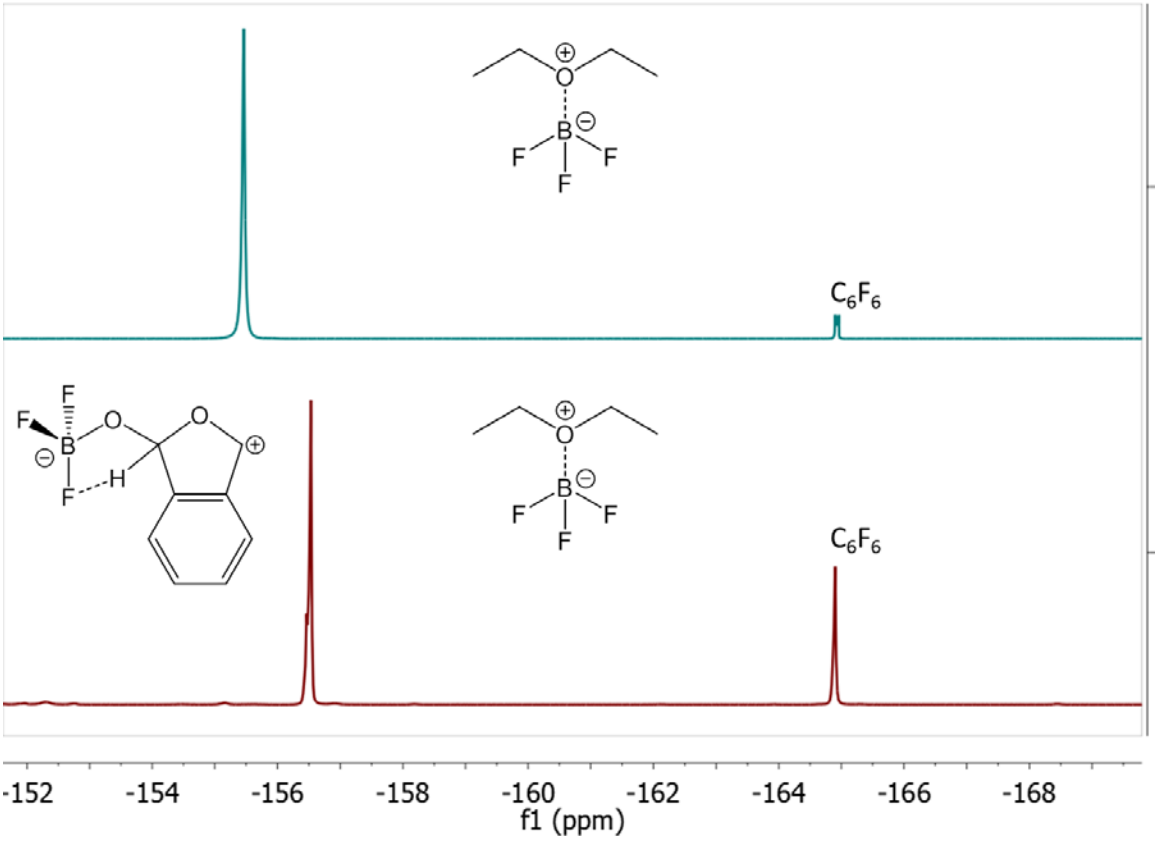

Figure 4.4. ^{19}F NMR spectra of BF_3-OEt_2 at room temperature (top) and phthalaldehyde and BF_3-OEt_2 mixture at -80°C (bottom).

The catalyst appears to play a more complex role in the polymerization than simply opening and closing insertion sites with the presence of a counter ion like previous reports suggest.[63] A polymerization with phthalaldehyde and BF_3-OEt_2 probably has two thermodynamic driving forces: creation of a stable polymer chain as determined by the ceiling temperature phenomenon and the complexation of BF_3 with the aldehyde monomer units or polyether backbone.[86] Figure 4.3 is a proposed mechanism for the insertion of additional monomer into a pre-existing polymer chain. The polymer chain complexes with a BF_3 molecule, as shown in Figure 4.3 (A). This complexation can promote the rearrangement of BF_3-OEt_2 to form a boron anion and carbocation, as previously shown in Figure 4.1 (C). An additional BF_3-monomer complex can insert

between the anion and cation of the polymer as shown in Figure 4.3 (B), conserving charge and allowing for close proximity of the BF_3 complexes with neighboring carbocations. The BF_3 complex and carbocation can rearrange back to a closed polymer chain, Figure 4.3 (C). Rapid exchange of the BF_3 molecules between free monomer, diethyl ether, and polyether backbone allow further insertion of monomer or oligomer units into the growing polymer chain.

A traditional cationic addition mechanism could provide chain growth until backbiting occurs to allow the BF_3 complex to close the cyclic polymer chain. An alternate explanation for the BF_3 catalyzed polymerization of phthalaldehyde could be that multiple BF_3-monomer complexes come together to form an ionically aligned group that allows the BF_3 rearrangement shown in Figure 4.3 (C) to close the cyclic polymer chain.

4.2.3 Polymerization Yield Comparisons for Poly(phthalaldehyde)

To further probe the role of BF_3 in the polymerization of phthalaldehyde, reactions were quenched at various times. Figure 4.5 shows the yield fraction, molecular weight, and polydispersity index ($Đ$) of these reactions. There is little change in molecular weight and yield fraction for the polymerization of phthalaldehyde catalyzed by BF_3-OEt_2. The shortest reaction time of 15 minutes seems to be sufficient to reach equilibrium. The $Đ$ may decrease slightly with reaction time supporting the NMR observations.

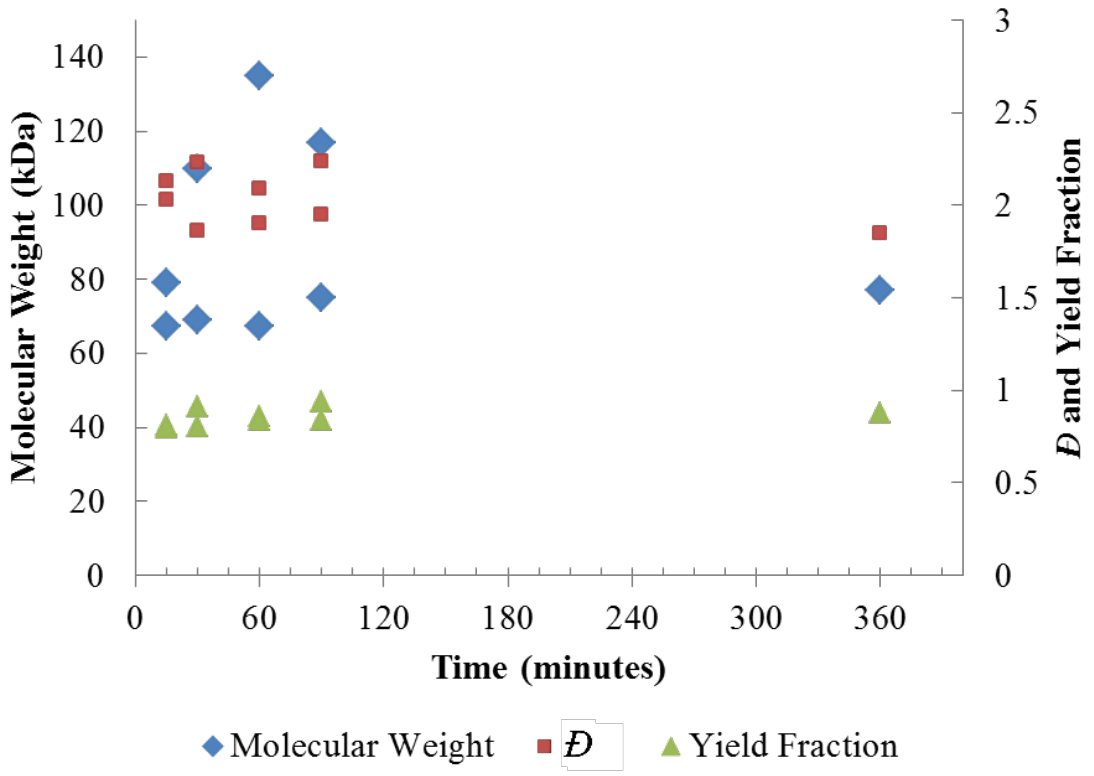

Figure 4.5. Molecular weight in kDa (diamonds, left axis), *Đ* (squares, right axis), and Yield Fraction (triangles, right axis) versus reaction time in minutes of polyphthalaldehyde.

A fast cationic growth mechanism with rapid initiation and exchange of the active propagation site can explain the high *Đ* values, as seen for BF_3-OEt_2 catalyzed phthalaldehyde polymerization.[88,89] Yield fraction, molecular weight, and *Đ* would be expected to be unchanged with time if the Scheme II mechanism was true.[63,72,77] The polymer chains quickly mature and reach an asymptotic equilibrium due to the ability of monomer units to be easily removed and inserted. Some of the differences in the experiments are the amount of catalyst used for the polymerization. In previous studies, much larger quantities of BF_3-OEt_2 were used.[62] With a larger amount of BF_3, the catalyst could simultaneously interact with multiple locations on the polymer chain,

allowing the removal and insertion of oligomers of phthalaldehyde, as proposed in Figure 4.3.

Multiple polymerizations were performed to determine the effect of catalyst loading on molecular weight. A theoretical molecular weight can be inferred by assuming that each catalyst initiates one chain. Each chain then propagates equally until the monomer is fully consumed. This results in a $Đ$ of 1.0. Figure 4.6 shows the molecular weight in kDa versus monomer-to-catalyst ratio for the experimental data (individual points) as well as the theoretical molecular weight from a $Đ$ of 1.0 (line).

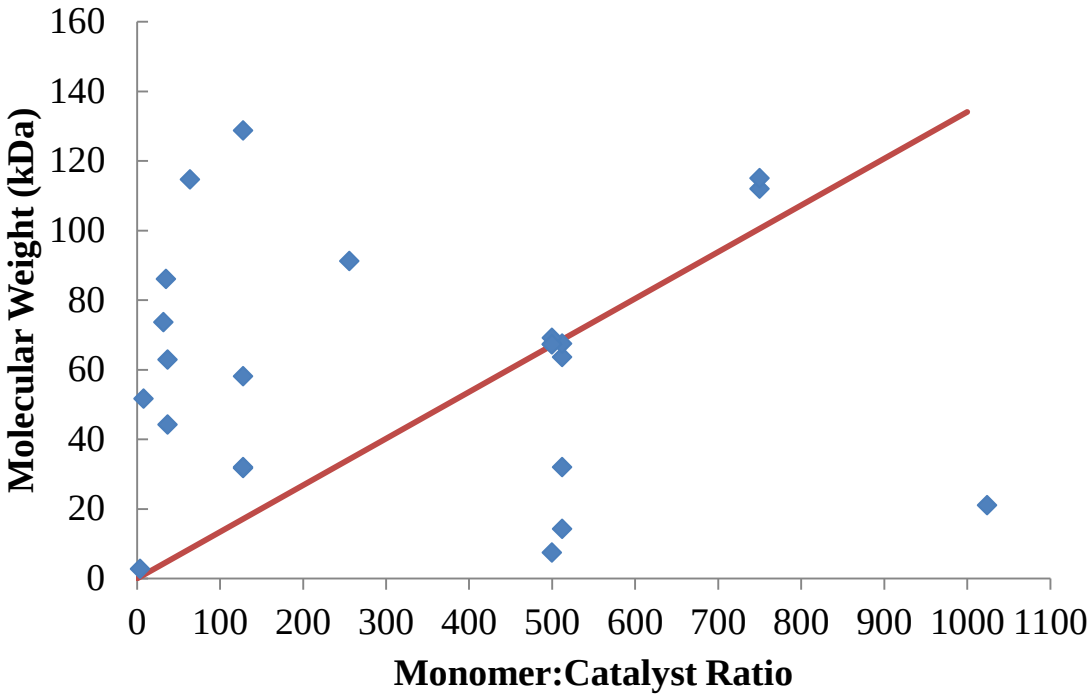

Figure 4.6. Molecular weight in kDa versus monomer:catalyst (phthalaldehyde:BF_3-OEt_2) ratio. A lower monomer-to-catalyst ratio means larger amounts of catalyst.

The polymerizations from Figure 4.6 were re-plotted to show the effective utilization of the monomer. Figure 4.7 shows the polymerization yield versus molecular

weight in kDa. A trend line is shown for ease of viewing. The top right is shaded to show desired polymerization results. The molecular weight increases with monomer utilization. This is expected if the polymerization proceeds with traditional propagation and termination. This also shows a lower and upper limit of the molecular weight of PPHA formed with BF_3-OEt_2 catalyst. Low monomer utilization leads to low molecular weight and the upper limit of molecular weight appears capped. A minimum molecular weight is not unreasonable due to the steric strain that could occur in the cyclic polymer. The oligomer must be of a certain size before it can backbite to form the cyclic polymer. The reproducibility of the polymerization with BF_3-OEt_2 catalyst can be seen from the data in Figure 4.6 and Figure 4.7. Each data point is a separate reaction. In many cases, there was no intentional change in procedure, although, it is recognized there are minor changes in experimental conditions that occur over a period of months. At low monomer-to-catalyst ratio (i.e. more catalyst) a higher than expected molecular weight is observed. Most of the previously published reports use a low monomer-to-catalyst ratio with BF_3-OEt_2 catalyst.[63,77] As the catalyst loading decreased (increasing monomer-to-catalyst ratio), there is considerable scatter in the results. The exact cause of the reaction-to-reaction scatter is still under investigation. This data does show the sensitivity of the reaction to what may be subtle changes in reaction conditions. One such condition, glove box humidity, is known to limit yield by forming a hydrate with the phthalaldehyde monomer.

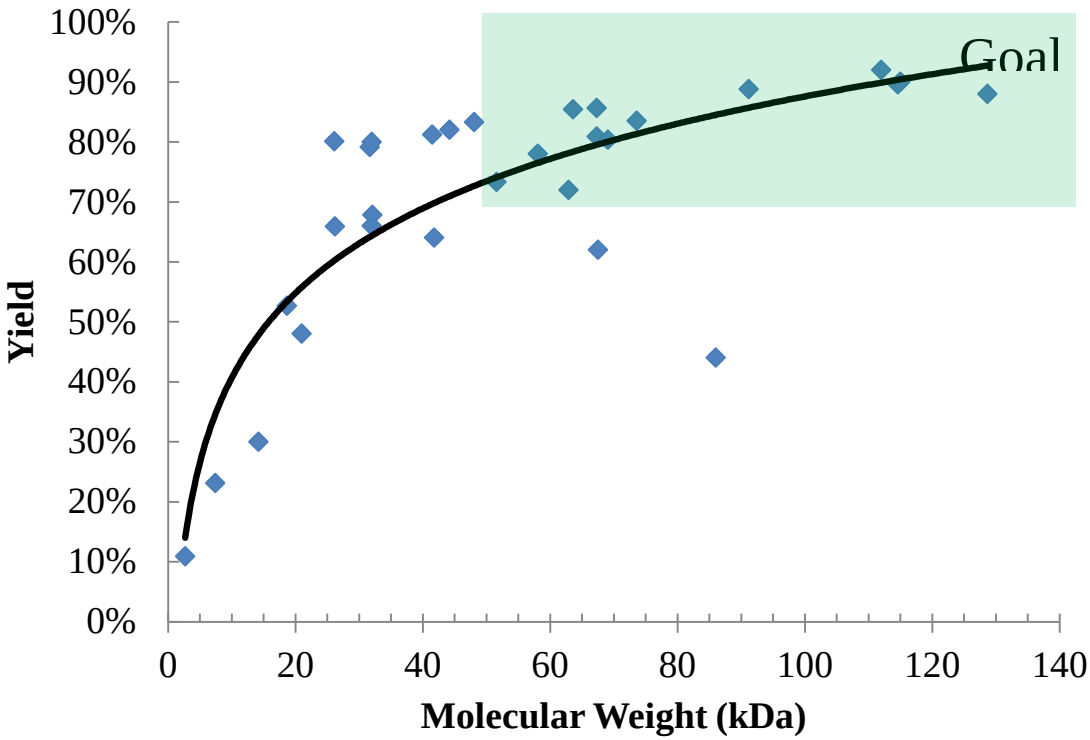

Figure 4.7. Yield of phthalaldehyde polymerizations with BF_3-OEt_2 versus molecular weight as determined by GPC in kDa.

4.2.4 Improvement of Poly(phthalaldehyde) Shelf-life

The ambient stability of PPHA has been a major concern for its use and commercialization. Unpredictable depolymerization of PPHA has been common. Some polymers have depolymerized in six months, and some have depolymerized within days. Reports of anionic PPHA decomposition suggest a slow loss of material that can be described as 1% depolymerization per day.[32] This could be due to the stability of the end-caps, the likely weakest bonds of the anionic material. The stability of PPHA was studied here by accelerated aging of the BF_3-initiated polymers purified by methods reported in literature.[63]

Isothermal gravimetric analysis at 70°C, 80°C, 90°C, 95°C, and 100°C was used to determine the Arrhenius parameters for the depolymerization reaction. The natural log of the mass was plotted versus the time at elevated temperature and linear regression was used to determine the rate of depolymerization at each temperature. The natural log of the rate obtained from the Arrhenius expression at each temperature was plotted versus the reciprocal of temperature, the relationship for first order kinetics, in Figure 4.8. A linear regression was used to determine the Arrhenius parameters from these data points. The activation energy was found to be 50 kcal/mol, and the pre-exponential was 2.6×10^{26}.

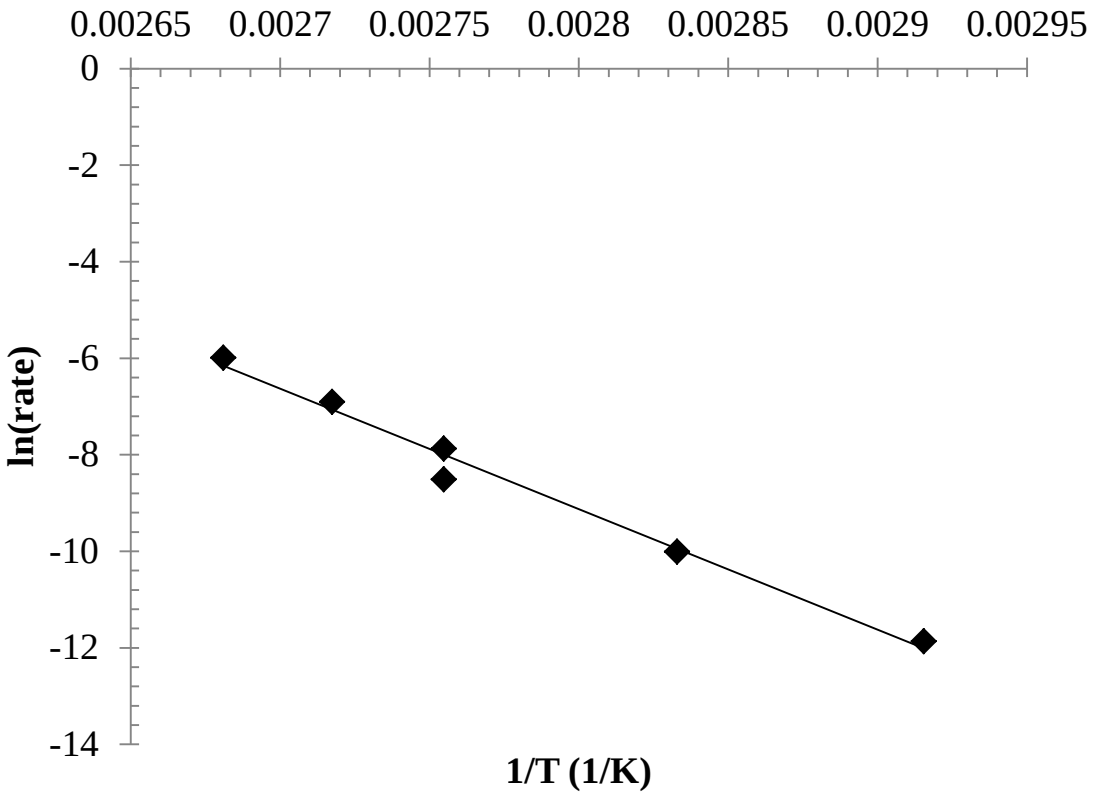

Figure 4.8. Arrhenius plot for the degradation rate at various isothermals for PPHA.

The activation energy is close to the reported values for the bond strength of an ether C-O bond, which is the expected weakest bond in the PPHA polymer chain.[90] Using these parameters, lifetime estimations were made for PPHA at various temperatures. At 40°C, the polymer would be expected to last 21 days before 1% loss of material occurs. At ambient storage conditions in a laboratory (20°C), the polymer is expected to last 13 years before 1% loss of material. These values for the cationic polymerization are contrary to past experiences and previous reports for the anionic polymerization where ambient temperature shelf-life was much shorter.[32] These results show that BF_3-OEt_2 catalyzed PPHA is inherently stable and suggests that an external stimulus is the likely cause of the stochastically observed depolymerization.

Samples of the BF_3-OEt_2 catalyzed polymer were sealed in vials to observe the decomposition over time. A transition from a white solid polymer to a transparent solid preceded depolymerization. ^{1}H NMR was performed on a polymer that was undergoing depolymerization to try and identify the cause of the depolymerization. The NMR spectrum showed a surprisingly large peak at 6.4 ppm, which corresponds to the BF_3-polymer complex. The BF_3 catalyst was thought to be removed by drying each sample until the mass no longer changed. This appeared to be confirmed by ^{1}H NMR of the polymer post-drying showing no such peak at 6.4 ppm. However, it appears that a small quantity of catalyst remained in the polymer. Only after depolymerization began did the peak at 6.4 ppm become apparent. Due to the catalytic nature of the depolymerization of PPHA, described above, a small amount of catalyst remaining in the polymer would be detrimental to its stability. As a consequence of the complex formed between BF_3 and

the polymer backbone, the removal of BF_3 appears to be difficult and could have led to the stochastic instability previously observed.

To address the issue of residual BF_3 catalyst, a new purification procedure was developed. Previously, the polymer was purified according to previous reports by redissolving the PPHA in DCM followed by precipitation in hexane.[62,63] The new purification procedure involved solvents with higher binding energies to BF_3 than the PPHA ether or OEt_2 to help remove residual BF_3. THF, which has a higher binding energy to BF_3 than diethyl ether and DCM, was used to redissolve the polymer. TEA, which has a higher binding energy to BF_3 than pyridine, was added to the polymer solution.[86] Finally the polymer was precipitated and dried as described above. The new purification procedure has provided stable polymer at ambient conditions for months without signs of decomposition. Small samples of PPHA were stored at ambient temperature in sealed vials containing atmospheres saturated with acetic acid (glacial), hydrochloric acid (30-38% in water), n-methyl pyrrolidone, pyridine, TEA, THF, water, trifluoroacetic acid, and isopropyl alcohol. Only the vial containing a strong acid, trifluoroacetic acid, resulted in PPHA decomposition, as expected. After 350 days, the date of this manuscript, all other samples remain stable. Low temperature storage should further improve stability during storage.

4.2.5 Scale-up of High Molecular Weight Phthalaldehyde

High molecular weight syntheses are readily achievable and the most significant next step for the polymerization of phthalaldehyde is the scale-up to large quantities of the stable polymer. Some efforts were made here to increase the batch size and obtain

high molecular weight PPHA in appreciable quantities. Table IV shows the molecular weights and yields obtained for a few different batch sizes attempted.

Table IV. Molecular weight and yield for cationic synthesis of phthalaldehyde with different batch size.

Starting Monomer Amount (g)	Monomer: Catalyst Ratio	Yield	MW (kDa)
1	128	88.0%	128.7
9	128	79.1%	31.7
1	500	62.0%	67.5
4	500	89.0%	91.9
8.9	500	40.6%	98.9

All of these batches were performed in 100 mL round bottom flasks. As can be seen, either molecular weights or yields were negatively affected by substantial differences in the size of the reaction vessel. The head space could be made similar in future batches of polymer.

4.3 Conclusions

The role of BF_3-OEt_2 in the polymerization of high molecular weight poly(phthalaldehyde) was investigated. The Lewis acidity and presence of fluorides for hydrogen bonding appear to make it uniquely suited for PPHA synthesis. A complex interaction of BF_3 with the monomer and polymer chains was observed by in-situ NMR. The polymerization time was less than 15 minutes to reach equilibrium. High molecular weight can be consistently achieved in the polymerization of PPHA by selecting the correct monomer-to-catalyst ratio, which promotes high yield. PPHA in the process of depolymerization showed residual catalyst remained despite traditional purification. An improved method of removing residual catalyst was effective at stabilizing the polymer

and improving shelf-life. Accelerated aging of PPHA suggests the polymer is stable for long time periods.

4.4 Recommendations

The commercial application of polyaldehydes is limited due to the sizes of polymerization currently in use. As the size of a polymerization of phthalaldehyde increases, yield and molecular weight suffer slightly. Over the course of this thesis, syntheses up to 10 g were attempted with limited success. Eventually, kilograms of polymer will be necessary for quite a few uses, especially if the fabrication of any number of printed wiring boards becomes necessary.

CHAPTER 5. COPOLYMERS OF ALDEHYDES

This study attempts to take the high vapor pressure of small molecule aldehydes and incorporate them into a stable copolymer with phthalaldehyde. The polymerization of aldehydes without phthalaldehyde was not successful in providing more than trivial quantities of stable solid. There is some evidence in Japanese patents of stable aliphatic polyaldehydes. Some combination of acetaldehyde, propionaldehyde, and butyraldehyde provided stable material in sufficient quantities to warrant a patent. This, however, was never reproduced successfully.[91]

5.1 Motivation

The emergence of transient electronics has generated multiple means of accomplishing the triggered disappearance.[43,45] Several reports have focused on the use of an external solvent, like water, to initiate the transience over timescales of minutes to hours.[44,64,92] More reliable and sensitive triggers are desirable. In this study, photo-initiated depolymerization was investigated as a means of triggering the transient event. Fast evaporation of the depolymerized monomers is an important second step after photo-triggering. Self-immolative polymers have been shown to offer the fast depolymerization required for transient applications.[37,40,93] Depolymerization rapidly converts the polymer backbone into monomer units leaving evaporation as the rate limiting step in material vaporization.

Polyaldehydes have shown promise as a self-immolative polymer, especially in situations where the polymer cannot be heated to high temperature.[29,94,95] Polyaldehydes

can have a low ceiling temperature (T_c), such as poly(phthalaldehyde) with T_c = -40°C. Above T_c the polymer can rapidly depolymerize back to monomer.[33,56,57,70] However, selecting aldehyde monomers with high vapor pressure at the desired transience temperature, which can also be kinetically trapped as polymers until triggered (above T_c) with suitable mechanical properties, is challenging.

Aliphatic aldehydes have a tendency to form highly crystalline polymers that become insoluble in common organic solvents.[58,91] This insolubility can cause growing chains to precipitate out of solution during polymerization before being kinetically stabilized. Further, solvent insolubility prevents solvent casting the polymer into its functional shapes. Monomers that form an amorphous polymer, which remain solvent soluble, tend to have low vapor pressure.[58,91] Low vapor pressure limits the applications of the transient polymer to situations that allow long times for transience. One approach to avoiding polymer crystallization and long monomer evaporation time is to use copolymers with one monomer that forms amorphous polymers and another that has high vapor pressure. The crystallinity of the polymer can be disrupted by a larger monomer increasing solubility and maintaining moderate vapor pressure at the transient temperature.

High molecular weight polyaldehydes have not been achieved through anionic polymerization of aliphatic aldehydes.[59] The acidic α-protons of the aldehyde inhibits chain propagation and acts as a chain transfer agent, creating a new initiation site for polymer propagation.[59] This interruption of a growing chain causes the molecular weights to be relatively low and creates high dispersity. On the other hand, a cationic growth mechanism is capable of achieving high molecular weight polyaldehydes.

In this study, the synthetic route to forming high molecular weight copolymers from phthalaldehyde (PHA) and butyraldehyde (BA) has been investigated. Utilizing both monomers avoids the crystallization problems and improves the monomer evaporation rate. A procedure for evaluating the depolymerization and evaporation rate of low ceiling temperature polymers catalyzed by a photo acid generator (PAG) is also described.

5.2 Results and Discussion

5.2.1 Butyraldehyde

The polymerization of a high molecular weight PHA-BA copolymer is desired for achieving adequate mechanical properties and rapid vaporization after transience. However, the formation of a BA trimer complicates the formation of a high molecular weight PHA-BA copolymer.[59,96] It is hoped that the copolymerization of PHA and BA, Figure 5.1, inhibits BA trimer formation. The previously reported cyclic nature of the PHA homopolymer is expected to also occur with the PHA-BA copolymer.[63]

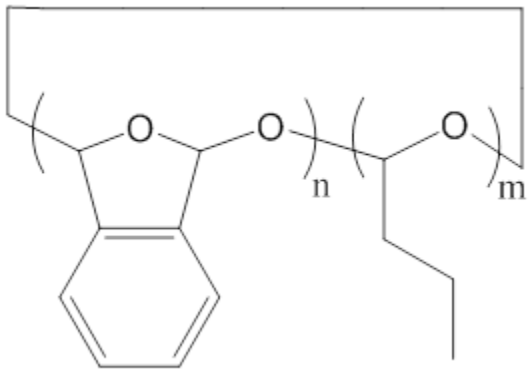

Figure 5.1. Structure of PHA-BA copolymer.

PHA-BA copolymerization was performed with different catalyst loadings, reaction times, and reaction temperatures. Table V shows the yield, polydispersity, number average molecular weight, butyraldehyde ratio in the polymer and aldehyde-to-catalyst ratio (catalyst ratio). The PHA-to-BA molar ratio for all the experiments was 2:1. The BA uptake in the PHA-BA copolymer was determined by ^{1}H NMR by integration of the broad peak from 5.2 to 5.6 ppm that represents the BA polymer ether (later described in more detail in the in-situ NMR chapter). The PHA ether backbone has peaks from 6.4 to 7.2 ppm. The ratio between the PHA ether backbone and the BA ether backbone peaks was used to calculate the BA mole percentage in the polymer.

Table V. Reaction results for the copolymerization of phthalaldehyde and butyraldehyde. Catalyst ratio is the moles of aldehyde monomer per mole of catalyst.

Number	T (°C)	Time (min)	Catalyst Ratio	M_n(kDa)	*Đ*	Yield	BA mol%
1	-78	120	750	21.8	2.23	47%	8%
2	-78	120	187.5	17.4	3.02	60%	7%
3	-78	120	46.5	41.5	1.79	65%	6%
4	-78	120	24	48.1	1.82	66%	6%
5	-78	120	6	32.1	1.66	54%	5%
6	-78	30	750	103.5	2.27	60%	12%
7	-87	480	750	26.9	1.67	36%	10%
8	-87	1440	750	34.9	1.65	15%	7%
10	-87	2880	750	29.5	1.73	33%	8%
9	-87	4320	750	23.4	1.66	50%	9%
11*	-78	30	750	66.3	1.95	58%	12%
12	-78	30	1125	20.7	1.70	37%	18%
13	-78	30	1536	22.9	1.70	29%	19%
14	-78	120	3	26.2	1.56	53%	3%
15	-78	120	2	18.7	1.47	42%	1%

The reaction time and temperature did not have a significant effect on the polymer properties. The temperatures were well below the ceiling temperature of PHA polymer, which was shown to produce polymer with high yield. Long polymer reaction times were not expected to affect the polymerization reaction because it was found that polymer equilibrium could be achieved within 30 min.[19,24] Experiment numbers 6 to 9 in Table V show that extending the reaction time from 30 to 4320 min did not have a significant effect on the synthesis. It was previously shown that equilibrium was achieved within 30 min for PHA homopolymer.[97] The ability of BF_3 to randomly open and close aldehyde bonds during polymerization has been shown previously.[62] However, Table V shows that only a limited amount of BA incorporation into the polymer was achieved. The molecular weight tended to be higher with less catalyst (i.e. higher monomer to catalyst ratio, Catalyst Ratio in Table V), however, there is considerable scatter in the data. This lack of a clear trend of molecular weight with monomer-to-catalyst ratio can be understood by considering the role of BF_3 in the polymerization. BF_3 not only initiates the polymerization, it also opens polymer ether bonds and inserts additional monomer units into the growing polymer.

It is desirable to increase the BA ratio in the PHA-BA copolymer so as to improve the vaporization rate of after depolymerization. Lower catalyst loadings (i.e. higher monomer-to-catalyst ratio) favor higher incorporation of BA in the copolymer. Figure 5.2 shows the BA mol% versus BF_3 concentration on a log scale. More catalyst appears to negatively affect the ability of BA to copolymerize. One possible explanation is the availability of large amounts of catalyst facilitates formation of the BA trimer. Once the BA trimer forms, it is likely less active in the copolymerization with PHA because BF_3

does not depolymerize the BA trimer like it does the growing PHA polymer. Another possible explanation is that the catalyst has a much stronger preference for the PHA. Recall that BF_3 actively opens the growing polymer chain and inserts additional PHA monomer units, which may be favored over BA. This has the net effect of forcing BA out of the growing polymer chain.

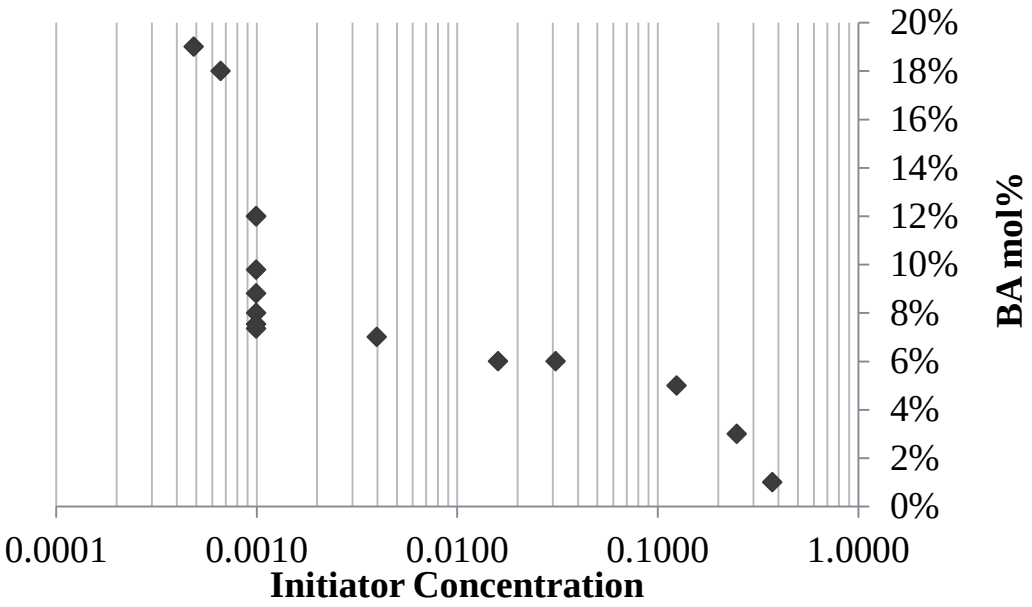

Figure 5.2. Butyraldehyde mol% versus initiator concentration for the copolymerization of phthalaldehyde and butyraldehyde

Higher incorporation of BA into the copolymer is desired. Additional reactions were performed to explore ways to increase the BA concentration in the polymer. Avoiding the formation of BA trimer may be one approach to the increasing the BA mole ratio in the copolymer. One method to avoid BA trimer is to rapidly cool the reaction below the T_c of PHA, or to cool the reaction before addition of catalyst. A reaction solution was prepared as described above without catalyst. The reaction solution was brought to the reaction temperature of -78°C, and the catalyst added (750:1 ratio). The

reaction was allowed to proceed for 30 min followed by quenching with pyridine. This reaction produced polymer with 12 mol% BA, which is toward the high end of the variation observed with the standard polymerization method.

A reaction mixture without catalyst was frozen with liquid nitrogen before addition of catalyst. The reaction was allowed to warm to -78°C until the monomer redissolved followed by addition of pyridine. There was a total of 9 min between the addition of catalyst and quenching with pyridine. The polymer formed by this method contained 16 mol% BA, which is at the high end of the BA mole ratio within the experiments performed in Table V.

One challenge is to use the BA trimer which forms prior to PHA polymerization in the copolymer to produce a BA-rich copolymer. Additional experiments were performed by changing the polymerization temperature to allow equilibrium of the BA trimer to occur, Table VI.[96] One reaction was held at -24°C for 19 hours and quenched in an attempt to form BA-rich polymer. Another was held at -24°C for 20 hours, followed by slowly lowering the temperature to -85°C at a rate of 0.5°C/min to facilitate PHA incorporation. The mixture was quenched after 10 min. A third mixture was held at -40°C, just below the PHA ceiling temperature, for 1 h to encourage BA incorporation over PHA. A fourth mixture was held at -40°C for 30 min in an attempt to incorporate a lower amount of PHA because PHA polymerization is incomplete at this temperature. This was followed by slowly lowering the temperature to -85°C at a rate of 0.5°C/min to facilitate additional incorporation of PHA, and quenching after 10 min. As shown in **Error! Reference source not found.**, there was no improvement in the incorporation of BA. There was little or no BA in the polymer and the yield for each was near zero.

Reacting the mixtures for prolonged time near the PHA ceiling temperature is detrimental to polymer formation. This is somewhat surprising because each of the monomers by themselves are reversible with BF_3-OEt_2 as the catalyst.[98] It is possible that very low molecular weight polymer was formed but could not be precipitated under the conditions used.

Table VI. Reaction results for warmer copolymerization of phthalaldehyde and butyraldehyde.

Number	Temp (°C)	Time (min)	Catalyst Ratio	Yield	BA mol%
1	-25	1140	500	0%	n/a
2	-25/-85	1200/10	500	4%	3%
3	-40	60	500	0%	n/a
4	-40/-85	60/10	500	5%	7%

The reason for the apparent limit in BA content is still under investigation. The PHA is known to establish a stable complex with BF_3.[97] The preference of the catalyst for PHA over BA appears to be a limiting factor in the mechanism and incorporation of BA in the copolymer. Preference of one BF_3 complex over another could be attributed to the enthalpy of complex formation. It is also possible that the high molecular weight copolymer with a large mole fraction of BA creates the same crystallinity problems that are observed with the BA homopolymer.

Determination of the rate of depolymerization and evaporation separately for the BA-PHA copolymer is difficult. Differential scanning calorimetry provides some information regarding the depolymerization energy, but it also captures the heat of

evaporation and melting for conversion of the polymer to monomer. Thermal gravimetric analysis can also be used, however exposure of the polymer to acid prior to measuring mass changes creates either an increase in mass when an acid vapor is used or extraordinarily long exposure times when a PAG is used.

A QCM was used to differentiate the depolymerization reaction from monomer evaporation. The Butterworth-van Dyke equivalent circuit model for the electrical response of a QCM crystal provides information on the softening (i.e. depolymerization) and evaporation (i.e. mass loss) of the polyaldehyde films. The mass change can be monitored by the change in frequency (inductive changes) as a consequence of addition or removal of mass. The depolymerization rate can be monitored by the change in QCM resistance, corresponding to changes in viscosity. As the polyaldehyde depolymerized and formed a liquid, a sharp rise in the resistance of the QCM was observed as a consequence of viscous losses during oscillation. The liquid formation also caused a decoupling of the mass from the frequency response in the quartz crystal, giving an apparent decrease in the recorded mass. The frequency recovered as the liquid monomer eventually solidified due to the removal of heat by evaporation and convection, which also returned the resistance to a minimum value. The resistance changes are used to determine the depolymerization rate, and the frequency changes are used to determine the evaporation time.

The resistance was normalized to the maximum observed value within each measurement to compare changes across multiple samples. The time was zeroed to the moment of photo-exposure, which created the photoacid from the PAG and initiated the depolymerization. The depolymerization was often complete part way into the photo-

exposure of the PAG. The time to complete depolymerization was taken as the point of maximum QCM resistance. The resulting data was fit to an exponential curve of the form $R_{norm} = exp(b(t\text{-}c))$, where R_{norm} is the normalized resistance, t is time in seconds, and b and c are fitting parameters. Both parameters can provide quantitative values for the physical occurrence of depolymerization with b being the rate of depolymerization and c being the delay in the response to light irradiation. Figure 5.3 shows the normalized resistance from QCM versus time in seconds for the depolymerization of polymer 3 in Table V. The best fit line, obtained by minimizing the sum of squared error, for an exponential equation of the form above is also shown.

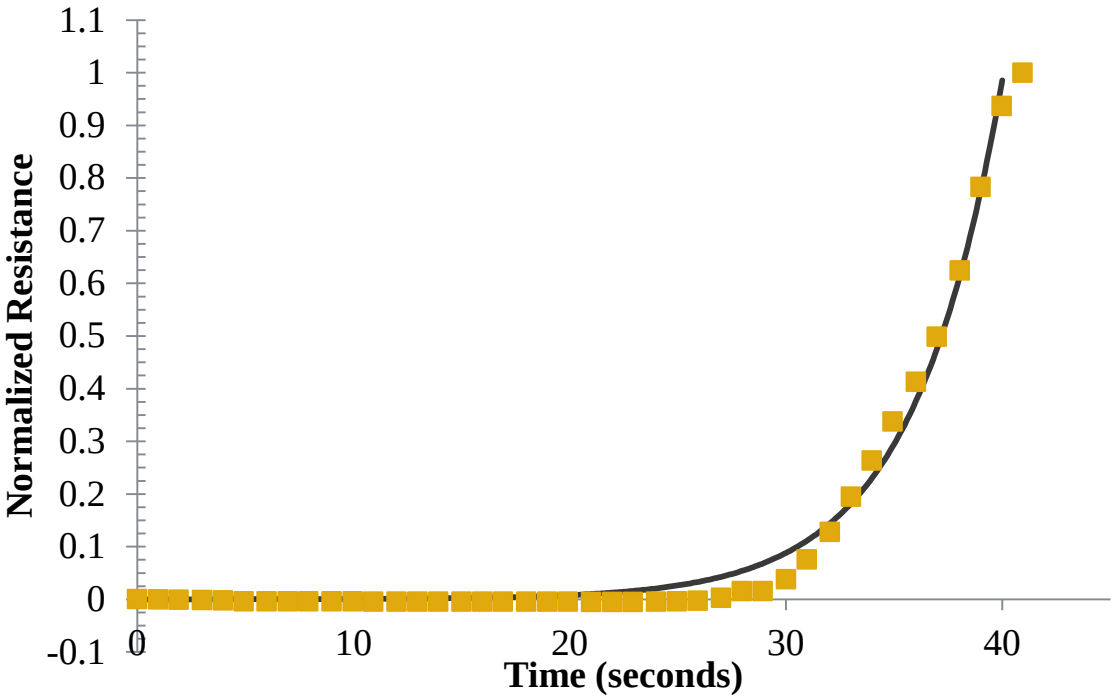

Figure 5.3. Representative QCM resistance for the depolymerization of a butyraldehyde copolymer, 6 mol% BA and 41.5 kDa.

The best fit parameters for the data shown in Figure 5.3 are 0.24 s^{-1} and 40 s for b and c, respectively. A larger b parameter implies a faster depolymerization rate. A

smaller c implies a higher sensitivity to acid, which is desirable to ensure complete depolymerization of the polyaldehyde. The b and c parameters for many samples were compared to determine trends in the depolymerization of the polyaldehydes versus butyraldehyde content. Figure 5.4 shows the depolymerization rate constant, b, versus butyraldehyde mol%. An increase in butyraldehyde mole fraction generally trends towards a higher rate constant, which is desired. However, there is considerable scatter in the data. Figure 5.5 shows the delay, c, versus butyraldehyde mol%. An increase in butyraldehyde percentage does not affect the delay.

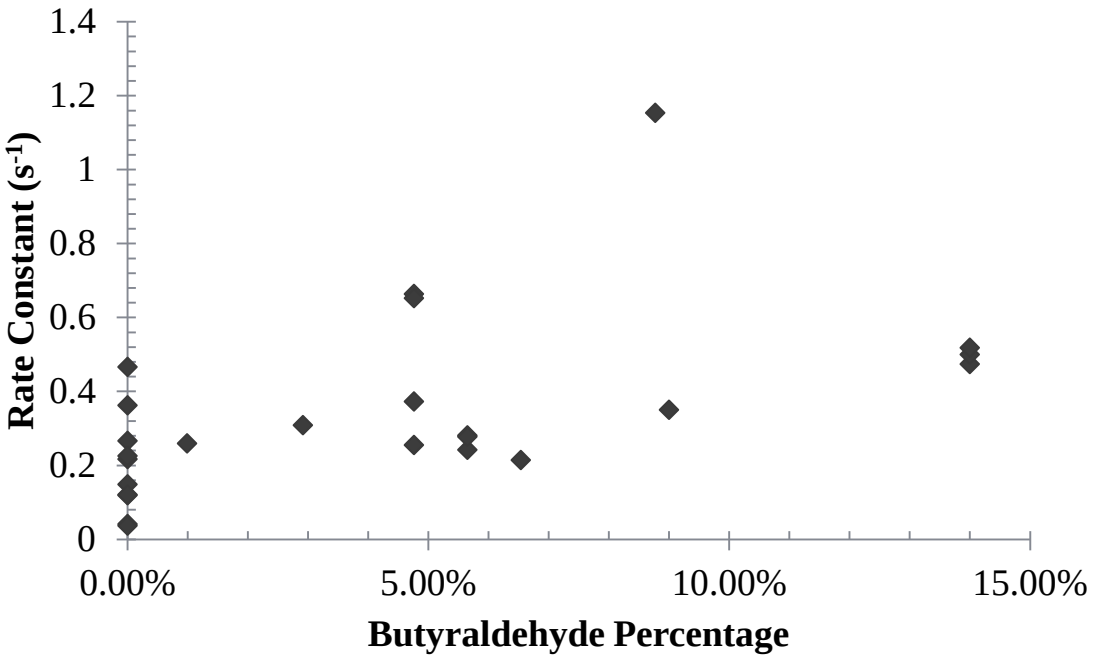

Figure 5.4. QCM resistance rate constant versus butyraldehyde percentage for the photoacid catalyzed depolymerization of copolymer films.

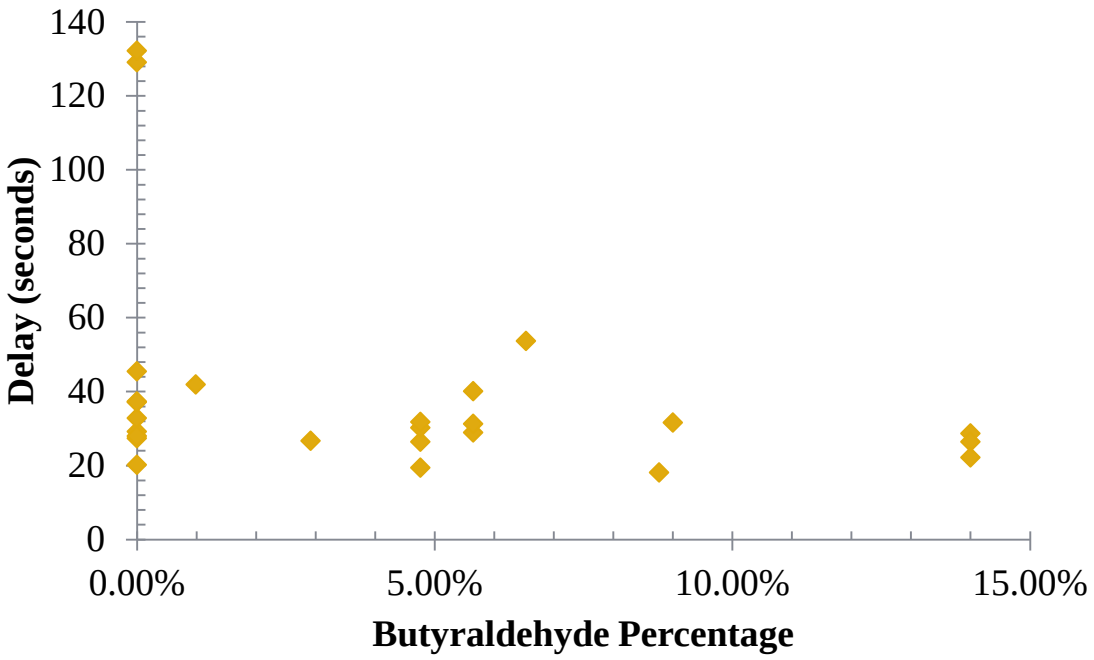

Figure 5.5. QCM resistance delay versus butyraldehyde percentage for the photoacid catalyzed depolymerization of copolymer films.

A higher mol% of butyraldehyde in a copolymer likely increases the depolymerization rate by increasing acid diffusion because BA is a low viscosity liquid at room temperature whereas PHA is either a solid or high viscosity liquid. As a copolymer depolymerizes into PHA and BA, the liquid BA can help acid diffuse to unreated polymer chains. The PHA also liquefies during depolymerization as well due to the highly exothermic reaction, but BA promotes acid diffusion by maintaining the liquid state longer than the time for PHA to solidify. The benefit of this liquid state becomes more apparent as thicker films of polymer are used. The delay shown in Figure 5.5 is unaffected by the BA content, because it is not a function of the polymer matrix. Rather, it is dependent on the type and amount of PAG used.

The benefit of incorporating BA into the copolymer is seen in the evaporation time, as determined by QCM, of the depolymerized polymer. A homopolymer of PHA takes 2.5 days for 90 wt% of the monomer to evaporate after depolymerization. The copolymer of PHA and BA evaporated in 5.25 h, which is an order of magnitude improvement.

An unintended consequence of the incorporation of BA is the increase of the thermal stability of the polyaldehyde, irrespective of the BA incorporation level. The representative dynamic TGA curves of a PHA homopolymer and a BA-PHA copolymer are shown in Figure 5.6. The homopolymer has a molecular weight of 63 kDa. The copolymer has a molecular weight of 66 kDa and a BA incorporation of 12 mol%. The onset of thermal degradation is 107°C for the homopolymer and 141°C for the copolymer.

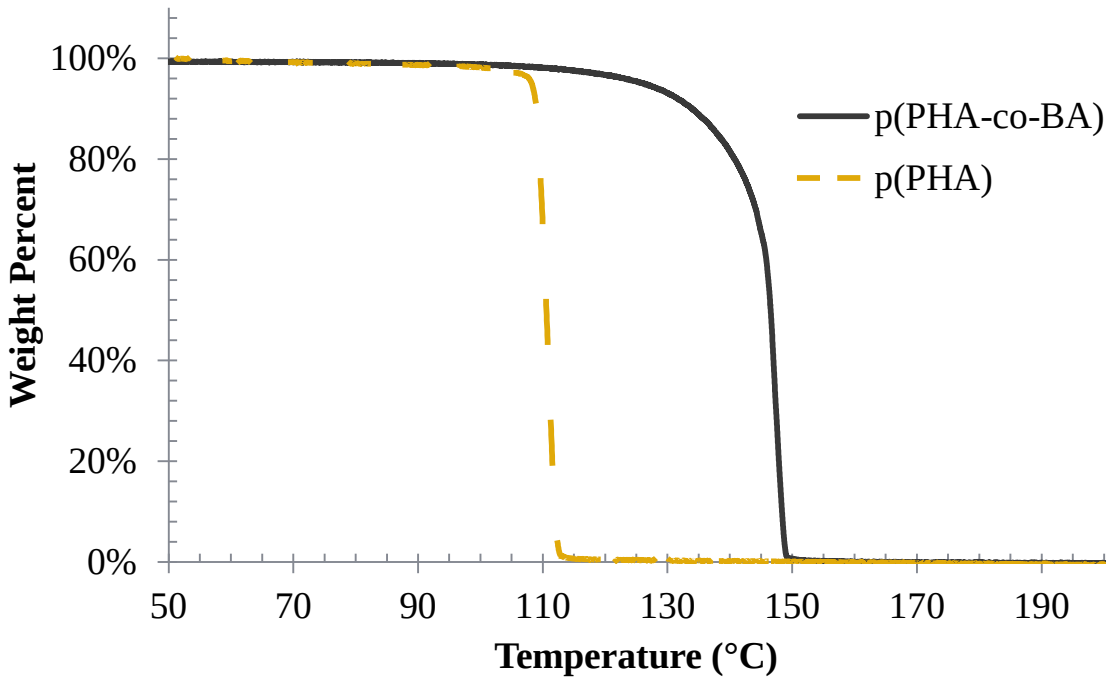

Figure 5.6. Dynamic TGA of a homopolymer of phthalaldehyde (61 kDa) and the copolymer of phthalaldehyde and butyraldehyde (12 mol% BA, 66 kDa).

5.2.2 Other Aldehydes

Beyond the copolymerization of butyraldehyde, attempts at the incorporation of other aldehydes provided mixed success. Figure 5.7 shows all of the aldehydes that were used in the copolymerization with phthalaldehyde in the course of this thesis. All of the aldehydes in this section were used as-received with the exception of 4-TBA, which was synthesized in-house. Each aldehyde was also used in a homopolymerization, none of which produced yield. With the exception of pivalaldehyde and furfural, all polymerizations with the comonomers in Figure 5.7 provided yield of some polyaldehyde polymer.

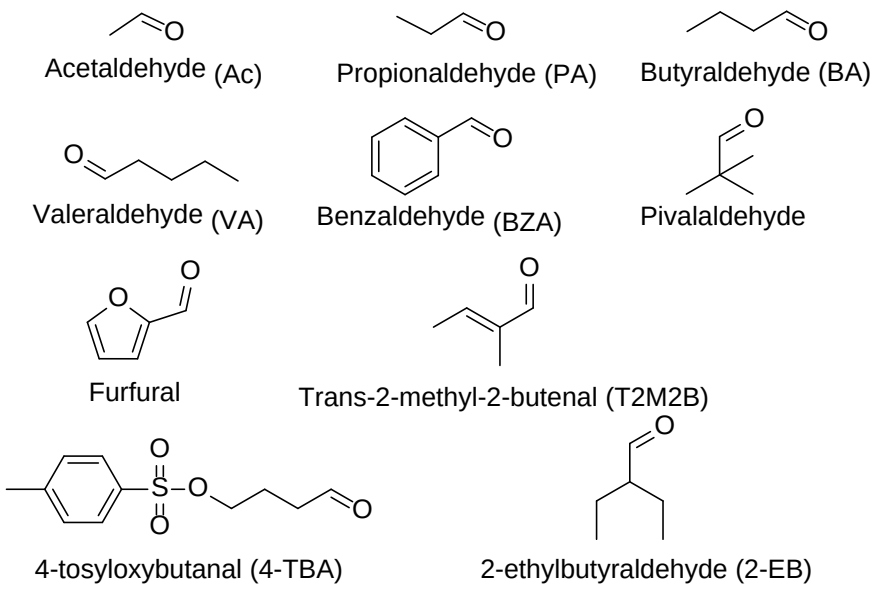

Figure 5.7. Structures of aldehydes used as comonomers in the polymerization with phthalaldehyde.

Appendix B contains a table of all of the polymerization results for coaldehydes other than butyraldehyde. The copolymerization of some aldehydes was not verifiable by ^{1}H NMR. BZA ^{1}H NMR peaks are masked by the large range of peaks for poly(phthalaldehyde). Evidence for benzaldehyde incorporation comes from long-live liquid states observed in QCM and the increased sensitivity from contrast experiments. Similarly, T2M2B, PA, VA, and Ac were never observed in ^{1}H NMR, but all showed trends in the thermal stability and contrast experiments that are unexplainable without some interaction with the phthalaldehyde polymer. These polymers will be referred to as copolymers of phthalaldehyde and the respective monomer for ease of discussion, although the polyaldehyde incorporation is small.

Copolymerization of aldehydes other than phthalaldehyde affects the thermal stability of the polyaldehyde. Figure 5.8 shows the dynamic TGA traces for all of the copolymers with yield. A rate of 5°C/min was used. Each coaldehyde affects the

polymer thermal stability in a different way, however some trends are apparent. Molecules with sterically large structure, like BZA, T2M2B, and VA, will not affect the stability of the polymer. The small size of Ac destabilizes the polymer. The 3 and 4 carbon aldehydes, PA and BA, significantly stabilize the polymer. The 4-TBA copolymer has a very low onset, likely due to the 4-TBA monomer breaking apart into a tosyl acid, facilitating a faster depolymerization. The cause of these trends for the coaldehydes is not well understood, however, the ability of PA and BA to form crystalline polymer cannot be ignored. Previous reports have consistently held the crystallinity of homopolymers of PA and BA.[56] If crystalline regimes of PA and BA occur in the respective copolymers with PHA, the significant thermal stability could be explained.

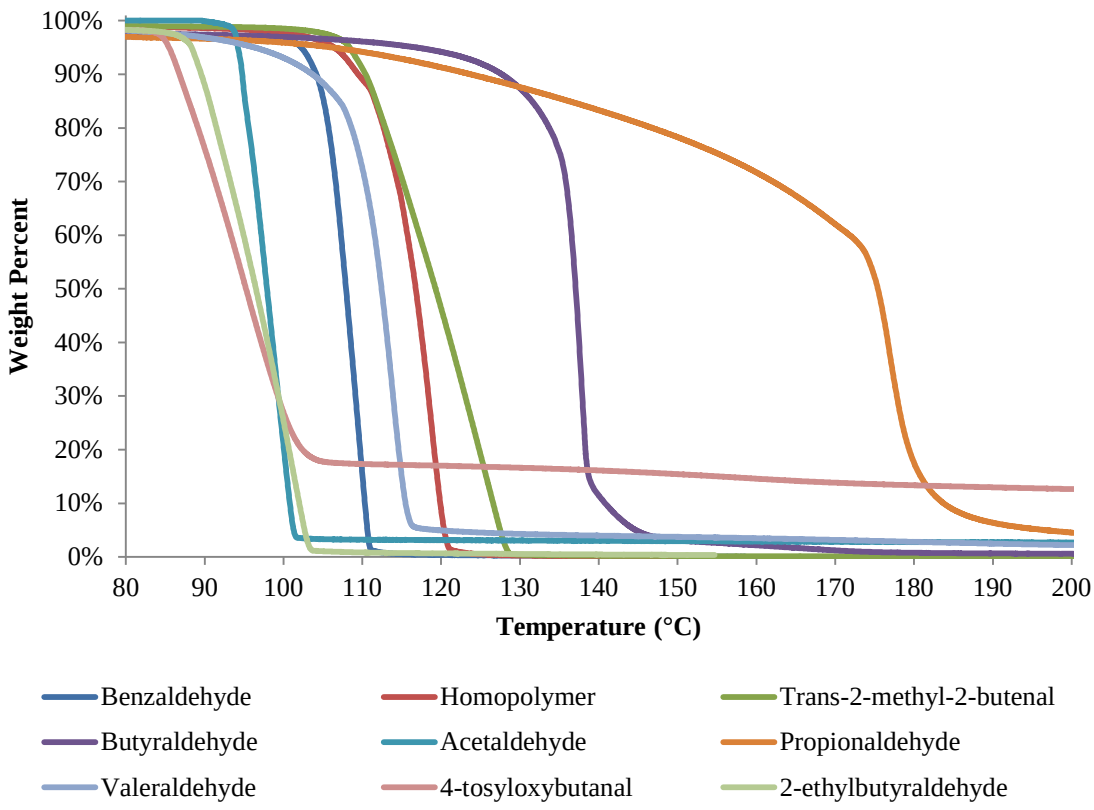

Figure 5.8. Dynamic TGA traces for copolymers.

The purpose of incorporating 4-TBA into a polyaldehyde is to provide a tethered acid capable of depolymerizing the polymer. The thermal decomposition of the 4-TBA copolymer confirms this when isothermal conditions are used. Figure 5.9 is the 70°C isothermal TGA mass loss versus time for PPHA and the copolymer of PHA and 4-TBA. The depolymerization of the 4-TBA copolymer is orders of magnitude faster than that of phthalaldehyde homopolymer.

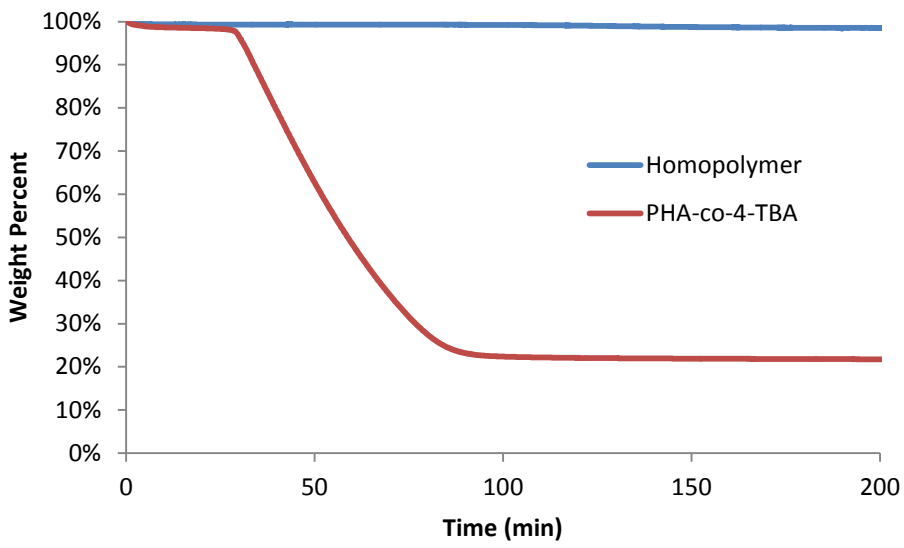

Figure 5.9. 70°C isothermal mass loss versus time for homopolymer and copolymer with tethered acid generator.

QCM was also performed for all of these copolymers except the 4-TBA monomer due to the residue. Nothing of note came out of the QCM rates and delays, however some observations were qualitatively apparent. BZA copolymers exhibited long-lived liquid states that would last for minutes, whereas the PHA homopolymer would only stay a liquid for less than a minute. Ac copolymers exhibited little to no liquid state as the acetaldehyde monomer would evaporate almost immediately.

Another method of determining the effect of coaldehydes on the acid catalyzed depolymerization of a polymer is contrast curves. Thin polymer films with 10 pphr of Rhodorsil FABA PAG were spin-cast onto pieces of silicon. The polymer films were exposed at 248 nm irradiation through a variable density mask and allowed to evaporate overnight. The resulting changes in thickness were recorded. The normalized thickness versus the log of the exposure dose for four polyaldehydes is shown in Figure 5.10 below. A lower value for D_{100} (the x-axis intercept) is desirable.

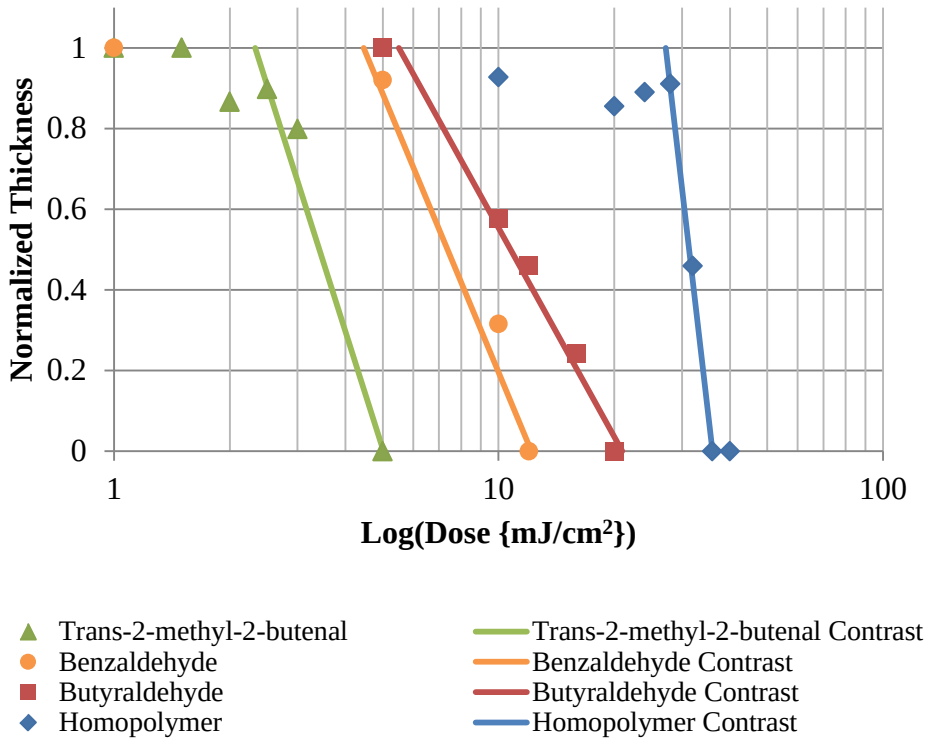

Figure 5.10. Contrast curves for four polyaldehydes.

The incorporation of any coaldehyde shown decreases the sensitivity of the polymer. The depolymerization of the polyaldehydes causes a liquid state due to the rapid exothermic reaction. The presence of an aldehyde that is liquid at room temperature, like BA, T2M2B, or BZA, allows acid to diffuse over longer periods of time. This prolonged liquid state allows less acid to depolymerize a specified volume of polymer giving rise to the more sensitive polymer.

Some terpolymers were also synthesized. These terpolymers all had limited yield but exhibited complex thermal decomposition profiles. Figure 5.11 shows the dynamic TGA traces for the terpolymers with a homopolymer decomposition curve for comparison. A ramp rate of 5°C/min was used. In some cases, as with terpolymers with BZA and BA, BA and 2-EB, Ac and 2-EB, and 2-EB and VA, bimodal decomposition

curves are observed. The sharp decline of the Ac and T2M2B, Ac and BZA, and 2-EB and T2M2B curves are more typical of polyaldehyde decomposition profiles.

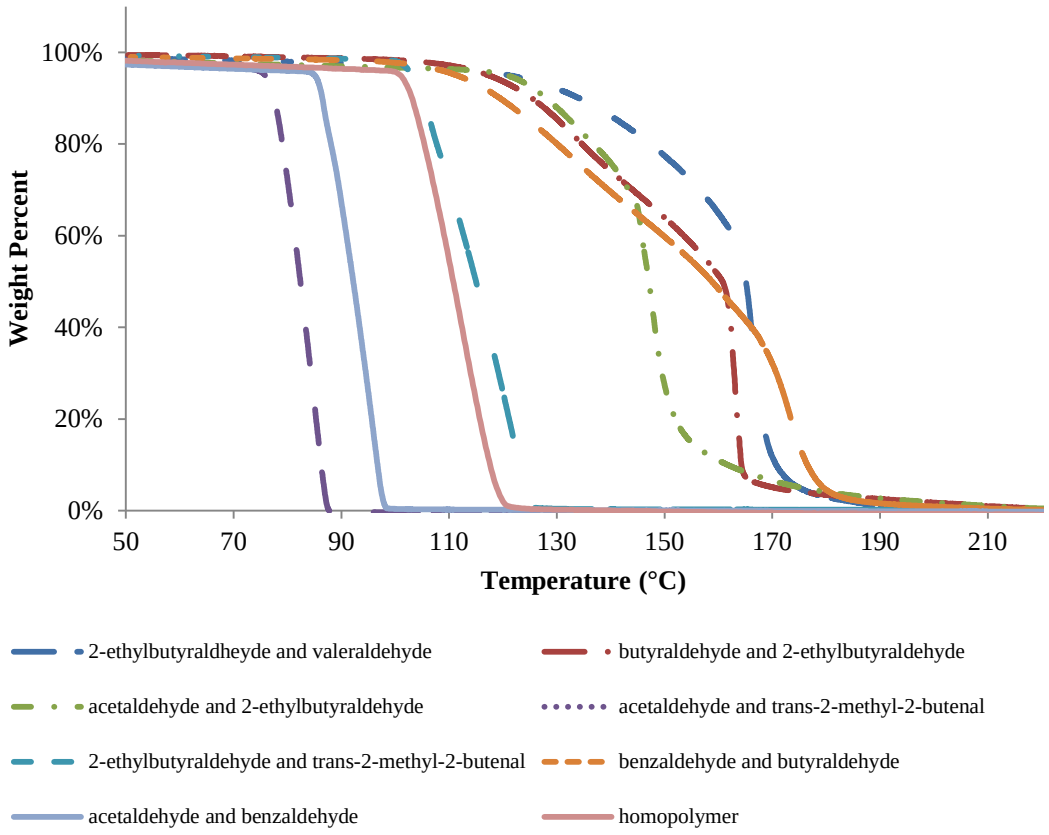

Figure 5.11. Dynamic TGA traces for terpolymers.

There is a significant amount of complexity observed for these decomposition profiles, but there is information from the onset temperatures for each terpolymer. Terpolymers with Ac tend to be less thermally stable than the homopolymer. Long aliphatic chain aldehydes, especially BA, tend to stabilize the polymer. Incorporation of monomer with similar structure to PHA, like BZA, does not shift thermal decomposition and is instead guided by the third aldehyde. These observations are consistent with what was observed for the onset temperatures shown previously in Figure 5.8 for copolymers.

While these co- and terpolymerizations were successful, the coaldehydes presented in this subchapter provided less desirable properties than butyraldehyde for the application. Therefore, butyraldehyde was the focus of further polymerizations, as seen previously. Revisiting terpolymers could, however, be valuable as further applications of polyaldehydes become apparent.

5.3 Conclusions

The copolymerization of PHA and an aliphatic aldehyde has been achieved, which improves the monomer evaporation time for a depolymerized polymer film. A method of determining the coupled evaporation and depolymerization of polyaldehydes is also presented. The incorporation of BA into poly(PHA) was limited. BA was been found to have a significantly different T_c and forms a trimer upon polymerization. These factors limit the degree of polymerization with PHA. It was found that depolymerization of the polyaldehyde occurs quickly and complete vaporization is limited by the rate of monomer evaporation. The copolymerization of other aldehydes has also been achieved, which affects the thermal stability of the polyaldehyde.

5.4 Recommendations

Finding a different co-catalyst that will act as a stronger binding initiation site to the coaldehydes could prove valuable. Correct selection of the right ratio of co-catalyst to facilitate the incorporation or polymerization of coaldehydes while not interfering with the polymerization kinetics of the phthalaldehyde is important.

Coaldehydes used for this study were limited to those available for purchase commercially. No attempts were made to synthesize an aldehyde that could be either a higher vapor pressure or be more reactive in the polymerization. Screening of more coaldehydes would be beneficial to find trends in the reactivity, vapor pressure, solubility, and even potentially a lower dielectric constant. If an aldehyde could be synthesized with heavy fluorination, the electron with-drawing nature of the fluorine could provide a more reactive aldehyde as well as decrease the dielectric constant. The increased size of the fluorine could also help increase the solubility of the resulting polymer over the hydrogenated form.

As always, the push for higher vapor pressure is very desirable. Polymerization, either by homopolymerization or copolymerization, of high vapor pressure monomers is a continual improvement to be made. High molecular weight, high vapor pressure polyaldehydes seems to currently be limited by the available chemical structures that will facilitate not only good reaction kinetics, but also amorphous polymer that retains solubility in the reaction solvent. The correct selection of a catalyst for forming polymer with high incorporation of the higher vapor pressure aldehyde is also a continual improvement to be made. The terpolymerization of aldehydes may be an option for the polymerization of amorphous and highly volatile polyaldehydes. The incorporation of dissimilar aldehyde structures may also be benefitted by the terpolymerization of aldehydes.

Cross-linking of a polyaldehyde would be beneficial to the mechanical strength, especially when high molecular weights can not be achieved, as is the case with some coaldehydes. The cross-linking reaction, however, needs to be compatible with the

polymer. Acids and bases are therefore, not an option for catalyzing the polymerization reaction. Similarly, a photo-catalyzed reaction is not desirable as this could interfere with the depolymerization reactions. Therefore, the curing must be thermal, below the decomposition temperature, and must occur over short times to minimize the PPHA that may decompose into monomer.

One possible pathway involves the incorporation of alkenes into a monomer to create sites for radical cross-linking via a thermal radical generator. The choice of thermal radical generator also needs to avoid decomposition products that could cause the depolymerization of a polyaldehyde or interfere with the acid-catalyzed decomposition. Any radical generators containing nitrogen, which could potentially interfere with an acid, should be avoided. Additionally, peroxides that decompose into strong acids must also be avoided. Most radical generators will consume acid if thermal degradation has not already occurred. Quantities of radical generator also need to be controlled to minimize interactions with acid. Preliminary tests show a PPHA film remains stable when exposed to benzoyl peroxide.

The incorporation of an alkene monomer could prove difficult. The most reactive version would be the incorporation of a vinyl phthalaldehyde. Alternatively, a benzaldehyde (styrene aldehyde) with a vinyl group could be used. The reaction kinetics for either of these two monomers could prove sufficient to create a copolymer with phthalaldehyde. The vinyl phthalaldehyde would have to be synthesized. Figure 5.12 shows two routes to the vinyl phthalaldehyde monomer.

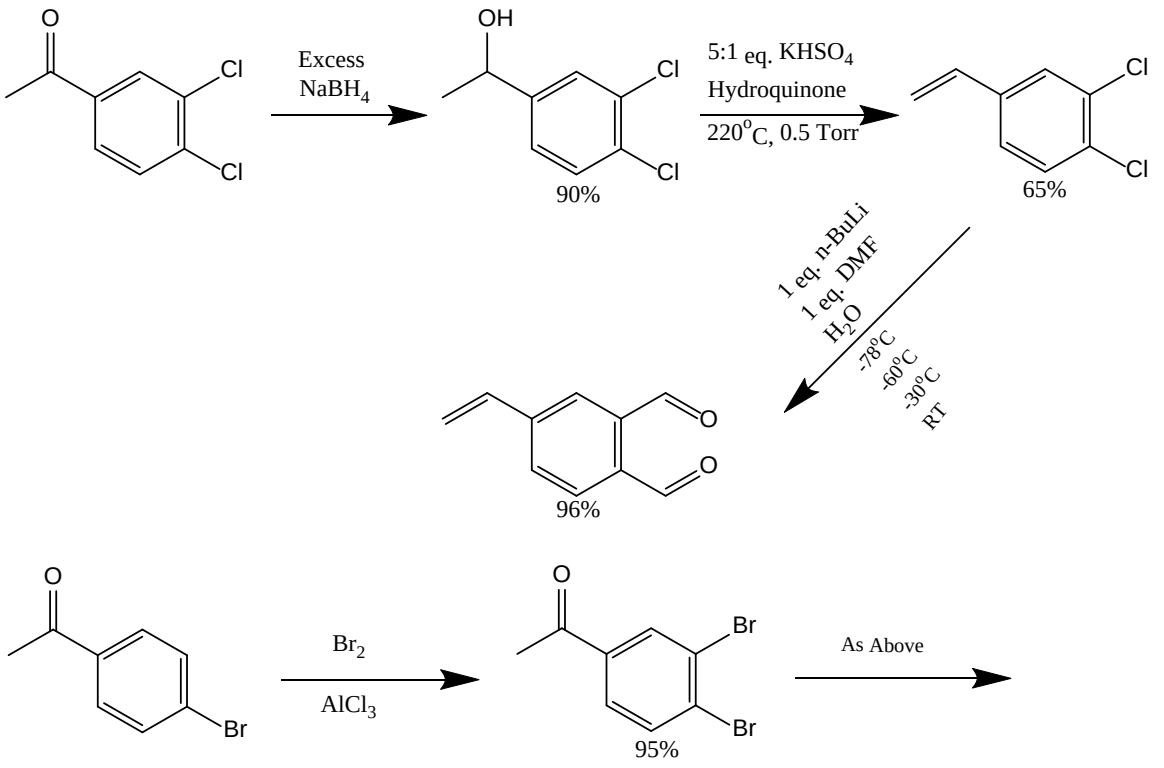

Figure 5.12. Synthesis route to vinyl o-phthalaldehyde.

CHAPTER 6. IN-SITU NMR TECHNIQUE FOR DETERMINING LOW CEILING TEMPERATURE THERMODYNAMIC VARIABLES

This study used variable temperature (VT) ^{1}H NMR to find the ceiling temperature and thermodynamic variables of low ceiling temperature polymers. Previously, the ceiling temperature and thermodynamic values were determined by finding the saturation yield of polymerizations at various temperatures. There is one report that showed the determination of the saturation yield by VT NMR, but did not report thermodynamic values.[91,99]

6.1 Motivation

Knowing the ceiling temperature of a polymer is essential to determining the optimum reaction conditions for high yield and high molecular weight polymer synthesis. Measuring the saturation yield involves measuring the concentration of the monomer as a function of temperature. The most common method for calculating the ceiling temperature of a polymer involves measuring the saturation yield of the monomer by evaluating the polymer yield after polymerization.[100,101] Many factors can negatively affect accuracy of the polymer yield, including human error and erroneous polymer properties. For example, self-immolative polymers may not be easily dried of solvent due to their low thermal stability and lack of glass transition temperature. A higher yield would be apparently achievable despite the reality of a solvent-rich weight.

Aso, et al. were successful in developing an in-situ IR method for monitoring the monomer concentration for poly(phthalaldehyde) polymerization, but were limited by the temperature control. [72,78] The variable temperature NMR method for measuring monomer concentration and polymer thermodynamics has been disclosed but has been largely unused.[91,99] In this paper, variable temperature ^{1}H NMR was used to measure the polymer ceiling temperature and to provide additional insight into the thermodynamics of polymerization for several low ceiling temperature polymers. It is shown that a wide range of temperatures are readily accessible in the NMR experiment for finding the true "region of ceiling temperature". [70,71] Similar to polymer yield experiments, the equilibrium monomer concentration at each temperature is used to determine the ceiling temperature by extrapolation of a linear fit of natural log of monomer concentration vs inverse of absolute temperature. This method can also be used to help identify the depolymerization/polymerization kinetics, either by examining the catalyst interactions or by identifying temperature regions dominated by polymerization and depolymerization. In this paper, the enthalpy and entropy of polymerization are determined by in-situ, variable temperature ^{1}H NMR for three low ceiling temperature polyaldehydes.

6.2 Experimental

For the in-situ NMR of poly(phthalaldehyde), a solution of 0.75M purified PHA in DCM-d_2 was prepared with 0.05 mL BF_3-OEt_2 in dry nitrogen glovebox. For the polymer yield experiments, 2 g (15 mmol) of PHA was dissolved in 20 mL DCM in a 100 mL round bottom flask in a nitrogen purged glovebox. To the monomer solution, 0.03 mmol of BF_3-OEt_2 was added and the flask was sealed with a septum. The reaction was cooled to the target temperature and allowed to react for 30 minutes. The reaction

was quenched with 0.12 mL (1.5 mmol) pyridine to remove the BF_3-OEt_2. The solid was precipitated by addition of methanol and filtered. The precipitate was redissolved in THF, and 0.05 mL (0.36 mmol) of triethylamine was added per gram of precipitate to help remove residual catalyst. The polymer was precipitated into hexanes, filtered, and allowed to dry until constant weight.

A solution of 0.93M purified PHA (0.56 mmol) and BA (0.21 mmol) in DCM-d_2 was made for the in-situ NMR of the BA-PHA copolymer. The solution was added to an NMR tube with 0.6 µL BF_3-OEt_2 (0.005 mmol) in a dry nitogen glovebox. Similarly, a solution of only distilled BA (0.56 mmol) in DCM-d_2 was prepared and added to an NMR tube with 0.05 mL BF_3-OEt_2 for the BA only polymerization.

6.3 Results and Discussion

6.3.1 Poly(phthalaldehyde)

The poly(phthalaldehyde) data was previously reported by Schwartz, et al.[97] NMR of PHA monomer has peaks at 10.45 (2H, aldehyde, singlet), 7.98 (2H, phenyl, quadruplet), and 7.79 (2H, phenyl, quadruplet). BF_3-OEt_2 alone has peaks at 4.21 (4H, -CH_2-, quadruplet) and 1.40 (6H, -CH_3, triplet). The integration of the ^{1}H peaks was normalized to the residual dichloromethane solvent peak at 5.32 ppm. Integrations of the PHA aldehyde peak provided the saturation concentration of monomer at each temperature. Equilibrium between the PHA monomers and BF_3-OEt_2 catalyst was reached within 15 minutes at each temperature. The temperatures were chosen based on previous reports of the ceiling temperature for poly(phthalaldehyde) (PPHA).[72] Figure 6.1 shows the ^{1}H NMR spectra for PHA in the PHA polymerization between -25°C and -

35°C. The peaks at 7.34 and 7.42 ppm are polymerized phthalaldehyde phenyl protons. The peak at 6.45 ppm is the proton on the carbon in the PPHA polymer backbone next to the ether linkage which is complexed with BF_3.

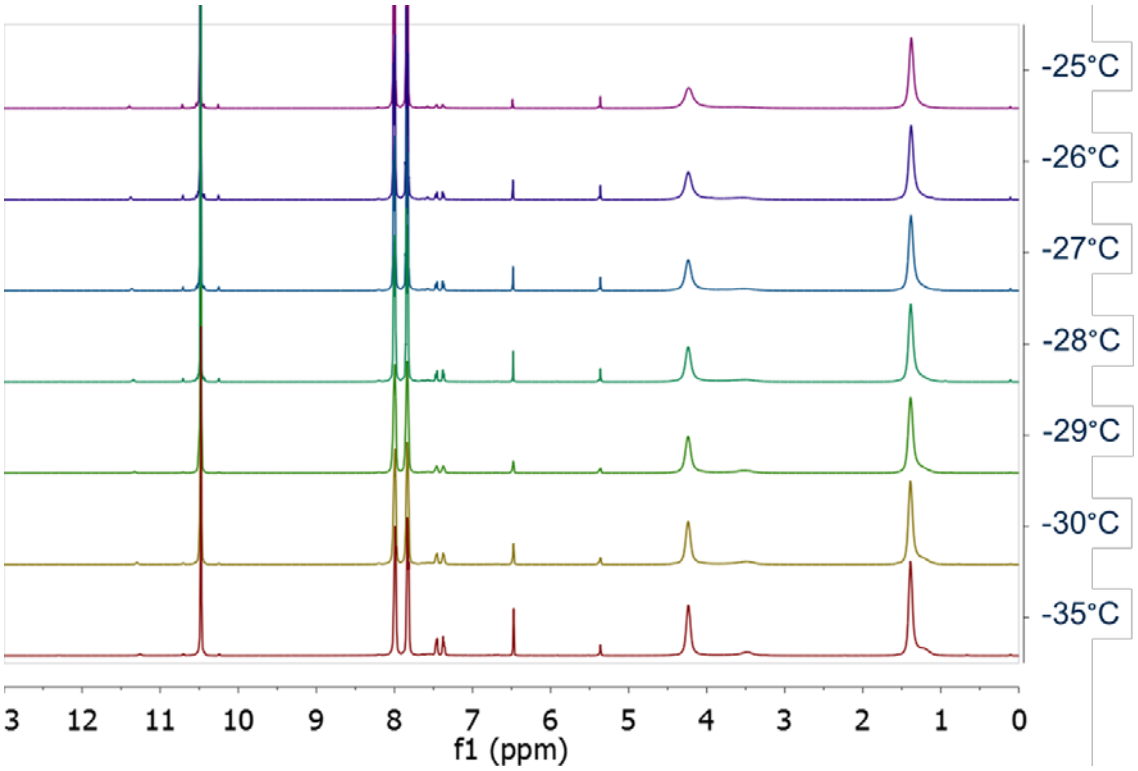

Figure 6.1. In-situ ^{1}H NMR spectra for the polymerization of phthalaldehyde for the temperature range of -25°C to -35°C.

The increase in the two doublet peaks at 7.34 and 7.42 ppm shows the formation of PHA polymer. At temperatures slightly above the ceiling temperature, Figure 6.1, some polymer yield is observed. This small polymer yield asymptotically approaches the initial monomer concentration, as observed when the ceiling temperature phenomenon was first reported.[100] In this case, the asymptotic approach could be due to the catalyst, which lowers the activation energy for both the polymerization and the depolymerization reactions. At temperatures between -25°C and -35°C, the depolymerization reaction

dominates the polymerization reaction and only a small polymer yield is observed in the peaks at 7.34 and 7.42 ppm.

Also of note in Figure 6.1 is the change in the diethyl ether corresponding to free diethyl ether (3.48 ppm) and diethyl ether complexed with BF_3 (4.21 ppm). At -25°C, the peaks are from a singlet at 4.21 ppm (complex with BF_3) and a small, broad peak at 3.48, corresponding to $-CH_2-$ protons for free diethyl ether. At lower temperature in Figure 6.1, the $-CH_2-$ protons shifted from 3.48 ppm to 3.43 ppm and become better defined. Similarly, the peak at 1.35 ppm, corresponding to $-CH_3$ protons from diethyl ether, split as the temperature decreased. This peak shift reflects BF_3 forming a complex with PHA monomer and the poly(phthalaldehyde) ether backbone.

Figure 6.2 shows the ^1H NMR spectra for PHA polymerization from -42°C to -80°C. As the temperature was lowered to -42°C, the monomer was consumed as shown by a decrease in the peak height at 10.45 ppm. As the temperature was lowered to -80°C, a near complete conversion of the monomer to polymer was observed. Similar to the higher temperature spectra in Figure 6.1, peaks corresponding to formation of polymer at 7.4 ppm increased in area. The broad-shaped peaks from 6.4 to 8.0 ppm, which are typical of polymer formation, became more pronounced as the temperature decreased. At -80°C, almost all of the monomer was consumed, leaving only a small monomer peak at 10.45 ppm.

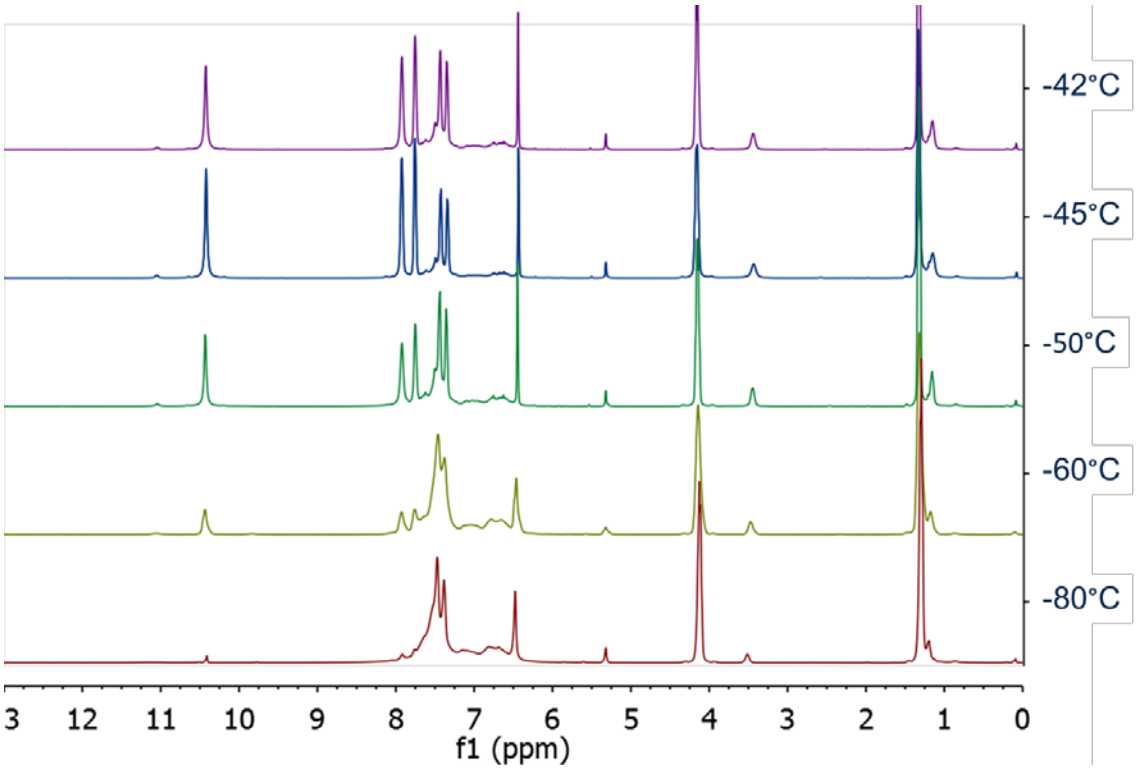

Figure 6.2. In-situ ^{1}H NMR spectra for the polymerization of phthalaldehyde for the temperature range of -42°C to -80°C.

Integrations of the monomer peak at 10.45 ppm provided the monomer concentration at each temperature. The area of the peak at room temperature was used as a reference for the initial monomer concentration of 0.75M. The natural log of the monomer concentration was then plotted versus the inverse of absolute temperature, as shown in Figure 6.3. The dashed line in Figure 6.3 shows the original monomer concentration at temperatures well above the ceiling temperature, and the solid line shows the linear approximation of the monomer concentration at temperatures below the ceiling temperature. The intersection of the dashed and solid line in Figure 6.3 gives the ceiling temperature at -35.4°C. The slope and intercept of the solid line can be used to obtain the enthalpy and entropy for the polymerization (Eq. 2), -36.5 kJ/mol and -151 J/mol-K, respectively.

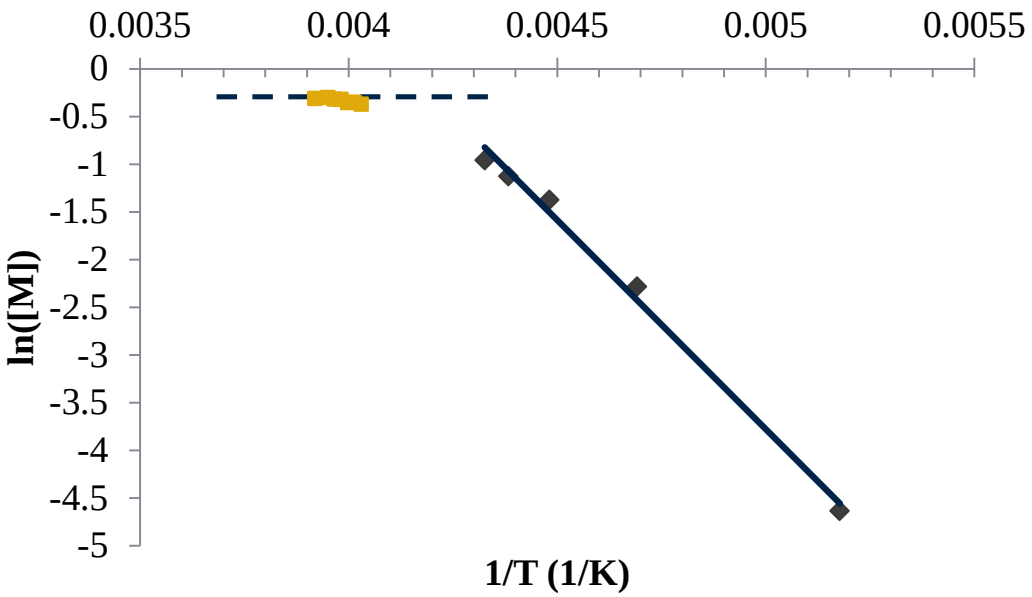

Figure 6.3. Natural log of the equilibrium monomer concentration versus inverse temperature as determined by the ^{1}H NMR spectra (diamonds) with initial concentration (dashed line) and line through the region of ceiling temperature (solid line).

Additional syntheses were performed in the region of the ceiling temperature, -78°C, -64°C, and -45°C, to the ceiling temperature and thermodynamic values from polymer yield experiments. The polymer yield, as determined by weighing the polymer after synthesis, was subtracted from the starting concentration of monomer to determine the monomer saturation concentration at each temperature. Figure 6.4 shows a comparison of the experimental results of polymer yield (solid line) to the results obtained for monomer concentration (dashed line)with ^{1}H NMR. The resulting linear regression through the polymer yield data provided an enthalpy and entropy of polymerization of -19.2 kJ/mol and -79.6 J/mol-K, respectively, and a ceiling temperature of -38.6°C.

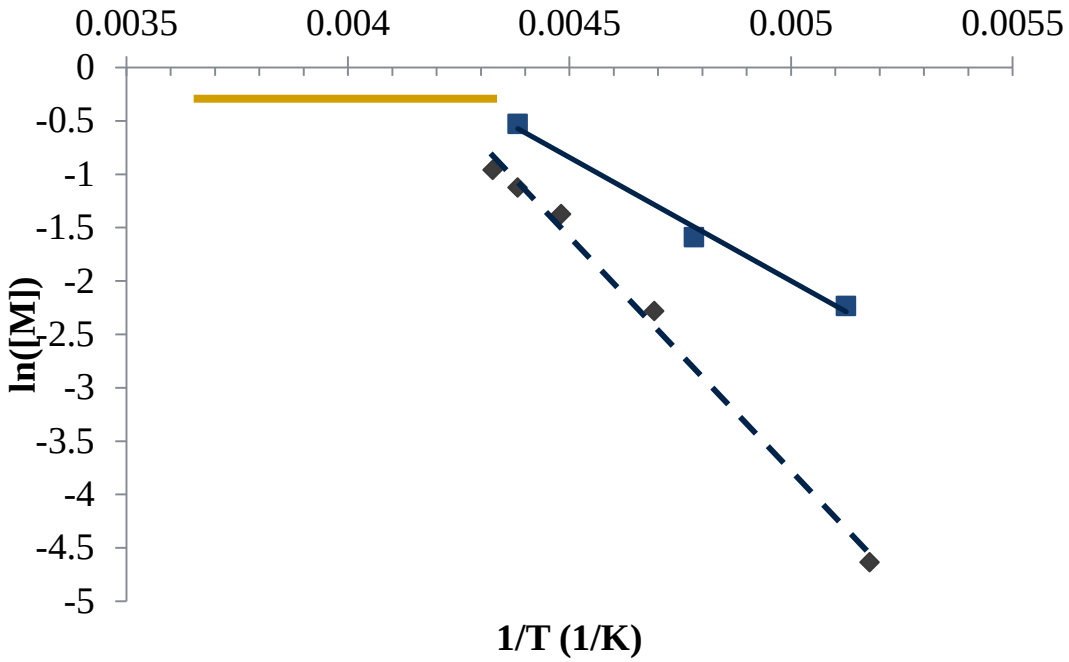

Figure 6.4. Comparison of polymer yield (squares) and ^{1}H NMR-based (diamonds) saturation concentrations with linear regressions through regions of ceiling temperature for both polymer yield (solid line) and NMR (dashed line). The bold line represents initial concentration.

Table VII shows the thermodynamic variables and ceiling temperature for the two methods in this study and a previous report for comparison. Results from the polymer yield data are closer to previously reported values because both sets of data were obtained by the same method. However, the in-situ NMR has fewer sources of error and uncertainties because the monomer concentration can be directly measured at each temperature while the polymer yield data can be distorted by loss of product during isolation or improper purification of polymer leading to slight depolymerization or presence of residual solvent.

Table VII. Comparison of poly(phthalaldehyde) thermodynamic variable methods.

Source	ΔH (kJ/mol)	ΔS (J/mol-K)	T_c
Polymer Yield (Aso, et al.)	-22.2	-96.2	-43.0°C
In-situ NMR	-36.5	-151	-35.4°C
Polymer Yield (this study)	-19.2	-79.6	-38.6°C

6.3.2 Butyraldehyde Trimer

Copolymers with PHA have been previously synthesized, but the equilibrium thermodynamic data has not been reported.[62,95] The contribution of each type of aldehyde to the forming polymer was determined by in-situ NMR. The interaction of BA with BF_3-OEt_2 has previously been studied.[96] Hashimoto, et al. used gas chromatography to determine the amount of residual monomer from aliquots of a reaction between BA and BF_3-OEt_2. The cyclic trimerization of BA was found to occur at temperatures below 22°C. Similar to ceiling temperature equilibrium, the trimerization yield increased with decreasing temperature. This interaction of BA with BF_3-OEt_2 is important in understanding the copolymerization of BA with PHA.

In-situ NMR was performed with BA monomer and BF_3-OEt_2 catalyst in DCM-d_2 to investigate the role of BA trimerization. The resulting thermodynamic variables were obtained for BA polymer and compared to previous values. Figure 6.5 shows the ^1H NMR spectra for the reaction of BA with BF_3-OEt_2 between 25°C and -30°C. BA monomer has peaks at 9.72 (H, aldehyde, singlet), 2.39 (2H, -CH_2-, triplet of doublets), 1.62 (2H, -CH_2-, multiplet), and 0.94 (3H, -CH_3, triplet) ppm. The aldehyde peak for BA at 9.72 ppm was used to monitor the concentration of BA monomer, just as in the case for PHA. Significant changes in the spectra occurred for the reaction of BA with BF_3-OEt_2

as the temperature decreased. A peak at 4.84 ppm (H, -OCH-, triplet) corresponding to BA trimer formation appeared at 10°C and becomes larger at lower temperatures. Peaks corresponding to the $-CH_2-$ protons of BA also shifted upfield as a result of trimer formation to multiplets at 1.37 and 1.58 ppm. The 1.58 ppm multiplet is somewhat obscured by the monomer peak at 1.62 ppm.

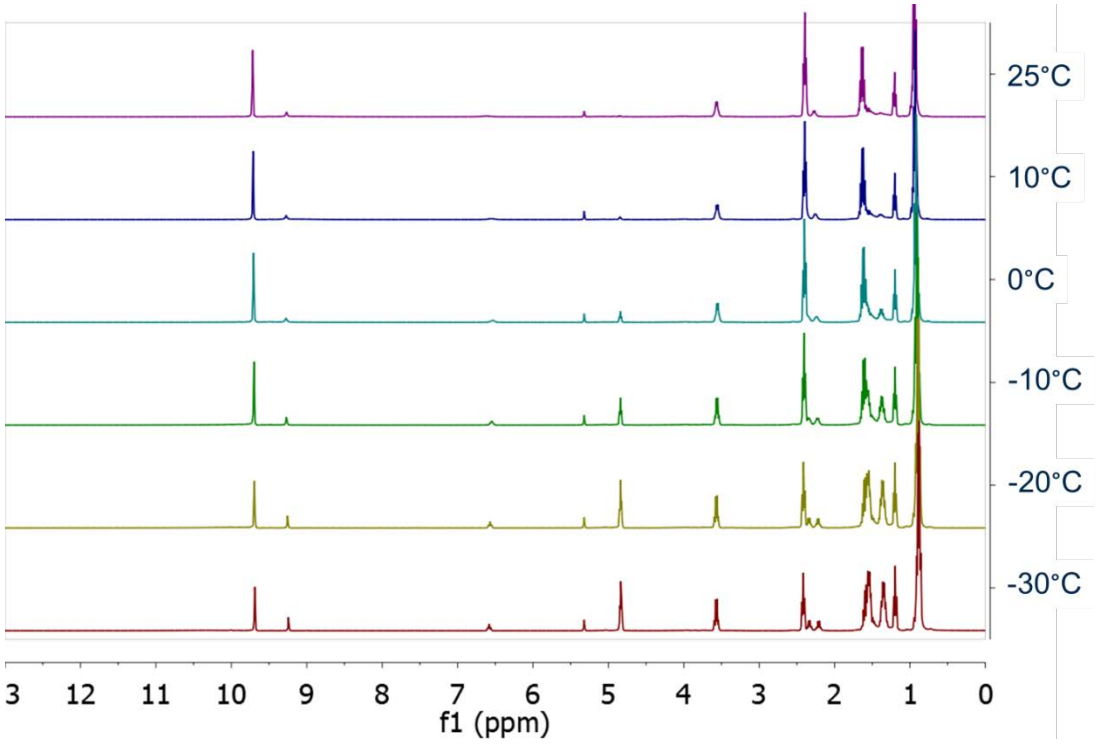

Figure 6.5. ^{1}H NMR spectra for the reaction of butyraldehyde with BF_3-OEt_2 in the temperature range of 25°C to -30°C.

Two additional peaks appear in the spectrum as the temperature decreased. The first, at 9.23 ppm, is most likely due to complexation of BF_3 with the aldehyde functionality of BA, because BF_3 is known to complex easily with aldehydes. This could cause this upfield shift in the aldehyde proton upon complexation.[85,86] The second peak which increased as the temperature decreased is at 6.59 ppm. This peak most likely corresponds to the complexation of BF_3 with the ether bonds of the BA trimer, shown in

Figure 6.6. There is no significant change in the ^{1}H NMR spectra for the reaction of BA with BF_3-OEt_2 at temperatures between -30°C and -80°C. This shows that that the BA/BF_3-OEt_2 reaction is complete below -30^{o}C, and there is no further consumption of monomer or change in the oligomer (i.e. BA trimer).

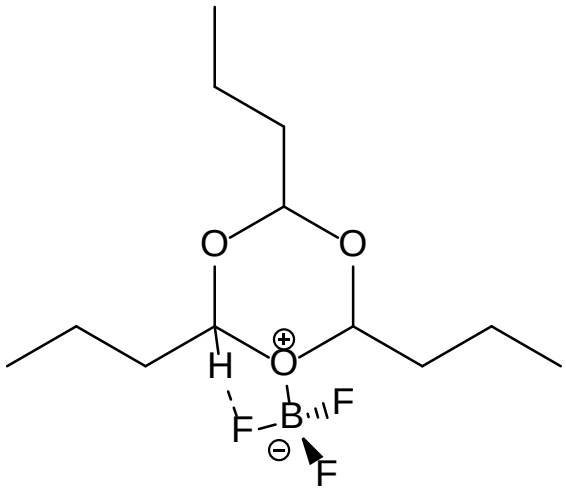

Figure 6.6. Butyraldehyde trimer with BF_3 complexed to ether oxygen

BA monomer concentration can be used to determine the thermodynamic variables for the BA/BF_3-OEt_2 reaction. **Error! Reference source not found.** is a graph of the natural log of the BA concentration versus inverse temperature. The BA monomer concentration decreased dramatically as the temperature was lowered from room temperature to -30°C. As observed in the NMR, below -30°C the BA concentration is almost constant with a small increase in the concentration at very low temperature. The ceiling temperature and thermodynamic values for BA trimerization were calculated using the aldehyde concentrations at or above -30°C. This is shown in **Error! Reference source not found.** by the linear regression fit (i.e. straight lines on the graph) through the temperature region near the ceiling temperature. The slope and intercept of the line

below 0°C yields the enthalpy and entropy values of -12.1 kJ/mol and -38.9 J/mol-K, respectively. The ceiling temperature for BA trimer is 20.6°C. These values are in agreement with those reported by Hashimoto, et al. who reported values of enthalpy and entropy of formation as -12.6 kJ/mol and -42.3 J/mol-K, respectively, and ceiling temperature of 22°C.[96]

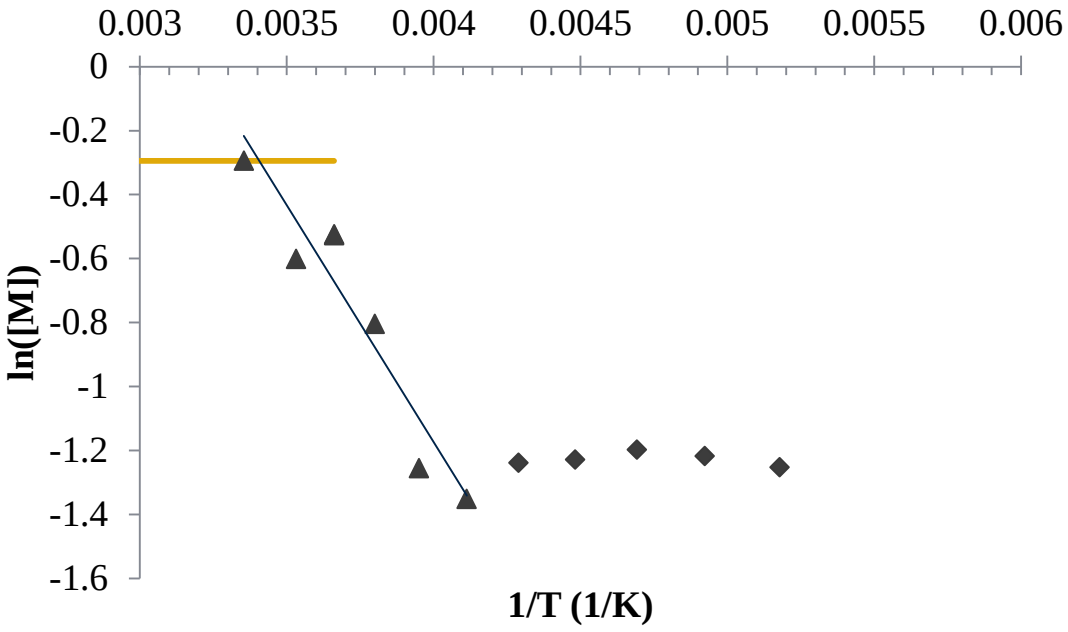

Figure 6.7 Natural log of the equilibrium concentration versus inverse temperature of butyraldehyde in the in-situ ^{1}H NMR reaction with BF_3-OEt_2 with the region of ceiling temperature (triangles) and saturated polymer concentration (diamonds). The bold line represents the initial concentration.

6.3.3 Poly(phthalaldehyde-co-butyraldehyde)

The copolymerization of BA and PHA was attempted using the same reaction conditions as described for the separate PHA and BA synthesis. The entropy and enthalpy of copolymer formation have not previously been reported. An in-situ NMR reaction was performed for the BA-PHA copolymer synthesis with BF_3-OEt_2 catalyst. The monomers were added at a mole ratio of 4 PHA to 1 BA, and the NMR analysis was

performed as before. The initial monomer peaks at room temperature were unchanged from previous experiments. Figure 6.8 shows the ^{1}H NMR spectra for the copolymerization of PHA and BA at temperatures between 25°C and -30°C.

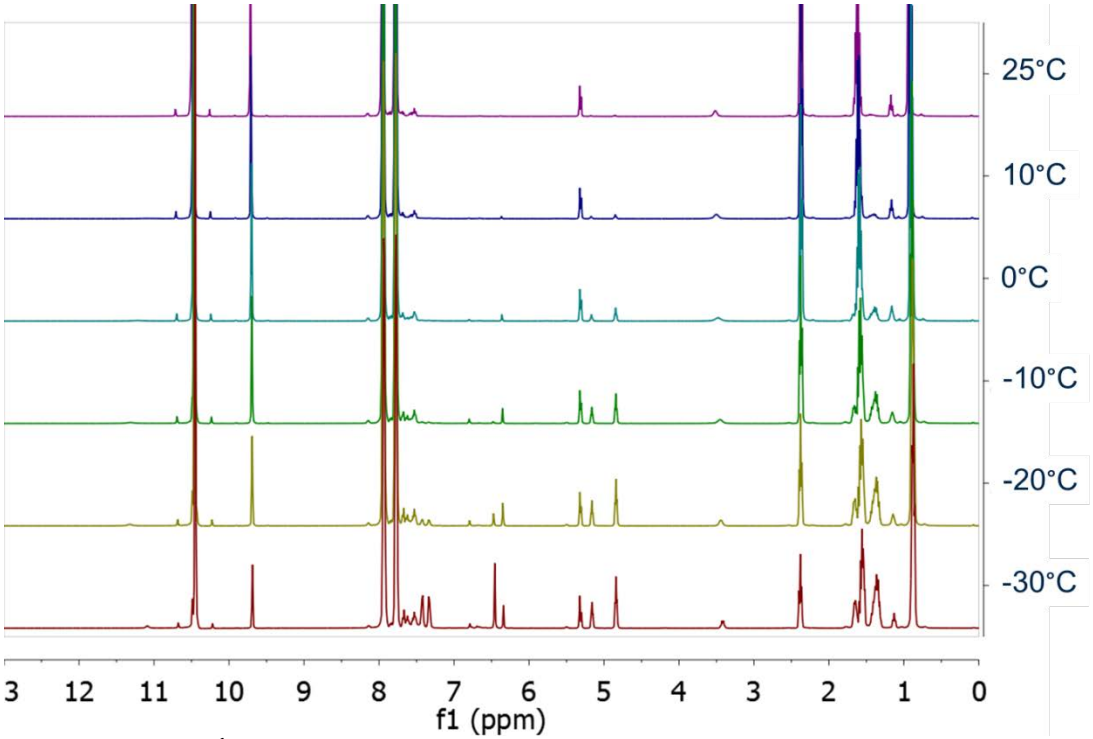

Figure 6.8. ^{1}H NMR spectra of the polymerization of butyraldehyde and phthalaldehyde for the temperature range of 25°C to -30°C.

As with the BA-only reaction, a peak corresponding to the formation of BA trimer at 4.84 ppm appeared at temperatures below about $10^{o}C$. There is not, however, a peak corresponding to the BA trimer/BF_3 complex, as was seen at 6.59 ppm with the BA-only synthesis. It appears that the reason for this is the affinity of BF_3 for the PHA monomer. The BF_3 catalyst preferentially bound to the PHA monomer over the BA monomer. This conclusion is supported by the observation that a peak at 6.34 ppm appears in the BA-PHA synthesis that is not present for the polymerization of the PHA or BA homopolymers. The peak at 6.34 ppm can be attributed to BF_3 complexed to a PHA ether that is covalently bonded to a BA, as shown in Figure 6.9. The number of BA or

PHA monomers involved in this structure could not be determined. The chemical structure shown in Figure 6.9 is to provide one possible structure that would satisfy the peak at 6.34 ppm. Similarly, another peak at 5.16 ppm appeared and increase in size as the temperature was lowered along with the increase in size of the peak at 6.34 ppm. The peak at 5.16 ppm could be the BA ether proton when covalently bonded next to a PHA monomer. As the temperature was lowered to approach the PHA ceiling temperature, the peaks associated with the formation of the poly(phthalaldehyde) ether backbone, broad peaks from 6.25 to 7.25 ppm, and the complexation of $BF_3$with the poly(phthalaldehyde) backbone, singlet at 6.45 ppm, also appeared.

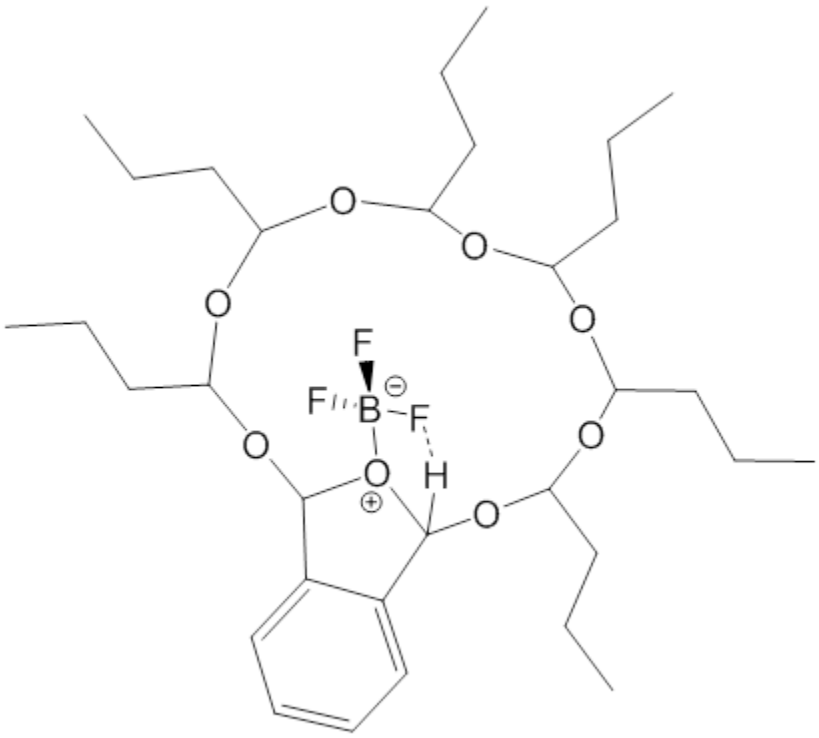

Figure 6.9. One possible structure for the polymer formed with one phthalaldehyde and multiple butyraldehyde monomers. A BF_3 molecule is also shown to illustrate a possible complexation structure to explain ^{1}H NMR peak at 6.36 ppm.

Lowering the temperature below -30°C allows PHA to copolymerize with BA, because PHA is below its ceiling temperature. Figure 6.10 shows the in-situ ^{1}H NMR spectra for the copolymerization of PHA and butyraldehyde from -30°C to -80°C. The broad polymer peaks at 6.25 to 7.25 ppm associated with polymerized PHA become more pronounced at lower temperatures. The butyraldehyde monomer and trimer peaks are unaffected by the drop in temperature from -30°C to -80°C, because the BA utilization is already at its maximum as observed in the BA-only NMR.

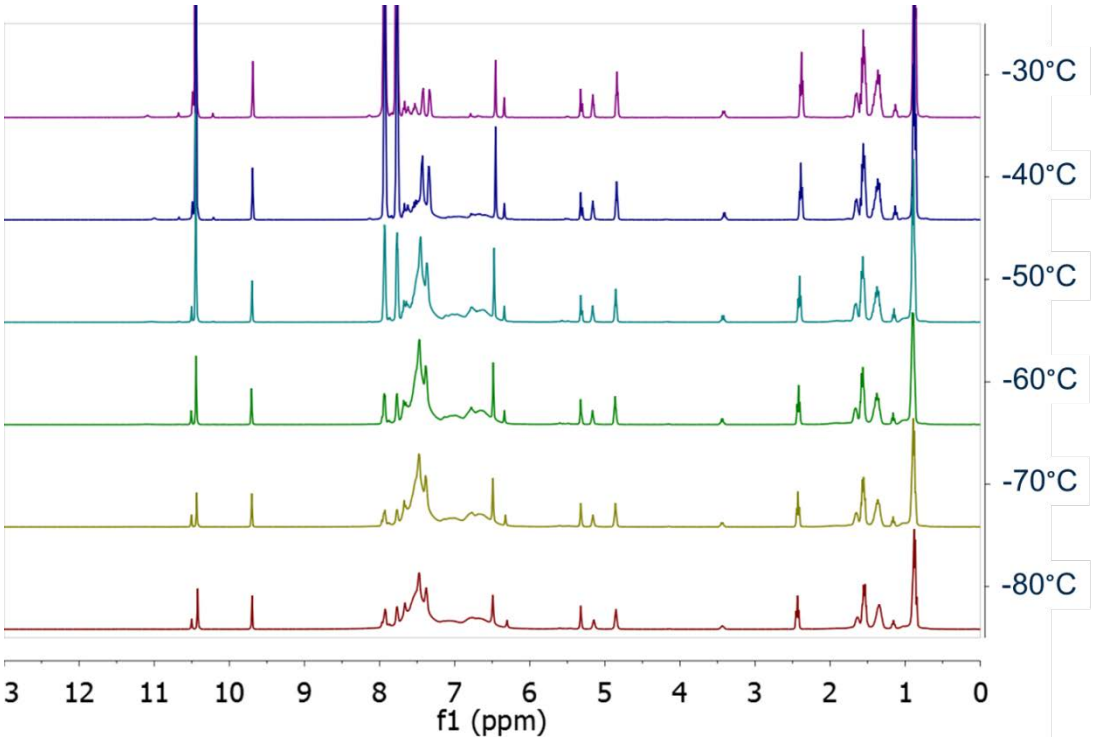

Figure 6.10. ^{1}H NMR spectra of the polymerization of butyraldehyde and phthalaldehyde for the temperature range of -30°C to -80°C.

Figure 6.11 is an expanded view of the copolymer ^{1}H NMR spectra for the range of -30°C to -80°C to better show the polymer peak associated with butyraldehyde incorporation into the BA-PHA copolymer. The broad peak from 5.3 to 5.6 ppm is associated with protons of the butyraldehyde ether when the BA is incorporated into the

BA-PHA copolymer. At the lowest temperature, -80°C, the BA content in the BA-PHA copolymer is 5 mol% butyraldehyde.

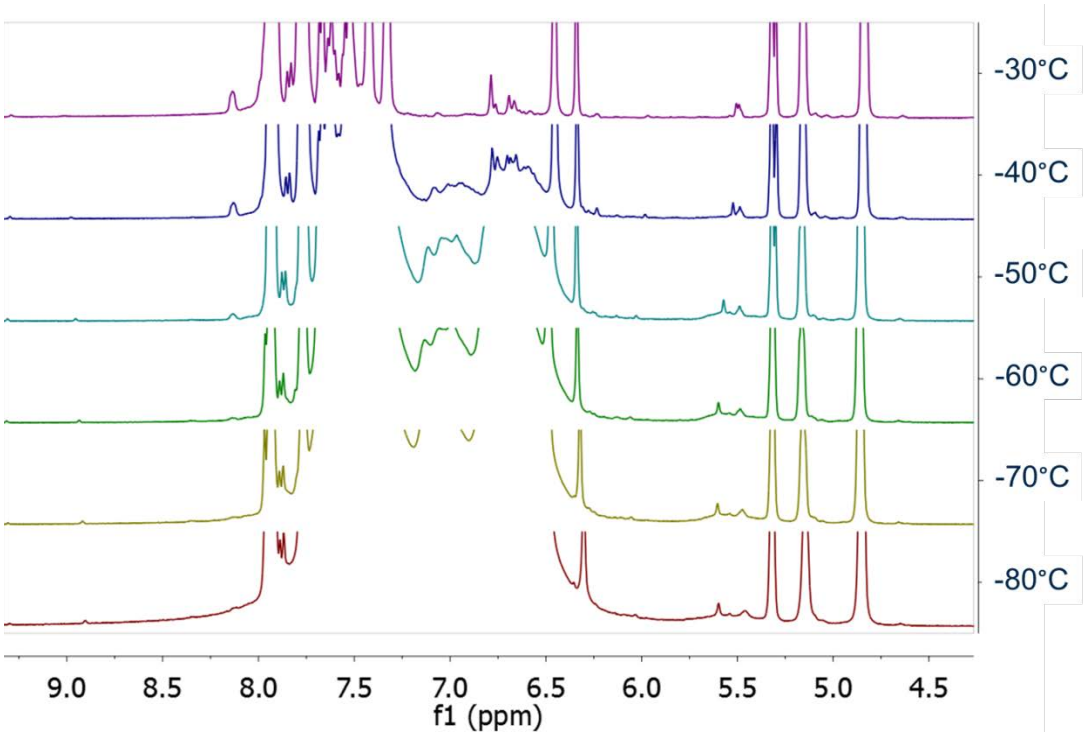

Figure 6.11. Enlarged section of the ^{1}H NMR spectra of the polymerization of butyraldehyde and phthalaldehyde for the temperature range of -30°C to -80°C.

The effect of temperature on the BA-PHA copolymerization can be examined by measuring the BA and PHA monomer concentrations. The natural log of BA monomer concentration versus inverse temperature is shown in **Error! Reference source not found.**. Unlike the case with the BA only polymerization, BA uptake in the polymerization reaction does not begin until the temperature drops to about 0°C. This is likely due to participation of PHA in the reaction. Similar to the BA-only reaction, the BA monomer concentration drops only until the temperature is about -30°C. Below -30°C, the BA monomer concentration does not decrease further. Linear regression of the log of BA vs 1/T in the linear region of the BA ceiling temperature gives a ceiling

temperature for BA of -0.3°C, enthalpy of formation of -15.1 kJ/mol, and entropy of formation of -44.9 J/mol-K. Table VIII shows the thermodynamic values and ceiling temperatures for BA trimer and the copolymer synthesis. The copolymer values are slightly more exo-enthalpic and exo-entropic than those for the BA trimer. This implies that PHA is changing the thermodynamic equilibrium for BA polymerization by allowing BA to form a larger molecule than just a trimer.

Table VIII. Comparison of butyraldehyde variables for trimer and copolymer formation.

Source	ΔH (kJ/mol)	ΔS (J/mol-K)	T_c
BA Trimer (Hashimoto, et al.)[96]	-12.6	-42.3	22.0°C
BA Trimer (This study)	-12.1	-38.9	20.6°C
BA in p(PHA-co-BA)	-15.1	-44.9	-0.3°C

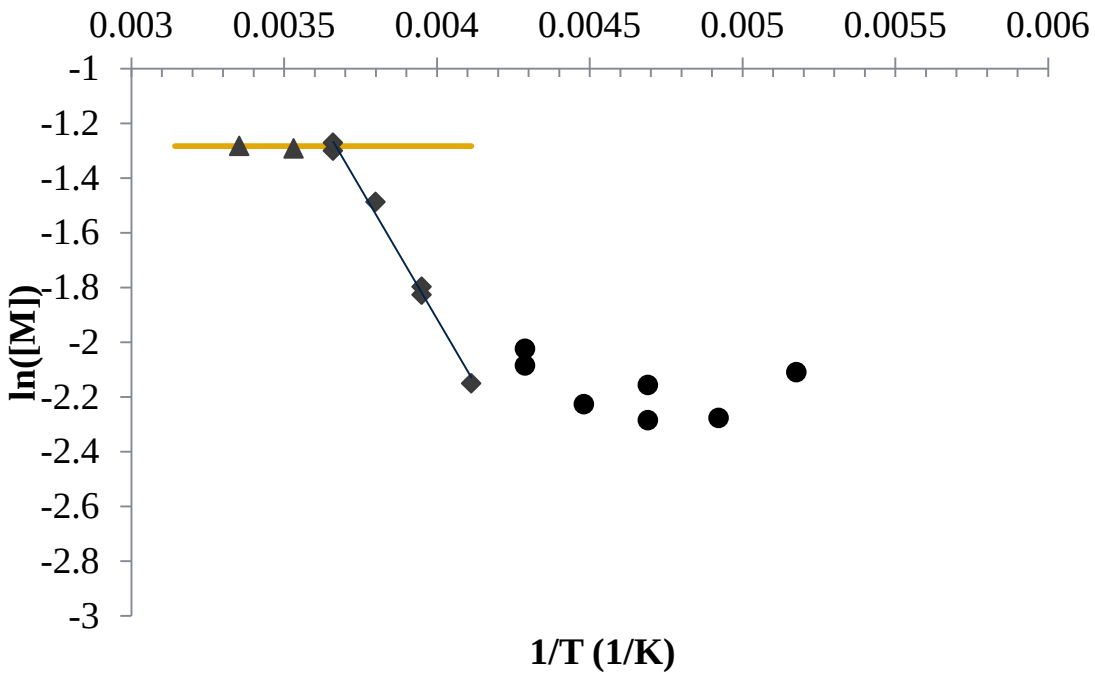

Figure 6.12. Natural log of the saturation concentration of butyraldehyde versus inverse temperature as determined by the ^{1}H NMR spectra in the polymerization of butyraldehyde and PHA with region of minimal polymer formation (triangles), region of ceiling temperature (diamonds), and saturated polymer (circles). The bold line represents initial concentration.

The incorporation of PHA into the copolymer helps maintain the solubility of the polymer in the solvent during polymerization by breaking up the high crystallinity of BA polymer.[56] As shown, the yield of PHA copolymer is higher at colder temperatures. This is shown in Figure 6.13, where the log of PHA monomer concentration is plotted vs inverse temperature. The PHA monomer concentration drops with temperature, just as with PHA homopolymer synthesis except at -80°C where the PHA monomer concentration increased slightly. This could be due to the insolubility of copolymer formed, or the fact that the equilibrium with BA was negatively impacted by lowering the temperature to colder values. Linear regression of Figure 6.13 in the region of the ceiling

temperature yielded thermodynamic variables associated with PHA copolymerization: enthalpy and entropy of formation are -25.9 kJ/mol and -104.0 J/mol-K, respectively, and the ceiling temperature is -30.2°C. The thermodynamic values are significantly less negative than for the PHA polymerization. One explanation could be that the low molecular weight copolymer formed with BA creates an unfavorable pathway to achieving a high molecular weight copolymer. An alternative explanation could be that initiation of a copolymer chain involves a ratio of the two individual monomer energies of formation, giving an apparent increase (less exo-enthalpic and exo-entropic) in the PHA thermodynamic values. PHA in the copolymer has a warmer ceiling temperature, which can be attributed to the incorporation of PHA into a low molecular weight BA copolymer.

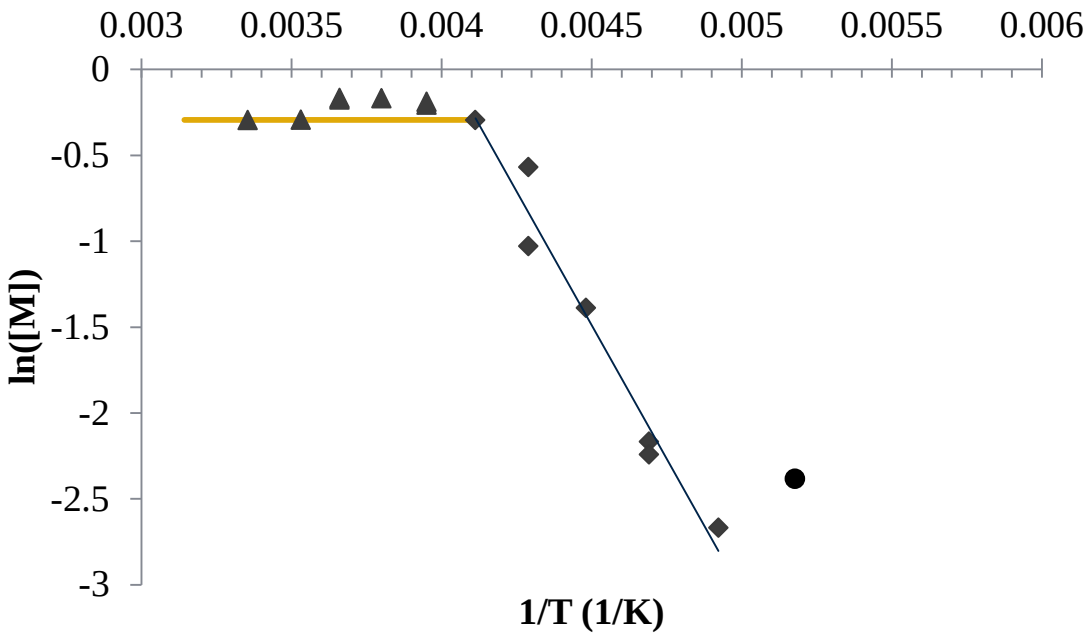

Figure 6.13. Natural log of the saturation concentration of PHA versus inverse temperature as determined by the ^{1}H NMR spectra in the polymerization of butyraldehyde and PHA with region of minimal polymer formation (triangles), region of ceiling temperature (diamonds), and region of saturated polymer concentration (circles).

6.3.4 Poly(γ-butyrolactone)

The evaluation of thermodynamic variables by in-situ ^{1}H NMR can easily be extended to other low ceiling temperature polymers. One such polymerization, poly(γBL), was attempted with the technique. Some yields at various temperatures for the polymerization of p(γBL) have been previously reported.[65] The yields did not completely capture a region of polymer formation that could be used for measuring the ceiling temperature and accompanying thermodynamic variables. The polymerizations were recreated to capture a region of polymer formation that could be described by the linear regression used previously. The polymer was initiated with benzyl alcohol. Polymerizations were performed in THF over 4 hours, as described in Hong, et al.[65] Polymerizations at 25°C, 0°C, and -18°C yielded no polymer. Figure 6.14 shows the natural log of the monomer saturation concentration based on polymer weight yield versus the inverse of temperature in Kelvin. Figure 6.14 also includes the conversion percentage reported by Hong, et al. at the temperature reported.[65]

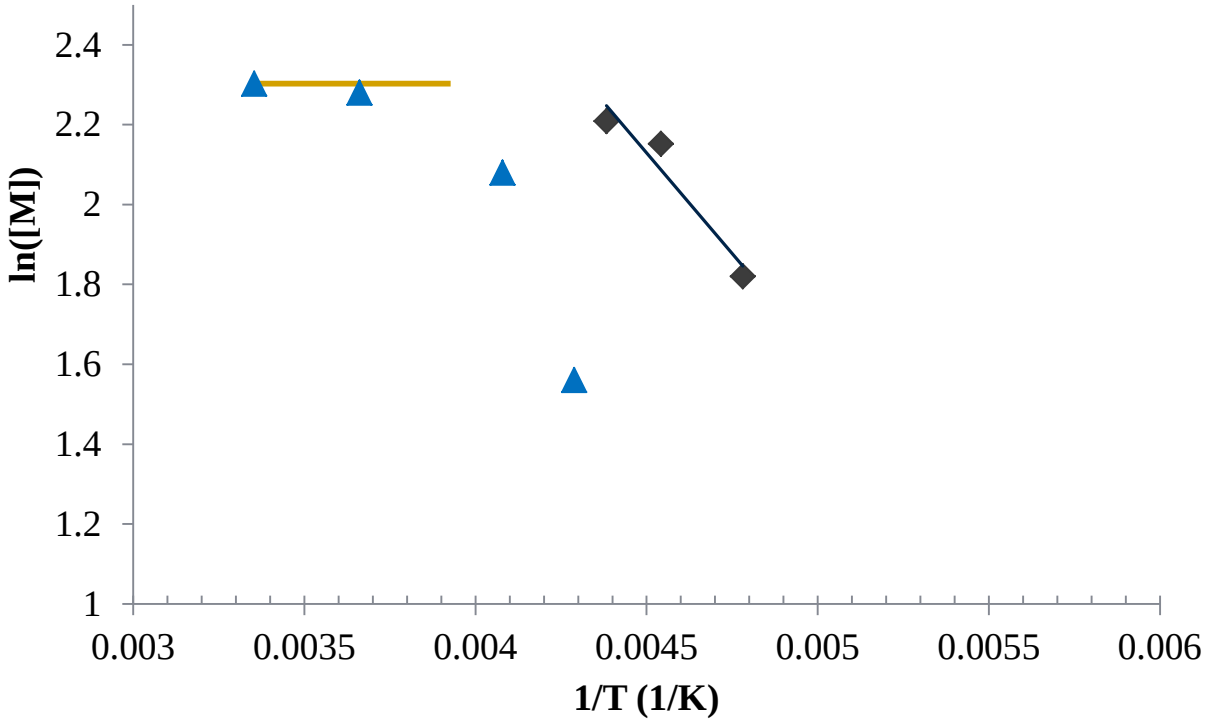

Figure 6.14. Natural log of the saturation concentration versus inverse temperature for the polymerization of p(GBL) as determined by conversion (Hong, et al., triangles) and polymer yield (this paper, diamonds).

The evaluation of the thermodynamic variables associated with the p(γBL) can be done for both the data calculated in this report and the data available from Hong et al. For the data collected in this report, the enthalpy and entropy of formation are -8.4 kJ/mol and -55.4 J/mol-K, respectively, with a ceiling temperature of -42.1°C. For the data available from Hong et al., the enthalpy and entropy of formation are -20.6 kJ/mol and -101.2 J/mol-K, respectively, with a ceiling temperature of -22.5°C. The two data sets clearly are not in agreement. This could be due to a number of factors including the purity of reactants as well as the preparation of reaction glassware.

The evaluation of the thermodynamic variables by ^{1}H in-situ NMR should provide evidence of the true values. Figure 6.15 is the ^{1}H in-situ NMR spectra for the

polymerization of p(γBL) for the temperature range of 25°C to -55°C. The temperature of -55°C was chosen as the lower bound because the reaction solution will freeze at much colder temperatures. The monomer has peaks at 2.21 and 2.35 ppm in THF-d_8. There are no visible changes in the spectra at any temperature despite experimental evidence that polymer would form at these temperatures. The differences between the peak locations of the polymer and monomer are too small to be deconvoluted.

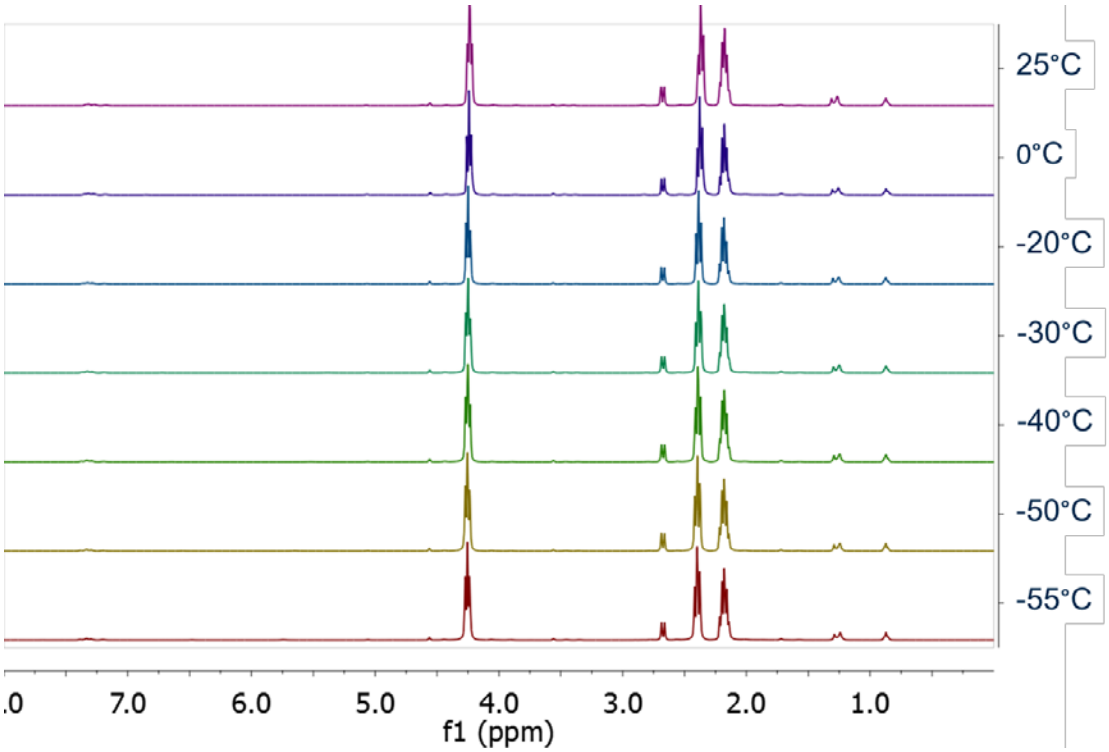

Figure 6.15. In-situ ^{1}H NMR spectra for the polymerization of p(GBL).

There are a few peaks, not associated to the monomer, that shift. These peaks, at 5.75 and 6.45 ppm, are most pronounced at the coldest temperature, -55°C. The integrations of these peaks are constant at all temperatures. The cause of this shift in peaks is unknown, but could be attributed to propagating polymer chains. Figure 6.16 is an enlarged version of the same spectra from Figure 6.16 to better elucidate small peak changes.

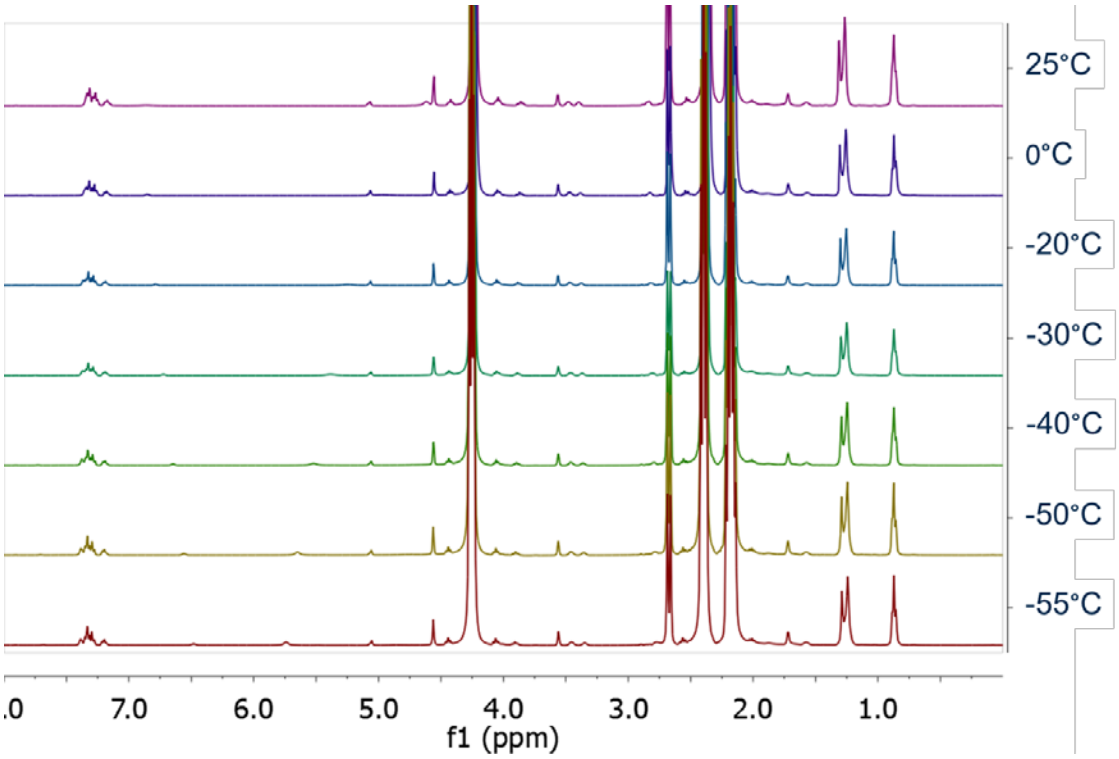

Figure 6.16. Enlarged view of the in-situ ^{1}H NMR spectra for the polymerization of p(GBL).

Unfortunately, the ^{1}H in-situ NMR technique will not work for every low ceiling temperature polymer. Polymers must be carefully chosen to have significantly different peak locations than their monomers.

6.4 Conclusions

The thermodynamic variables for three low ceiling temperature polymerizations were determined by ^{1}H NMR. The accuracy and ease of measuring the monomer saturation yield in-situ provide a reliable method for determining ceiling temperature. Additional thermodynamic information was obtained from the in-situ measurements, including thermodynamic values, the role of the catalyst, and insight into the mechanisms of polymerization. These insights into the equilibrium of low ceiling temperature polymers can lead to improved control over the polymer that is formed.

6.5 Recommendations

The continued evaluation of other coaldehydes in the polymerization of an aldehyde copolymer would prove valuable to finding a high vapor pressure polymer. Terpolymers of aldehydes could provide the necessary reactivity ratios and possibly help break crystallinity that is observed for the aliphatic aldehydes. In-situ ^{1}H NMR seems to provide a tool for finding the correct reaction conditions for a copolymerization. Prior to any attempts to polymerize other aldehydes, this technique could prove very valuable to the researcher to elucidate any limitations to the polymerization of any comonomers.

CHAPTER 7. ANIONIC POLYALDEHYDES

The use of the anionic mechanism for aldehyde polymerization allows two modes of decomposition to be used, namely end-cap removal and random bond scission, as described earlier. Having both mechanisms available for the depolymerization reaction may provide multiple means of triggering transience as well as potentially speeding up the depolymerization. Thus, the anionic mechanism was attempted first with the intent of utilizing multiple modes of decomposition.

This study attempts to elucidate all of the small changes to the polymerization reaction that could lead to high molecular weight polymer through an anionic initiation. The misleading and deceptive descriptions in literature are discussed for the anionic polymerization of phthalaldehyde. The results of attempts to recreate the conditions described in various reports show a conflicting and complex understanding for the anionic polymerization of phthalaldehyde. The anionic polymerization of phthalaldehyde is not understood as thoroughly as literature would suggest. Anionic Polymerization of Poly(phthalaldehyde) Data is the tabulated results of all anionic polymerization attempts.

7.1 Reproducibility of Syntheses

Synthesis of polyphthalaldehyde via the anionic route has been in literature for quite some time.[24] Recently, researchers discovered an easy way to alter both the initiator and the end-cap.[60] This allows the use of both ends of the polymer to initiate a triggered depolymerizaiton. Previously, only the end-cap was easily altered, limiting the sensitivity of the polymer to an external stimulus. The new method, shown in Figure 7.1,

uses a strong base to deprotonate an alcohol (I) which acts as the anion initiator for the phthalaldehyde (II). The polymerization is then quenched by the addition of pyridine and a strong electrophile that acts as the end-cap (III). Typically, the alcohol is one that is very easy to dry, and the end-cap has a good leaving group, like a halide.

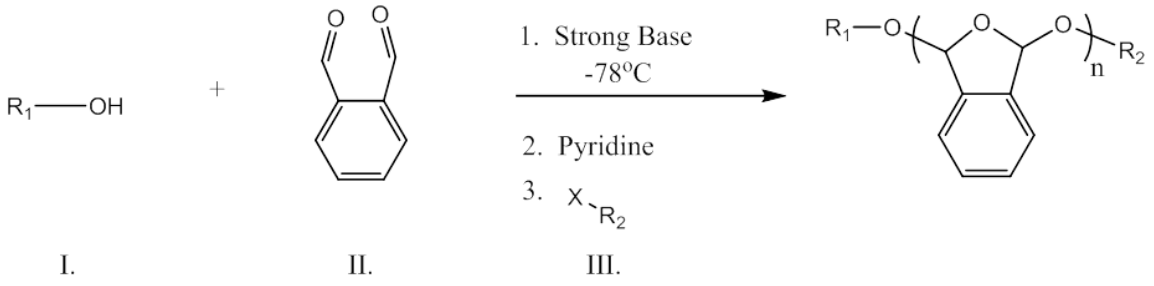

Figure 7.1. General procedure for the anionic polymerization of phthalaldehyde.

Changing the alcohol initiator, the strong base, the monomer purity, the reaction solvent, the end-cap, the reaction time, and the reaction vessel all affect the polymerization.[60,75,102] Targeting one cause for the success or failure between polymerizations is difficult due to the number of variables. The following sections use changes in these variables in an attempt to help the fundamental understanding of the anionic polymerization mechanism.

7.1.1 Targeting High Molecular Weight

Numerous reports discuss the synthesis of PPHA, although none target high molecular weight. Dilauro, et al. describe a scalable anionic synthesis of PPHA with reproducible molecular weights and yield.[60] De Winter, et al. attempt to minimize the Đ of PPHA to achieve high quality polymer with predictable molecular weight.[75] Others focus on the application more than the polymer itself, and once the polymer performs the function necessary for their application, syntheses end.[24,102,103]

In this project, recreating the previous reports was the initial focus. A thorough literature review revealed a few options for anionically produced PPHA that provided high molecular weight with at least moderate yields. Reproducibility was a key aspect of many of these papers. The purity of the starting materials was altered first to attempt to view the trends observed in these literature sources.

Polymerizations of phthalaldehyde were performed with different monomer purification procedures. Table IX shows the best yield and molecular weights achieved by the respective purification procedures. In some cases, different initiating alcohols and end-caps were used. This table represents the best case scenario for each purification procedure. Slight improvement is seen for purified material over the raw monomer. The results do not, however, show the same success seen in literature by improving the monomer purity. There are numerous possible explanations, especially when the purity of the reaction solvent and alcohol have not been improved.

Table IX. Yield, molecular weight, and *Đ* for different purification procedures for phthalaldehyde.

Monomer (PHA)		Solvent		Initiator		End cap	Yield	M_n Actual
Purification	g	Abbrev.	Distilled (Y/N)	$M_{n(th)}$	Abbrev.	Abbrev.	%	kDa
1X Recrystallized	2	THF	N	115.0	n-HOS	MC	2%	6.1
2X Recrystallized	2	THF	N	115.0	n-HOS	MC	3%	
3X Recrystallized	1	THF	N	50.0	2-NB	4-NPC	96%	7.0
4X Recrystallized	2	THF	N	115.0	n-HOS	MC	0%	
5X Recrystallized	1	DCM	Y	67.0	IPA	AC	81%	5.8
Raw	3	THF	N	23.0	2-NB	4-NPC	90%	6.2
Sub	1.5	THF	N	2398.8	2-NB	MC	84%	3.3
Toluene Azeotrope	1	THF	N	67.0	IPA	AC	0%	
Vac-Dried	4.2	THF	Y	115.0	IPA	MC	0%	

After the failure of monomer purification, different procedures were performed to purify THF for use in the reaction. First, Dri-Solv THF was purchased from and used in a polymerization. No yield was obtained. In another attempt, anhydrous THF was purchased from BDH. Approximately 200 mL was added to a round bottom flask with CaH_2 and purged with Ar. After 24 h of stirring, three freeze-pump-thaw cycles were performed to remove any gases remaining in the solvent. The THF was then distilled over molecular sieves, where three more freeze-pump-thaw cycles were performed. The resulting THF was distilled directly into a reaction vessel containing monomer that was kept under vacuum for 24 h. A solution of n-HOS and P_2-t-Bu was prepared prior to adding to the reaction. This solution was then added and the reaction proceeded as above. Again, no yield was obtained.

DCM was also used in various conditions. Table X shows the attempts made to vary solvent purity and solvent ratios to obtain the highest yield. All Polymerizations were based on 1 g of phthalaldehyde and monomer that was unpurified.

Table X. Yield, molecular weight, and *Đ* of the anionic polymerization of phthalaldehyde with different solvent systems.

Solvent			Initiator		End cap	Yield	M_n Actual	*Đ*
Abbrev.	Distilled (Y/N)	$M_{n(th)}$	mol/mol PHA	Abbrev.	Abbrev.	%	kDa	M_w/M_n
DCM	Y	67.0	0.0020	IPA	AC	21%	9.5	
DCM	N	44.0	0.0030	t-BDMS	AA	22%	9.1	2.1
THF/DCM	N	44.0	0.0030	t-BDMS	AA	8%	4.1	1.5
THF	N	44.0	0.0030	t-BDMS	AA	44%	12.3	1.8

Reaction size was another variable explored for obtaining high molecular weight polymer. All polymerizations were performed in as-received anhydrous THF with n-HOS as the initiator and VC as the end-cap. The phosphazene was held constant at a 2 to

1 molar ratio to the alcohol. In every case, the polymer was either not obtained in high enough yields to perform GPC, or the polymer depolymerized prior to successfully measuring molecular weights by GPC. Table XI shows the yield when changing the reaction size. Some variation in alcohol concentration was also used, but resulted in limited success in changing yield or molecular weight. Once again, obtaining high molecular weight polymer was unsuccessful.

Table XI. Yield for the anionic polymerization of phthalaldehyde with different reaction sizes.

Monomer (PHA)		Initiator			Yield
Purification	g	$M_{n(th)}$	mol/mol PHA	Abbrev.	%
Raw	4.7	9.0	0.015	n-HOS	72%
Raw	5	9.0	0.015	n-HOS	0%
Raw	4	9.0	0.015	n-HOS	0%
Raw	3	67.0	0.0020	n-HOS	29%
Raw	10	67.0	0.0020	n-HOS	11%

7.1.2 Initiation of Poly(phthalaldehyde)

Another aspect that can easily alter the quality of PPHA is the method of initiation. Different bases can be used to deprotonate the alcohol initiator. Choosing an alcohol that also creates higher quality polymer can be a challenge. The ability to remove water from the alcohol is probably most important, but the substituent groups on the alcohol can also have an effect on the resulting polymer. DBU, TBD, Phosphazene base choice. Instability of phosphazenes in DCM.[65,75]

The deprotonation of the initiating alcohol can be performed by a number of strong bases. Some strong bases that have been used are diazabicycloundecene (DBU), triazabicyclodecene (TBD), and phosphazene structures. Usually, phosphazenes are

favored due to their relative stability and base strength.[75] While bases like DBU and TBD do yield polymer, they either have low yields or very high dispersities.[75] Efforts here were focused on using phosphazene bases to initiate the polymerization of phthalaldehyde.

The first used in this study, P_2-t-Bu, was chosen as a result of the procedure described in the paper by DiLauro, et al. Table XII shows the polymerization molecular weights and yields as a result of adjusting the phosphazene ratio. There is seemingly no dependence on the catalyst loading.

Table XII. Yield, molecular weight, and dispersity for anionically initiated polymers with different catalyst ratios.

Monomer (PHA)		Initiator		P2-t-bu	End cap	Yield	M_n Actual	*Đ*
Purification	g	$M_{n(th)}$	Abbrev.	mol/mol PHA	Abbrev.	%	kDa	M_w/M_n
Raw	1	67.0	IPA	0.0040	AC	10%	8.9	1.9
Raw	1	67.0	IPA	0.0067	AC	11%	8.0	2.2
Raw	1	67.0	IPA	0.0093	AC	16%	8.5	2.0
3X Recrystal	3	115.0	n-HOS	0.0011	MC	0%		
3X Recrystal	2	115.0	n-HOS	0.00056	MC	0%		
3X Recrystal	2	115.0	n-HOS	0.00028	MC	0%		
3X Recrystal	2	115.0	n-HOS	0.00014	MC	0%		
3X Recrystal	2	115.0	n-HOS	0.0023	MC	2%	3.8	1.4

Further discussions with one of the authors of the DiLauro, et al. paper revealed that the combination of P_2-t-Bu and THF did not ever yield quality polymer.[60] The suggestion was to use P_2-t-Bu in DCM as some of the reproducible syntheses showed in literature. Since the publication of the procedure in 2011, there have been a few more self-immolative polymer synthesis papers published that utilize phosphazene bases in the reaction procedures.[75,104] Each report varied the reaction solvent to observe effects on polymer molecular weight. In each case, the catalyst did not yield a stable anion for

polymerization in DCM. The role of P_2-t-Bu in the polymerization of phthalaldehyde is not thoroughly understood. P_1-t-Bu was also used in literature for anionic PPHA. Similar to P_2-t-Bu, only a low molecular weight and minimal yield was obtained. This synthesis was performed in THF, which may have been an issue to the synthesis of phthalaldehyde as observed in the use of P_2-t-Bu. As shown in Appendix A, the majority of the work reproduced here was performed with THF as the reaction solvent.

Despite the apparent issues with the base catalyst, efforts were made to choose an alcohol to reproduce the highest molecular weights shown in literature. Trends showed electron donating groups for the initiating alcohol create higher molecular weight polymer. This is likely due to the strength of the anion formed once deprotonated. Multiple alcohols were attempted following this trend to maximize the yield and molecular weight of polyphthalaldehyde. Table XIII shows the molecular weights and yields obtained from 5 different alcohols.

Table XIII. Best case results for different alcohol initiators in the polymerization of phthalaldehyde.

Monomer (PHA)		Solvent	Initiator		P2-t-bu	End cap	Yield	M_n Actual	PDI
Purification	g	Abbrev.	$M_{n(th)}$	Abbrev.	mol/mol PHA	Abbrev.	%	kDa	M_w/M_n
3X Recrystal	4	DCM	67.0	1-PB	0.0047	AC	24%	22.0	2.1
Raw	3	THF	67.0	n-HOS	0.0040	AA	54%		
Raw	2	THF	67.0	IPA	0.0093	AC	24%	11.4	1.8
Raw	1	THF	44.0	t-BDMS	0.0093	AA	44%	12.3	1.8
Raw	3	THF	23.0	2-NB	0.011	4-NPC	88%	6.5	1.8

Generally, the more electron withdrawing substituents on the alcohol resulted in higher yield. Molecular weight, unfortunately, does not follow any particular trend. As seen in this table, molecular weights were limited to approximately 25 kDa.

Another means to facilitate higher molecular weights is reducing the number of potential initiation sites, or reducing the moles of alcohol in the reaction. The amount of alcohol was varied to target different molecular weights over the course of this study. Figure 7.2 shows the molecular weights achieved from each synthesis versus the theoretical molecular weight from a perfect polymerization where each alcohol initiates one polymer chain and propagates equally until full consumption of the monomer. The tabulated form of this data can be found in Appendix A.

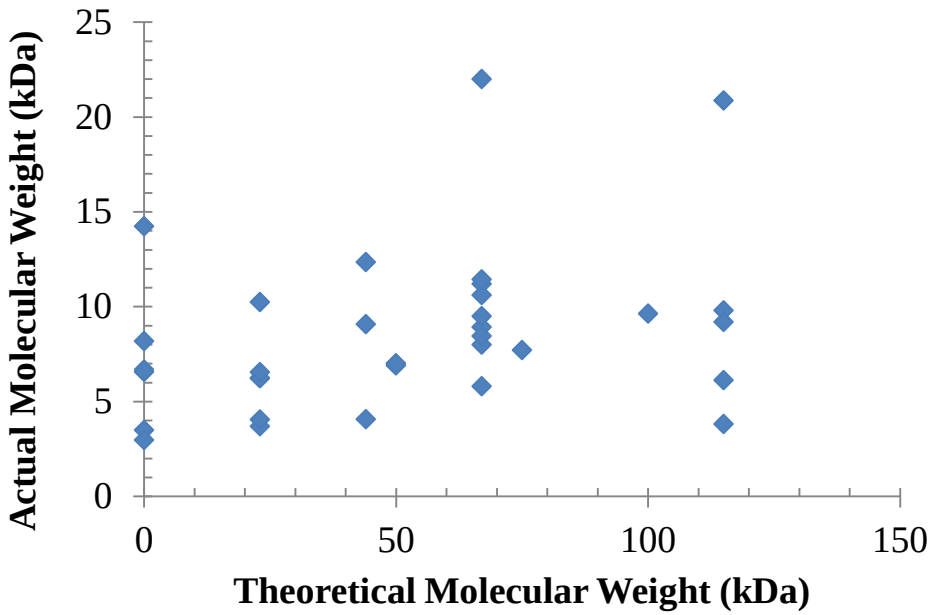

Figure 7.2. Actual versus theoretical molecular weight in the anionic polymerization of phthalaldehyde

Despite the lower amount of alcohol, there is not a trend towards higher molecular weight material. There is a maxima approaching only 25 kDa. Even without an alcohol initiator, polymer forms. This is likely due to the presence of water, or small impurities in the monomer or solvent that is remaining despite the purification by procedures reported in literature.

The procedure can be changed slightly to allow the phosphazene base, P_2-t-Bu, to react with the alcohol first. This should guarantee that the alcohol forms an anion prior to exposing it to the monomer. Unfortunately, over numerous attempts, this procedure did not yield any appreciable polymer.

7.1.3 End-capping of Poly(phthalaldehyde)

The end-capping of anionic-catalyzed PPHA is important for the overall stability of the polymer, but also can provide functionality. A wide range of end-caps were used to see which chemistry promoted the end-capping of high molecular weight material and provided stable material in good yield at room temperature. Another consideration is the reactivity of the end-cap when acting as the strong electrophile. A good leaving group, like a halide, and significant electron withdrawing substituents will promote the end-capping reaction.

In this project, finding an end-cap that provided material stable for long periods of time proved difficult. Either the reactivity of the end-cap was not sufficiently high enough to covalently bond to the polymer chains, or the resulting bonds were unstable at temperatures above the ceiling temperature of PPHA. The classification of end-caps that worked most often was chloroformates. The halogen leaving group and the formate electrophile are the likely reasons for the success of these end-caps.

Beyond the complications of finding an end cap that would provide stable material for any length of time, no end-caps were ever observed in NMR despite the low molecular weights. Low molecular weight is necessary to have a high enough concentration of ends compared to the monomer repeat units. Dilauro, et al. reported one

^{1}H NMR spectra with end-caps shown, however, this result was not reproducible. There is also evidence in literature of the lack of end-caps despite, again, lower molecular weight.[63] Despite claims of easy and reproducible end-capping of PPHA, the chemical characterization of PPHA shows that it may not proceed as expected. A short shelf-life of the anionic-catalyzed PPHA would be expected. The short shelf-life was observed for all anionically polymerized phthalaldehyde.

7.2 Anionically Polymerized Copolymers of Aldehydes

Despite the frustrations of the anionic polymerization route to polyaldehydes, efforts were made to synthesize copolymers of aldehydes. The only success was the polymerization of butyraldehyde with phthalaldehyde. Varying ratios of phthalaldehyde and butyraldehyde were used, but the only ratio to provide yield was 4 moles of phthalaldehyde to 1 mole of butyraldehyde. Table XIV summarizes the limited results obtained from this anionic synthesis of the copolymer prior to abandoning the anionic synthesis altogether.

Table XIV. Summary of anionic butyraldehyde copolymer syntheses

Poly #	M_n Target	M_n Actual	PDI	PHA:BA Ratio	Yield
1	20	7.1	2.1	15	62.0%
2	20	14.2		50	25.0%
3	20	15	1.6	17	43.9%

Similar to the results observed for the hompolymer, high molecular weights were never achieved, although also not attempted. Yields are similar to those achieved from the anionic synthesis of the homopolymer. The molar content of butyraldehyde is inconsistent across the polymerizations.

7.3 Conclusions

The reproducibility of PPHA via the anionic mechanism is suspect. Yields for the anionic mechanism never consistently exceeded 60%. Molecular weights never exceeded 25 kDa, which is the most significant drawback to the anionic synthesis. High molecular weight is necessary to achieve free-standing films due to the chain entanglement. Without molecular weights above 60 kDa, films would have no structural integrity. When polymer was obtained, the average shelf-life of the material was short.

Literature sources provided deceptive procedures and results that are not reproducible. Despite attempting to combine the best-case scenarios from numerous reports, high molecular weight was never achieved. While this is not direct evidence of the anionic mechanism being impossible, it does cast doubt on previous reports.

7.4 Recommendations

Reports of the anionic polymerization of phthalaldehyde suggest a simple and reproducible method for high quality and high molecular weight polymer. The details required for the easily reproduced reaction are likely incomplete. Information regarding the procedures of cleaning glassware and observations of any appreciable color changes could be important to understanding achieving good yield. The procedure for the purification of the monomer could be improved upon as well. Throughout the experiences attempting to purify phthalaldehyde, any contact with moisture in lab air would cause an insoluble and unusable diol to form. There was never mention of this in any of the purification procedures presented in literature, and as the attempts above wore

on, a significant portion of our efforts to purify monomer involved avoiding contact with moisture.

CHAPTER 8. SACRIFICIAL BRACING OF HIGH ASPECT RATIO SILICON STRUCTURES AT THE NANOMETER SCALE

This project focuses on the use of low molecular weight polyaldehydes as a sacrificial bracing material. Substantial work has been performed in trying the sacrificial bracing procedures on different high aspect ratio structures. Pictures are presented when they are available.

8.1 Motivation

The reduction of the size of microelectronics devices has driven industry to create inventive ways of utilizing space more efficiently. Features now tend to use three dimensions as effectively as possible. This means features are taller, thinner, and closer together. As a result of this shrinkage in pitch and exponential increase in the aspect ratio (height to width ratio), there are many traditional operations that will cause the complete destruction of these features. Any wet processing steps now have to be concerned with the collapse of features as a result of stiction, or the surface tension of a drying liquid pulling weak structures together. Higher aspect ratios are especially susceptible to this phenomenon. Methods are desired to allow traditional wet processing steps in areas on a wafer without these structures. This requires bracing of the structures with a sacrificial material.

The best illustration of this unique difficulty comes from a U.S. patent for the removal of a sacrificial bracing material by dry etching in a plasma tool.[105] Sirard, et al. describe the filling of high aspect ratio (HAR) structures with a material that can easily

be removed by an oxygen dry etch. Figure 8.1 shows a cartoon version of the general structure and procedure required to brace and remove the bracing material without causing collapse. This procedure has its limitations, however, especially when minimal oxidation to the underlying features is desired. The use of a low ceiling temperature polymer that has the ability to vaporize directly is an effective solution to this problem.

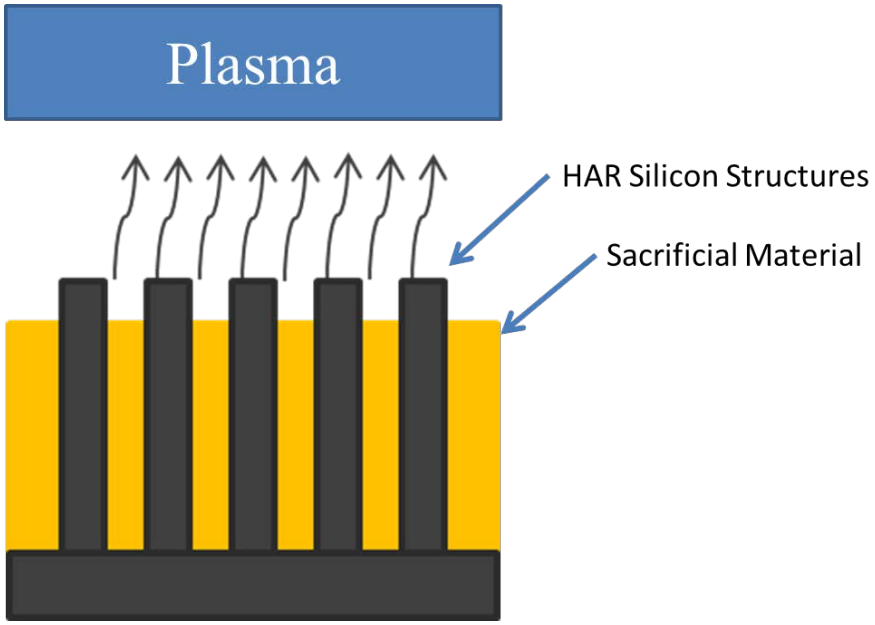

Figure 8.1. Schematic of plasma etching of sacrifical bracing material.

If the depolymerization reaction of a polyaldehyde can be controlled to allow the monomer to evaporate before liquefying, stiction will no longer be a problem. The effective removal of monomer before liquification requires control over a number of variables. The depolymerization rate, the vapor pressure of the monomers, the temperature during decomposition, and the pressure of the environment can all help minimize any liquid state. Depolymerization rate can be controlled by the addition of catalyst, in this case a photo or thermal acid catalyst. Copolymerization of higher vapor pressure aldehydes can help the need for increasing vapor pressure. The vapor pressures

of the monomers can then be increased by using high temperature. By initiating the depolymerization (thermally or photo-catalytically) while operating at a pressure lower than the vapor pressure of the monomer at a specific temperature, the depolymerizing polymer will sublimate, eliminating any surface tension. Figure 8.2 is a cross-sectional image of the silicon HAR pillars being used for this study. The pillars in Figure 8.2 are 430 nm tall and 44 nm wide, a 10:1 aspect ratio, with a 50 nm half pitch.

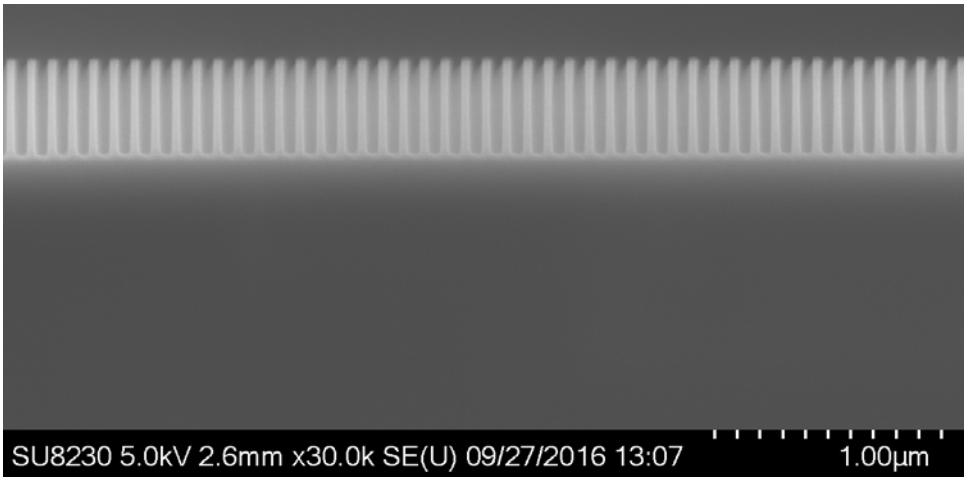

Figure 8.2. Cross-section of untreated silicon pillars.

8.2 Imaging with Heated Stage Microscope

The acid-catalyzed decomposition of polyaldehydes results in a highly exothermic reaction that melts any monomer present even while at room temperature. While this is great for improving the diffusion of acid for thick films, thin films, like those used for the HAR structures, do not need the additional acid diffusion. The liquification of polyaldehydes is a significant concern for the use as a bracing material between HAR structures. Before studying the collapse of HAR structures, a microscope with a heated and pressure-controlled stage was used to verify the importance of temperature, pressure,

and coaldehyde incorporation. A high temperature, low pressure, and high coaldehyde incorporation should all result in minimal liquid formation. Formation of liquid in the microscope is obvious as the polymer changes from a solid to melted monomer.

Polymer films were cast on pieces of bare silicon to observe the formation of liquid. In each case, 10 pphr PAG (Rhodorsil FABA) was also added. The silicon pieces with polymer were placed in the pressure and temperature-controlled microscope. Once at the desired temperature and pressure, the films were exposed to 248 nm light and irradiated for 5 minutes. While decomposing, pictures were taken to visualize the formation of liquid. Table XV lists the comonomers and whether a liquid was observed at each temperature and pressure condition.

Table XV. Visible liquid formation in the depolymerization of polyaldehyde films with PAG.

	Liquid (Y/N)			
Comonomer	**25°C/1 bar**	**25°C/25 mbar**	**80°C/1 bar**	**80°C/25 mbar**
None	Y	Y	Y	Y
BA	Y	Y	Y	N
BZA	Y	Y	Y	Y
T2M2B	Y	Y	Y	N

Butyraldehyde and trans-2-methyl-2-butenal copolymers both showed no visible liquid formation at 80°C and 25 mbar. Only these two polymers are used in further studies for the sacrificial bracing of HAR features. Peak temperatures are higher than 80°C, and vacuum pressures are lower than 25 mbar for all samples hereafter.

8.2.1 Filling of HAR Pillars

Filling the gaps between features without causing collapse is not trivial. The molecular weight of the polymer and choice of solvent is critical to success. Polymer

with molecular weights that are too high will be physically incapable of filling gaps. The solvent needs to be sufficiently low vapor pressure to allow filling before evaporation. Too much solvent can cause collapse. Too little solvent can minimize the ability of polymer to fill gaps.

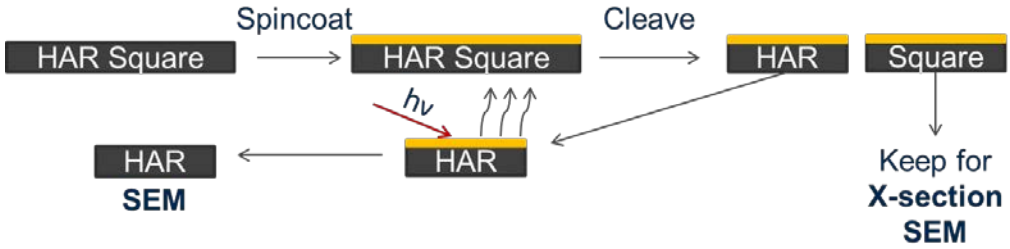

Figure 8.3. Schematic of procedure for HAR pillars decomposed in microscope.

Top-down views provide the best images to compare. The number of pillars collapsed into one focal point is considered for the quality of collapse. Figure 8.4 is an SEM image of an untreated sample for comparison. The rows of pillars (appearing as white dots) can be seen standing with no fallen pillars.

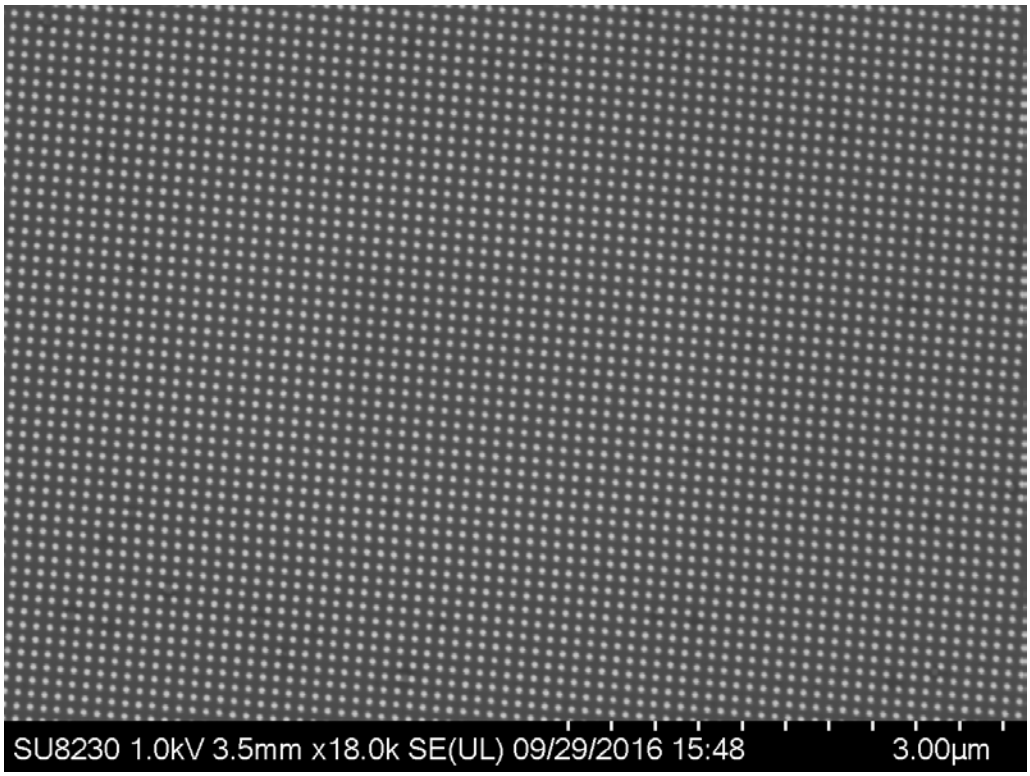

Figure 8.4. Top-down view of HAR pillars prior to any treatment.

Another good comparison to observe is the intentional collapse of the pillars by exposing them to common solvents that could be used during traditional washing procedures. Figure 8.5 are representative images of the collapse caused by dropping water (left) and PGMEA (right) onto 10:1 HAR pillars and allowing the liquid to evaporate. The image on the left shows extensive collapse. A whitening of the image when compared to an untreated sample is the most significant indicator of collapse. The majority of the pillars have collapsed into groups of four, which is common for these features. There are also pockets of collapse where tens of pillars have collapsed into one point. The large pockets of collapse are considered to be the worst case scenario. The sample treated with PGMEA shows far less collapse. The lines of white are groups of

four pillars that have collapsed together in a linear group. The dark spots are an impurity from the solvent, but the exact cause is unknown.

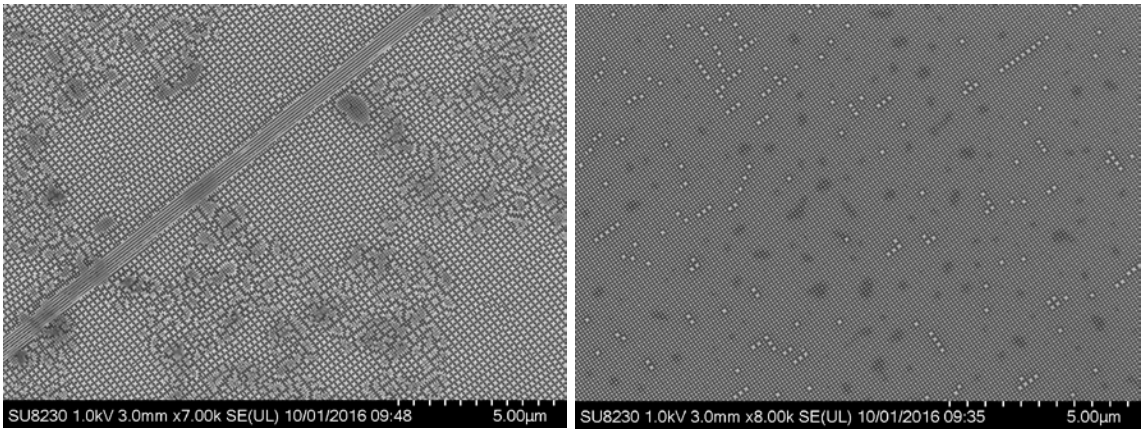

Figure 8.5. Top-down view of HAR pillars treated with water (left) and PGMEA (right), both of which were allowed to dry.

The best image showing the fill of any polymer film was made with a copolymer of phthalaldehyde and trans-2-methyl-2-butenal. The cationically synthesized p(PHA-co-T2M2B) polymer had a molecular weight of 11 kDa. The polymer was dissolved in PGMEA at 5 wt% polymer with 10 pphr PAG (Rhodorsil FABA). The formulation was spin-cast onto an HAR pillar piece with a ramp rate of 300 rpm/s to 1500 rpm sustained for 60 s. The resulting film was soft baked at 55°C for 5 min. The polymer-filled HAR structure was cleaved in half to obtain a cross-section image of the polymer fill. Figure 8.6 shows the cross-section SEM image of the p(PHA-co-T2M2B)-filled HAR pillars. As seen in the image, the polymer does not appear to fully penetrate the pillars. This incomplete filling also appears to have caused collapse of the pillars. It was later discovered this is likely not the case.

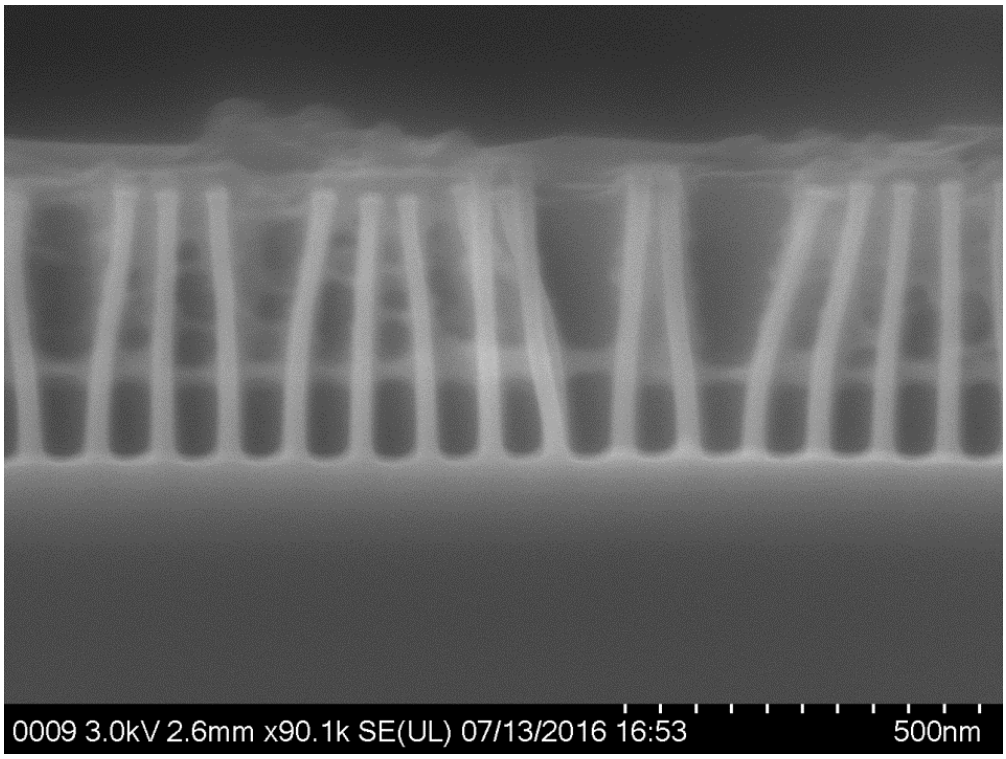

Figure 8.6. Cross-section of polymer filled pillars.

Through various attempts to image the fill of the polymer in the HAR pillars, it was discovered that the electron beam causes depolymerization of the polymer films. The polymer is too sensitive to be imaged by an electron beam. Signs of depolymerization were observed within seconds of focusing on a small section of polymer-filled pillars. It is unclear if the incomplete filling of the pillars or the uncontrolled depolymerization once the polymer was exposed to the electron beam is the cause of the collapse and incomplete filling seen in Figure 8.6.

Since the imaging of polymer-filled pillars proved difficult, a different solvent was chosen for spincoating to create thicker films. For a sustained, high decomposition temperature, a thicker film should not be a disadvantage for the pillars. The incomplete filling of pillars by a polymer film that is too thin should be the cause of extensive

collapse if any difference is observed. A phthalaldehyde copolymer (anionic synthesis route) with butyraldehyde with a molecular weight of 7 kDa and 7 mol% butyraldehyde incorporation was used. Two solvents were chosen, THF and PGMEA, which provided thicknesses of 1.5 μm and 0.5 μm, respectively, on a bare silicon wafer. Both samples were decomposed in the microscope at 0.7 mTorr with a ramp rate of 30°C/min to 200°C and an isothermal at 200°C for 30 min. Figure 8.7 shows representative pictures of the effect of decomposing the thicker (left) and thin (right) film on 11:1 HAR pillars. There is effectively no difference between the two thicknesses. This likely means that the thin polymer film does fully fill the silicon pillars. PGMEA as the casting solvent is used for all of the sacrificial bracing that follows. Based on the lack of difference between thicknesses, it is assumed that the polymer films are filling between the silicon structures, although this is still not known.

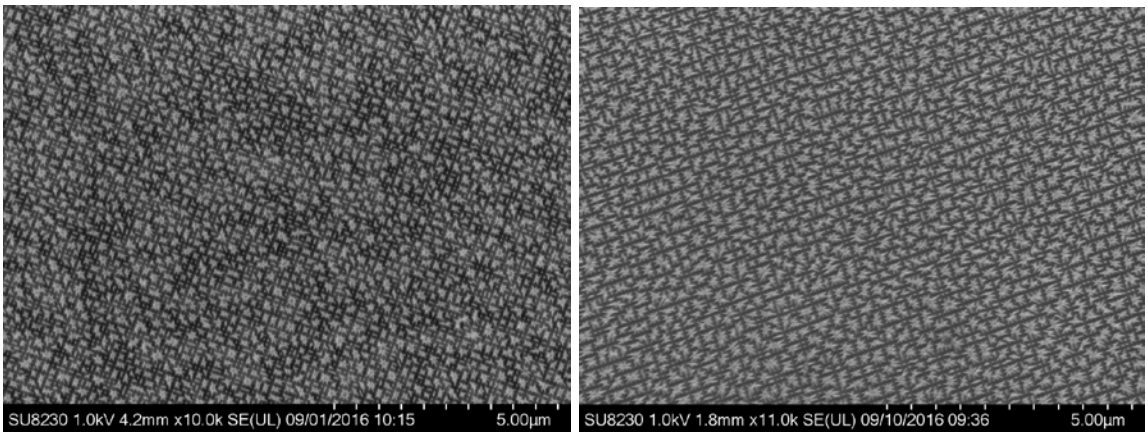

Figure 8.7. Representative SEM images of thick (left) and thin (right) films decomposed on HAR pillars.

8.2.2 *Low Pressure Decomposition of HAR Pillars*

In the same microscope used to determine the length and extent of the liquid states, polymer-filled HAR pillars were treated either to light (with PAG in the formulation) or temperature to remove the polymer. For PAG initiated experiments, a peak temperature of 125°C and a pressure of 0.7 mTorr was used.

The depolymerization of a butyraldehyde copolymer (cationic synthesis route, 20 kDa, 3 mol% BA) with a PAG was attempted first. A solution of 5 wt% polymer was made in PGMEA with 10 pphr PAG (Rhodorsil FABA). The polymer formulation was spin-cast onto an 11:1 HAR pillar sample with a ramp rate of 300 rpm/s to a maximum spin speed of 1500 rpm over 60 s. The resulting film was soft baked at 55°C for 5 min. The polymer-filled HAR sample was then placed in the microscope where a pressure of 0.7 mTorr and temperature of 125°C were sustained prior to exposure with 248 nm light. The sample was irradiated with 248 nm light until no visible changes were observed for 15 minutes. Figure 8.8 is a representative image of the pillar collapse caused by the PAG-initiated decomposition of the polymer film.

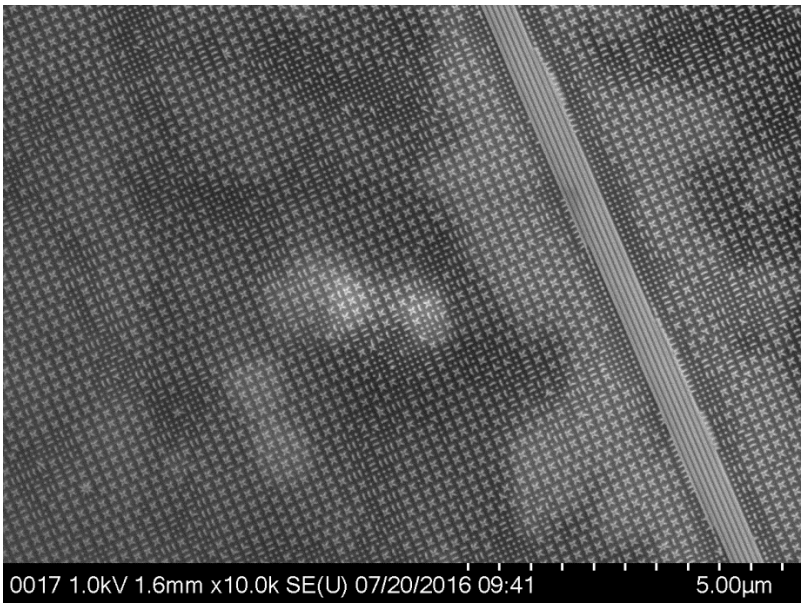

Figure 8.8. Representative SEM image of the HAR pillar collapse caused by the PAG-initiated decomposition of a p(PHA-co-BA) film.

The significant collapse observed is believed to be a consequence of the formation of liquid in the butyraldehyde copolymer films. Despite not observing a liquid state for the copolymer in the microscope, there is extensive formation of liquid to cause the amount of collapse seen in Figure 8.8. The bright spots are assumed to be residue left behind by the PAG. This salt is highly undesirable and led to the abandoning of the photo-catalyzed method.

8.3 Temperature Ramp Rate

Avoiding the liquid state of the depolymerization products will require higher temperatures or a different mode of decomposition than exposure of a homogeneous polymer and PAG film. The purely thermal decomposition of the sacrificial bracing material can achieve the higher temperatures necessary. For these thermal degradation experiments, temperature ramp rates were adjusted to reach the final desired temperature.

Two ramp rates, 1°C/min and 30°C/min, were used for the degradation in the temperature and pressure-controlled microscope. The final temperature of 250°C was held for 30 min. A pressure of 0.7 mTorr was used. Both polymer samples used the anionic synthesis route for p(PHA-co-BA). A 10 wt% solution in PGMEA of the butyraldehyde copolymer was used to cast films. Polymer films were spin-cast with a ramp rate of 300 rpm/s to a peak rpm of 1500 held for 60 s. Figure 8.9 shows representative SEM images of the thermal decomposition of the anionic polymer on 11:1 HAR pillars for the slow (left) and fast (right) ramp rates. Both images show extensive collapse with areas of white being groups of four to twenty pillars collapsed to one point.

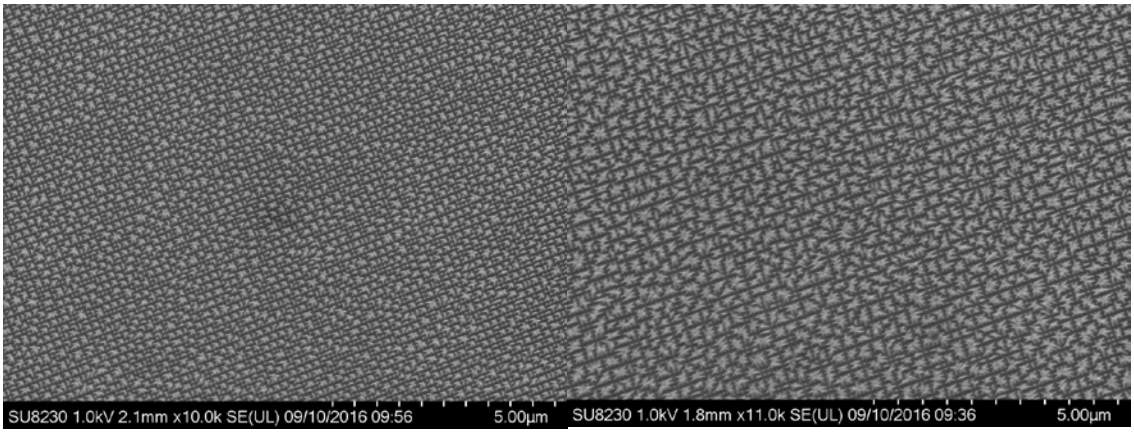

Figure 8.9. Representative pictures of the thermal decomposition of anionic butyraldehyde copolymer on 11:1 HAR pillars for a 1°C/min (left) and 30°C/min (right) ramp rate.

The slower ramp rate appears to have less collapse than the fast ramp rate. There are areas of minimal collapse and a few rows of still-standing pillars. The fast ramp rate seems to have caused significant collapse with more large groups of collapsed pillars when compared to the slower ramp rate. This is likely due to the formation of liquid as a result of the thermal degradation of the polymer prior to exceeding the vapor pressure necessary to have it rapidly vaporize.

The slower ramp rate seemed to improve the amount of collapse seen in the HAR pillars, but a fast ramp rate that can exceed the vapor pressure of the monomer could be beneficial. A low vacuum tool with IR lamps was used to achieve a faster ramp, similar to an RTA, to compare to the slower heating by the microscope. The thermal decomposition was achieved by a 75°C/min ramp rate to 425°C, which was held for 5 min. A vacuum of less than 0.5 mTorr was maintained for the thermal treatment. A 10 wt% solution of the anionic p(PHA-co-BA) in PGMEA was again used. The same spin-cast parameters as before were used. Figure 8.10 shows an SEM image of the RTA-like decomposition of the butyraldehyde copolymer on 10:1 HAR pillars.

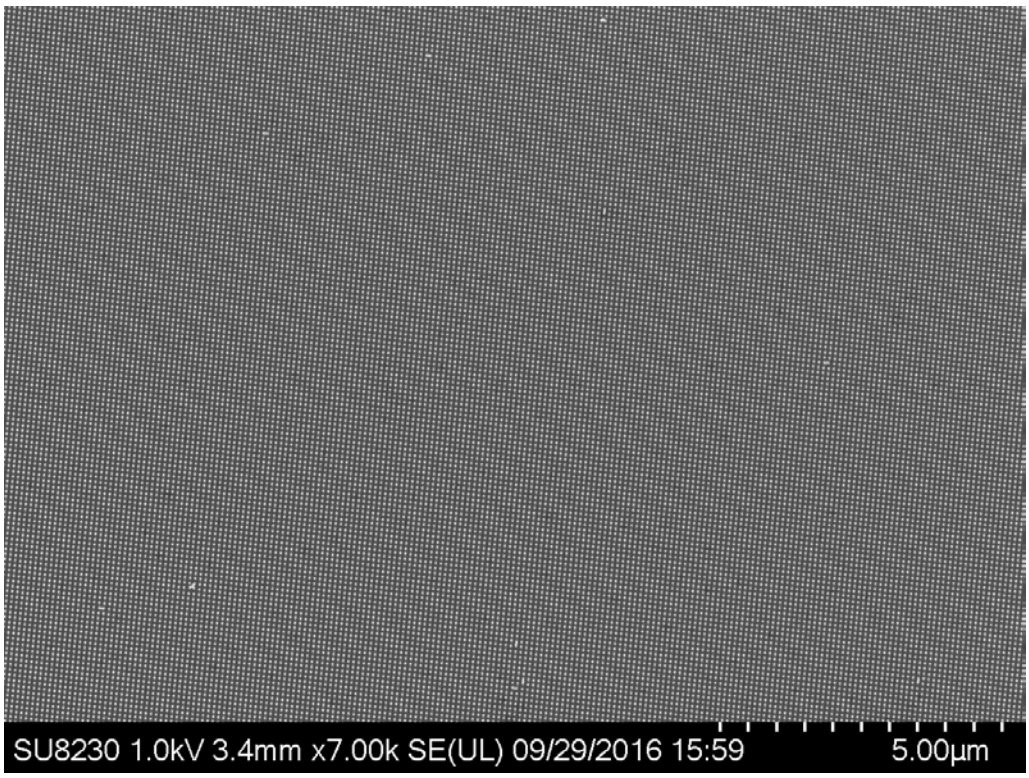

Figure 8.10. Representative image of the thermal decomposition of anionic butyraldehyde copolymer with RTA-like environment on 10:1 HAR pillars.

There is minimal collapse of any features for the rapid temperature ramp. There are a few pillars collapsed, but this could be due to handling of materials and solvents

prior to addition of the polymer. The success of this particular sample is unfortunately convoluted. The very fast ramp rate is probably beneficial to avoiding substantial polymer decomposition before surpassing the vapor pressure of the monomer. The aspect ratio is slightly smaller than some of the previous samples, 10:1 versus 11:1, which might withstand more liquid formation before collapse. There is an obvious success with this sample, and aspect ratios lower than 10:1 should perform equally or better.

8.4 Cleaning HAR Features

One possible explanation for the difficulty of decomposing a polyaldehyde without causing the collapse of HAR features is the surface prior to depositing polymer. Processes used in the fabrication of the HAR features could leave behind residue that could cause depolymerization of a polyaldehyde before it is desired. A procedure was created to remove the potential residue on 10:1 HAR pillars before adding polymer. Any washing requires low vapor pressure solvents that won't create significant surface tension before the polymer can be cast between the pillars. The pillars were first submerged in a bath of water with sonication for 2 min. The pillars were then quickly transferred to a bath of IPA with sonication for 2 min. The pillars were transferred again to a bath of GBL with sonication for 2 min. The solvent coated pillars were quickly moved to a spin-coater where a polymer solution was added before the GBL could evaporate. A similar procedure was used without sonication.

A set of pillars were used to ensure this procedure would not cause the collapse of any HAR features prior to adding polymer. Significant collapse was observed for

samples subjected to sonication. A representative picture is shown in Figure 8.11 (left). The white areas are collapse of pillars in groups of four. In the case of soaking in solvent, the pillars showed minimal collapse after the removal of the polyaldehyde by thermal decomposition at low pressure, as shown in Figure 8.11 (right). Again, the white areas are collapse of pillars in groups of four.

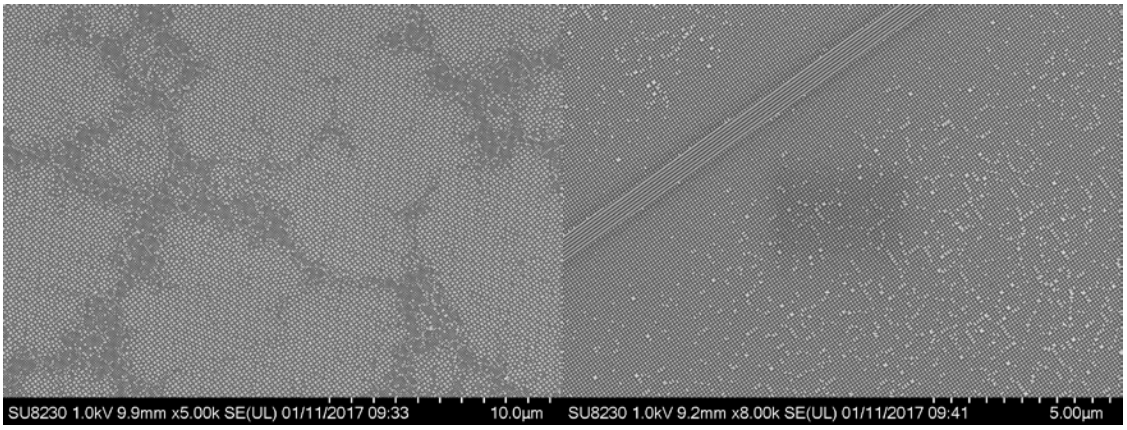

Figure 8.11. Representative pictures of the sonication wash (left) and the dip wash (right) for HAR pillars.

Optimization of the cleaning of the pillars prior to addition of the polymer is clearly needed. The likely cause of the collapse in the dip washed sample is the incomplete filling of the polymer due to the large amount of γBL present before addition of a diluted polymer solution. This will further dilute the polymer and cause incomplete filling. While the presence of cleaning solvents does not appear to cause significant collapse, the removal of residue on the surface of the pillars without creating any additional collapse is necessary.

8.5 Conclusions

The successful bracing of 10:1 HAR structures by a sacrificial polymer has been shown. The filling and decomposition of the polymer was achieved while not causing

collapse to the HAR pillars. The further evaluation of this polymer to achieve the sacrificial bracing of higher aspect ratios is ongoing.

8.6 Recommendations

The continued discovery of polyaldehydes that will depolymerize into higher vapor pressure monomers would be very valuable to the sacrificial bracing of HAR structures. Creating a method of depolymerization as a slow moving front of material could also benefit the bracing of these structures. One method could be introducing a thermal acid generator on the top of the polymer film and allowing the acid to slowly diffuse while maintaining the high vacuum. Another method could be heating purely from the top, which would require some method of radiating heat to only the top layer of the polymer film. Application of the procedures outlined above to other HAR pillars should be pursued. There are limitations to the specific procedures described, but the sacrificial bracing of other structures and aspect ratios is an obvious path forward. Imaging of the polymer fill may be possible through the use of cryogenic SEM. If the imaging were to take place at a temperature colder than the ceiling temperature of the polymer, minimal decomposition would be observed, and the electron beam will likely not cause significant damage.

APPENDIX A. ANIONIC POLYMERIZATION OF POLY(PHTHALALDEHYDE) DATA

Name	Monomer (PHA)			Solvent				Initiator			P2-t-bu	End cap		Pyridine	Yield	M_n Actual	Đ
	Purification	g	mol	[PHA]	mL	Abbrev.	Distilled (Y/N)	$M_{n(th)}$	mol/mol PHA	Abbrev.	mol/mol PHA	mol/mol PHA	Abbrev.	mol/mol PHA	%	kDa	M_w/M_n
20151215	3X Recrystal	4	0.030	0.60	50	DCM	Y	67.0	0.0020	1-PB	0.0047	0.1	AC	0.5	24%	22.0	2.1
20160108	3X Recrystal	2	0.015	0.60	25	DCM	Y	67.0	0.0020	1-PB	0.0047	0.1	AC	0.5	24%	11.2	2.2
20160125	3X Recrystal	1	0.007	0.60	12	DCM	Y	200.0	0.00067	1-PB	0.0047	0.1	AC	0.5	16%		
20150126Pan	Raw	3	0.022	0.60	37	THF	N	50.0	0.0027	2-NB	0.011	0.1	4-NPC	0.5	89%	6.9	1.9
20150127Pan	Raw	3	0.022	0.60	37	THF	N	100.0	0.0013	2-NB	0.011	0.1	4-NPC	0.5	86%	9.6	1.8
20150212APan	Raw	3	0.022	0.60	37	THF	N	200.0	0.00067	2-NB	0.011	0.1	4-NPC	0.5	93%		
20150212BPan	Raw	3	0.022	0.60	37	THF	N	0.0	0.0	None	0.011	0.1	4-NPC	0.5	92%		
20150224APan	Raw	3	0.022	0.60	37	THF	N	0.0	0.0	None	0.011	0	None	0.5	0%		
20150224BPan	Raw	3	0.022	0.60	37	THF	N	0.0	0.0	None	0.011	0	None	0	0%		
20150227Pan	Raw	3	0.022	0.60	37	THF	N	0.0	0.0	None	0.011	0.1	4-NPC	0.5	90%	6.7	1.8
20150302Pan	Raw	3	0.022	0.60	37	THF	N	0.0	0.0	None	0.011	0	None	0.5	0%		
20150303Pan	Raw	3	0.022	0.60	37	THF	N	0.0	0.0	None	0.011	0.1	4-NPC	0.5	89%	8.2	1.9
20150304Pan	Raw	3	0.022	0.60	37	THF	N	0.0	0.0	None	0.0071	0.1	4-NPC	0.5	89%	6.5	1.4
20150310Pan	Raw	3	0.022	0.60	37	THF	N	0.0	0.0	None	0.0036	0.1	4-NPC	0.5	17%		
20150311Pan	Raw	3	0.022	0.60	37	THF	N	0.0	0.0	None	0.011	0.02	4-NPC	0.5	88%		
20150312Pan	Raw	3	0.022	0.60	37	THF	N	0.0	0.0	None	0.011	0.006	4-NPC	0.5	77%		
20150317Pan	Raw	3	0.022	0.60	37	THF	N	0.0	0.0	None	0.011	0.1	4-NPC	0.5	83%	3.5	2.0
20150318Pan	Raw	3	0.022	0.60	37	THF	N	0.0	0.0	None	0.011	0.1	4-NPC	0.5	72%	3.0	1.9
20150506Pan	Raw	1	0.007	0.60	12	THF	N	23.0	0.0058	2-NB	0.011	0.1	4-NPC	0.5	71%	3.7	1.8
20150511Pan	Raw	1	0.007	0.60	12	THF	N	0.0	0.0	None	0.011	0.1	4-NPC	0.5	65%		
20150512Pan	Raw	1	0.007	0.60	12	THF	N	0.0	0.0	None	0.011	0.1	VC	0.5	78%		

20150513Pan	Raw	1	0.007	0.60	12	THF	N	0.0	0.0	None	0.011	0.1	4-NPC	0.5	69%		
20150514Pan	Raw	1	0.007	0.60	12	THF	N	0.0	0.0	None	0.0053	0.1	4-NPC	0.5	9%		
20150518Pan	Raw	1	0.007	0.60	12	THF	N	0.0	0.0	None	0.0053	0.1	4-NPC	0.5	0%		
20150526Pan	Raw	1	0.007	0.60	12	THF	N	0.0	0.0	None	0.0053	0.1	4-NPC	0.5	32%		
20150527Pan	Raw	1	0.007	0.60	12	DCM	N	0.0	0.0	None	0.0053	0.1	4-NPC	0.5	71%		
20150622Pan	Raw	1	0.007	0.60	12	THF	N	0.0	0.0	None	0.011	0.1	4-NPC	0.5	86%		
20150629Pan	Raw	1	0.007	0.60	12	THF	N	0.0	0.0	None	0.011	0.1	4-NPC	0.5	69%		
20150804Pan	3X Recrystal	1	0.007	0.60	12	THF	N	23.0	0.0058	IPA	0.011	0.1	MC	0.5	0%		
20150805Pan	3X Recrystal	1	0.007	0.60	12	THF	N	23.0	0.0058	IPA	0.011	0.1	VC	0.5	0%		
20150806Pan	3X Recrystal	1	0.007	0.60	12	THF	N	23.0	0.0058	IPA	0.011	0.1	VC	0.5	0%		
20150807Pan	3X Recrystal	1	0.007	0.60	12	THF	N	23.0	0.0058	IPA	0.011	0.1	4-NPC	0.5	0%		
20150819Pan	3X Recrystal	1	0.007	0.60	12	THF	N	50.0	0.0027	2-NB	0.011	0.1	4-NPC	0.5	0%		
20150820Pan	3X Recrystal	1	0.007	0.60	12	THF	N	50.0	0.0027	2-NB	0.011	0.1	4-NPC	0.5	0%		
20150827Pan	3X Recrystal	1	0.007	0.60	12	THF	N	50.0	0.0027	2-NB	0.011	0.1	4-NPC	0.5	82%	7.0	
20150831APan	3X Recrystal	1	0.007	0.60	12	THF	N	50.0	0.0027	2-NB	0.011	0.1	4-NPC	0.5	96%	7.0	
20150831BPan-reality	Raw	3	0.022	0.70	32	THF	N	115.0	0.0012	1-PB	0.000058	0.1	4-NPC	0.5	0%		
20150902Pan-reality	Raw	3	0.022	0.70	32	THF	N	115.0	0.0012	1-PB	0.000058	0.1	4-NPC	0.5	0%		
20150909Jared-realilty	Raw	3	0.022	0.60	37	THF	N	75.0	0.0018	n-HOS	0.0023	0.2	MC	0.5	9%	7.7	1.7
20150914Jared	3X Recrystal	3	0.022	0.60	37	THF	N	115.0	0.0012	n-HOS	0.0023	0.2	MC	0.5	79%	20.9	1.9
20150915AJared	Raw	3	0.022	0.60	37	THF	N	115.0	0.0012	n-HOS	0.0023	0.2	MC	0.5	33%	9.8	1.7
20150915B	3X Recrystal	3	0.022	0.70	32	THF	N	80.0	0.0017	1-PB	0.000058	0.1	4-NPC	0.5	0%		
20150917Jared	1X Recrystal	3	0.022	0.60	37	THF	N	115.0	0.0012	n-HOS	0.0023	0.2	MC	0.5	0%		
20150923AJared	3X Recrystal	3	0.022	0.60	37	THF	N	115.0	0.0012	n-HOS	0.0011	0.2	MC	0.5	0%		
20150923BJared	3X Recrystal	2	0.015	0.60	25	THF	N	115.0	0.0012	n-HOS	0.00056	0.2	MC	0.5	0%		
20150924AJared	3X Recrystal	2	0.015	0.60	25	THF	N	115.0	0.0012	n-HOS	0.00028	0.2	MC	0.5	0%		
20150924BJared	3X Recrystal	2	0.015	0.60	25	THF	N	115.0	0.0012	n-HOS	0.00014	0.2	MC	0.5	0%		
20150929Jared	1X Recrystal	2	0.015	0.60	25	THF	N	115.0	0.0012	n-HOS	0.0023	0.2	MC	0.5	2%	6.1	2.0

20150929BJared	2X Recrystal	2	0.015	0.60	25	THF	N	115.0	0.0012	n-HOS	0.0023	0.2	MC	0.5	3%		
20151001AJared	3X Recrystal	2	0.015	0.60	25	THF	N	115.0	0.0012	n-HOS	0.0023	0.2	MC	0.5	2%	3.8	1.4
20151001BJared	4X Recrystal	2	0.015	0.60	25	THF	N	115.0	0.0012	n-HOS	0.0023	0.2	MC	0.5	0%		
20151005Jared	5X Recrystal	2	0.015	0.60	25	THF	N	115.0	0.0012	n-HOS	0.0023	0.2	MC	0.5	13%	9.2	2.1
20151112A	Raw	1	0.007	0.60	12	THF	N	67.0	0.0020	IPA	0.0093	0.1	AC	0.5	26%		
20151112B	Toluene Azeotrope	1	0.007	0.60	12	THF	N	67.0	0.0020	IPA	0.0093	0.1	AC	0.5	0%		
20151117A	Raw	1	0.007	0.60	12	THF	N	67.0	0.0020	IPA	0.0093	0.1	AC	0.5	5%		
20151117B	Raw	1	0.007	0.60	12	DCM	Y	67.0	0.0020	IPA	0.0093	0.1	AC	0.5	21%	9.5	
20151117C	5X Recrystal	1	0.007	0.60	12	DCM	Y	67.0	0.0020	IPA	0.0093	0.1	AC	0.5	81%	5.8	
20151123B	Raw	1	0.007	0.60	12	DCM	Y	67.0	0.0020	IPA	0.0093	0.0	None	0.5	0%		
20151123C	5X Recrystal	1	0.007	0.60	12	DCM	Y	67.0	0.0020	IPA	0.0093	0.0	None	0.5	2%		
20151207A	3X Recrystal	1	0.007	0.60	12	DCM	Y	67.0	0.0020	IPA	0.0093	0.1	AC	0.5	10%		
20151207B	3X Recrystal	1	0.007	0.60	12	DCM	Y	67.0	0.0020	IPA	0.0093	0.1	AC	0.5	21%		
20151208A	3X Recrystal	0.5	0.004	0.60	6	DCM	Y	67.0	0.0020	IPA	0.0035	0.1	AC	0.5	1%		
20151208B	3X Recrystal	1	0.007	0.60	12	DCM	Y	67.0	0.0020	IPA	0.0093	0.1	AC	0.5	2%		
2015413Pan	Raw	3	0.022	0.60	37	THF	N	23.0	0.0058	2-NB	0.011	0.1	4-NPC	0.5	44%	10.2	1.7
2015414Pan	Raw	3	0.022	0.60	37	THF	N	23.0	0.0058	2-NB	0.011	0.1	4-NPC	0.5	80%	4.0	2.0
2015420Pan	Raw	3	0.022	0.60	37	THF	N	0.0	0.0	None	0.011	0.1	4-NPC	0.5	34%	14.2	1.7
20151022A	Raw	2	0.015	0.60	25	THF	N	67.0	0.0020	IPA	0.0093	0.1	AC	0.5	19%		
20151022B	Raw	2	0.015	0.60	25	THF	N	67.0	0.0020	IPA	0.0093	0.1	AC	0.5	15%		
20151021A	Raw	2	0.015	0.60	25	THF	N	67.0	0.0020	IPA	0.0093	0.1	AC	0.5	24%	10.6	1.8
20151021B	Raw	2	0.015	0.60	25	THF	N	67.0	0.0020	IPA	0.0093	0.1	AC	0.5	24%	11.4	1.8
20151015A	Raw	1	0.007	0.60	12	THF	N	67.0	0.0020	IPA	0.0040	0.1	AC	0.5	10%	8.9	1.9
20151015B	Raw	1	0.007	0.60	12	THF	N	67.0	0.0020	IPA	0.0067	0.1	AC	0.5	11%	8.0	2.2
20151015C	Raw	1	0.007	0.60	12	THF	N	67.0	0.0020	IPA	0.0093	0.1	AC	0.5	16%	8.5	2.0
20151016A	Raw	1	0.007	0.60	12	DCM	N	44.0	0.0030	t-BDMS	0.0040	0.1	AA	0.5	22%	9.1	2.1
20151016B	Raw	1	0.007	0.60	12	THF/DCM	N	44.0	0.0030	t-BDMS	0.0067	0.1	AA	0.5	8%	4.1	1.5

20151016C	Raw	1	0.007	0.60	12	THF	N	44.0	0.0030	t-BDMS	0.0093	0.1	AA	0.5	44%	12.3	1.8
20140923Jared	Raw	10	0.075	0.60	124	THF	N	9.0	0.015	n-HOS	0.0020	0.1	VC	0.5	11%		
20140929Pan	Raw	4.726	0.035	0.60	59	THF	N	9.0	0.015	n-HOS	0.0020	0.1	VC	0.5	72%		
20141001Pan	Raw	5	0.037	0.60	62	THF	N	9.0	0.015	n-HOS	0.0020	0.1	VC	0.5	0%		
20141104Pan1	Raw	4	0.030	0.60	50	THF	N	9.0	0.015	n-HOS	0.0020	0.1	VC	0.5	0%		
20141111Pan1	Raw	3	0.022	0.60	37	THF	N	9.0	0.015	2-NB	0.0020	0.1	4-NPC	0.5	5%		
20141111Pan2	Raw	3	0.022	0.60	37	THF	N	9.0	0.015	n-HOS	0.0020	0.1	VC	0.5	0%		
20141204Pan	Raw	3	0.022	0.60	37	THF	N	9.0	0.015	2-NB	0.0020	0.1	4-NPC	0.5	0%		
20141210Pan	Raw	3	0.022	0.60	37	THF	N	9.0	0.015	2-NB	0.0020	0.1	4-NPC	0.5	0%		
20141212Pan	Raw	3	0.022	0.60	37	THF	N	67.0	0.0020	n-HOS	0.0040	0.1	AA	0.5	54%		
20141215Pan	Raw	3	0.022	0.60	37	THF	N	23.0	0.0058	n-HOS	0.0072	0.1	AA	0.5	17%		
20141216Pan	Raw	3	0.022	0.60	37	THF	N	23.0	0.0058	2-NB	0.0072	0.1	AA	0.5	41%		
20141217Pan	Raw	3	0.022	0.60	37	THF	N	23.0	0.0058	2-NB	0.011	0.1	4-NPC	0.5	46%	6.2	1.8
20141218Pan	Raw	3	0.022	0.60	37	THF	N	23.0	0.0058	2-NB	0.011	0.1	4-NPC	0.5	51%		
20150107Pan	Raw	3	0.022	0.60	37	THF	N	23.0	0.0058	2-NB	0.011	0.1	4-NPC	0.5	90%	6.2	1.6
20150108Pan	Raw	3	0.022	0.60	37	THF	N	23.0	0.0058	2-NB	0.011	0.1	4-NPC	0.5	88%	6.5	1.8
20150115Pan	Raw	3	0.022	0.60	37	THF	N	9.0	0.015	n-HOS	0.011	0.1	VC	0.5	16%		
AS1-174	Sub	2	0.015	0.60	25	THF	N	1799.1	0.000075	n-HOS	0.0023	0.2	MC	0.5	20%	3.8	2.0
AS1-178	Sub	2	0.015	0.60	25	THF	N	1799.1	0.000075	n-HOS	0.0023	0.2	MC	0.5	0%		
AS1-179	Sub	2	0.015	0.60	25	THF	N	1799.1	0.000075	n-HOS	0.0023	0.2	MC	0.5	0%		
AS1-180	Sub	1.5	0.011	0.60	19	THF	N	2398.8	0.000056	1-PB	0.0023	0.2	MC	0.5	0%		
AS1-181	Sub	1.5	0.011	0.60	19	THF	N	2398.8	0.000056	2-NB	0.0023	0.2	MC	0.5	0%		
AS1-182	Sub	1.5	0.011	0.60	19	THF	N	2398.8	0.000056	2-NB	0.0023	0.2	MC	0.5	77%	2.1	1.4
AS1-183	Sub	1.5	0.011	0.60	19	THF	N	2398.8	0.000056	1-PB	0.0023	0.2	MC	0.5	8%	2.9	1.7
AS1-185	Sub	1.5	0.011	0.60	19	THF	N	2398.8	0.000056	2-NB	0.0023	0.2	MC	0.5	84%	3.3	1.7
JMS2-24B	Raw	3	0.022	0.60	37	THF	N	23.0	0.0058	n-HOS	0.011	0.2	VC	0.5	0%		
JMS2-27B	Raw	3	0.022	0.60	37	THF	N	23.0	0.0058	n-HOS	0.011	0.2	VC	1.5	0%		

JMS1-185	Raw	10	0.075	0.60	124	THF	N	67.0	0.0020	n-HOS	0.0020	0.1	VC	0.5	11%		
JMS1-200	Raw	3	0.022	0.60	37	THF	N	11.0	0.11	IPA	0.0020	0.1	VC	0.5	1%		
JMS3-1	Sub	2	0.015	0.60	25	THF	N	67.0	0.0020	n-HOS	0.0020	0.1	MC	0.5	2%		
JMS1-180	Raw	3	0.022	0.60	37	THF	N	67.0	0.0020	n-HOS	0.0020	0.1	VC	0.5	29%		
JMS2-181	Vac-Dried	4.2	0.031	0.60	50	THF	Y	115.0	0.0012	IPA	0.0023	0.1	MC	0.5	0%		
JMS2-182	Vac-Dried	5	0.037	0.60	60	THF	Y	50.8	0.0026	IPA	0.00037	0.1	MC	0.5	0%		
	Solvent	**DCM** - Dichloromethane, **THF** – Tetrahydrofuran															
	Initiator	**1-PB** - 1-pyrenebutanol, **2-NB** - ortho-nitrobenzyl alcohol, **IPA** - isopropyl alcohol, **n-HOS** - n-hydroxysuccinimide, **t-BDMS** - tert-butyldimethylsilanol															
	End-cap	**4-NPC** - 4-nitrophenyl chloroformate, **AA** - acetic anhydride, **AC** - allyl chloroformate, **MC** - methyl chloroformate, **VC** - vinyl chloroformate															

APPENDIX B. CATIONIC COPOLYMERIZATION DATA

Polymer Name	Coaldehyde(s)	Date Synth	Rxn T (°C)	Rxn Time (min)	Monomer: Catalyst Ratio	MW (kDa)	PDI	Approx Amount (g)	Yield	Sensitivity (mJ/cm^2)	Contrast	T_{onset} (°C)	$T_{d,50}$ (°C)	PHA:Coaldehyde Ratio
AS2-27	PA	2/17/2016	-78	150	7	3.2	2.59	0.04	4.10%			135.37	175.3	na
AS2-12	T2M2B	2/2/2016	-78	150	7	12.9	3.05	0.12	10.00%	20	2.03	109.6	117.7	na
AS2-14	T2M2B	2/3/2016	-78	150	7	17.4	1.69	0.4	35.00%	38.73	4.95	93.6	104.7	na
AS2-16	T2M2B	2/4/2016	-78	150	128			0.59	50.90%	5.025	2.99	104.71	119.2	na
AS2-25	T2M2B	2/16/2016	-78	150	7			0.3	40.00%	56.27	4.52	98.32	105.4	na
AS2-48	T2M2B	3/10/2016	-78	150	128	10.5	2.83	0.4	46.00%			111.53	117.6	na
AS2-11	VA	2/1/2016	-78	150	7			0.1	8.20%			105.38	112.4	na
AS2-23	2-EB	2/10/2016	-78	150	7			0.4	43.00%	28.84	5.77	84.67	96.4	na
AS2-31	2-EB and T2M2B	2/22/2016	-78	150	7	19.2	2	0.5	54.00%	61.27	5.07	99.23	114.9	289
AS2-35	2-EB and VA	2/24/2016	-78	150	7	4.7	2.68	0.23	24.00%	20	3.56	116.04	165.1	92
AS2-87	4-TBA	4/21/2016	-78	150	750	43	1.71	0.9	54.00%	178.5	2.32	81.23		124
AS2-22	Ac	2/10/2016	-78	150	7	7.4	3.28	0.24	27.00%			91.02	97.9	na
AS2-33	Ac and 2-EB	2/23/2016	-78	150	7	4.6	3.92	0.2	24.00%	20	3.29	117.22	147	118
AS2-29	Ac and BZA	2/18/2016	-78	150	7	9.1	3.68	0.3	37.00%	43.68	4.15	82.4	92.2	42
AS2-32	Ac and T2M2B	2/23/2016	-78	150	7	7.9	2.74	0.3	35.00%	77.44	4.1	73.43	83.4	15
AS2-49	Ac and T2M2B	3/10/2016	-78	150	128			0.4	46.00%			102.95	111.6	4
AS2-13	BZA	2/2/2016	-78	150	7	29.5	1.52	0.57	47.30%	12.18	2.29	100.6	107.9	na
AS2-24	BZA	2/16/2016	-78	150	7	6.3	4.44	0.3	33.00%	80.69	7.9	84.44	96	na
AS2-93	BZA	4/27/2016	-78	150	750	64	1.63	1.2	64.00%	49.46	1.56	118.24		na
AS2-30	BZA and BA	2/22/2016	-78	150	7	5.1	3.34	0.2	20.00%	63.08	4.75	102.66	158.4	1909

AS2-21	BZA and T2M2B	2/9/2016	-78	150	128	6	2.55	0.1	11.00%			101.88	110.2	na
AS2-34	BA and 2-EB	2/24/2016	-78	150	7	4.7	3.22	0.27	29.00%	31.34	7.81	108.62	160.5	153
AS2-20	BA and T2M2B	2/9/2016	-78	150	128	5.4	2.32	0.1	9.00%			100.84	107.4	na

REFERENCES

(1) Kohl, P. A. Low-Dielectric Constant Insulators for Future Integrated Circuits and Packages. *Annu. Rev. Chem. Biomol. Eng.* **2011**, *2*, 379–401 DOI: 10.1146/annurev-chembioeng-061010-114137.

(2) Tummala, R. *Fundamentals of Microsystems Packaging*; McGraw-Hill, 2001.

(3) Hall, W. J.; Williams, P. T. Separation and Recovery of Materials from Scrap Printed Circuit Boards. *Resour. Conserv. Recycl.* **2007**, *51* (3), 691–709 DOI: 10.1016/j.resconrec.2006.11.010.

(4) Lee, K. J.; Lee, J. A.; Kim, M. Multilayer Dielectric Cavity Antenna Design for Wide Bandwidth. *Microw. Opt. Technol. Lett.* **2012**, *54* (9), 2046–2049 DOI: 10.1002/mop.

(5) Maier, G.; Garching, D.-. Low Dielectric Constant Polymers for Microelectronics. *Prog. Polym. Sci.* **2001**, *26*, 3–65.

(6) Fritz, N.; Saha, R.; Allen, S. A. B.; Kohl, P. A. Photodefinable Epoxycyclohexyl Polyhedral Oligomeric Silsesquioxane. *J. Electron. Mater.* **2009**, *39* (2), 149–156 DOI: 10.1007/s11664-009-1031-9.

(7) Takala, M.; Karttunen, M.; Pelto, J.; Salovaara, P.; Munter, T.; Honkanen, M.; Auletta, T.; Kannus, K. Thermal, Mechanical and Dielectric Properties of Nanostructured Epoxy-Polyhedral Oligomeric Silsesquioxane Composites. *IEEE Trans. Dielectr. Electr. Insul.* **2008**, *15* (5), 1224–1235 DOI:

10.1109/TDEI.2008.4656229.

(8) *Polyimides: Fundamentals and Applications*; Ghosh, M. K., Mittal, K. L., Eds.; Marcel Dekker, Inc.: New York, 1996.

(9) Fukukawa, K.; Ueda, M. Chemically Amplified Photosensitive Polyimides and Polybenzoxazoles. *J. Photopolym. Sci. Technol.* **2009**, *22* (6), 761–771.

(10) Simpson, J. O. O.; St.Clair, A. K. Fundamental Insight on Developing Low Dielectric Constant Polyimides. *Thin Solid Films* **1997**, *308–309*, 480–485 DOI: 10.1016/S0040-6090(97)00481-1.

(11) Chisca, S.; Sava, I.; Bruma, M. Porous Polyimide Films Obtained by Using Lithium Chloride as Pore-Forming Agent. *Polym. Int.* **2013**, No. November 2012, n/a-n/a DOI: 10.1002/pi.4460.

(12) Jung, M.-S.; Lee, S. K.; Hyeon-Lee, J.; Park, M. K.; Jung, H.-T. Preparation of a Chemically Amplified Photosensitive Polyimide Based on Norbornene-End-Capped Poly(amic Acid Ethoxymethylester). *J. Polym. Sci. Part A Polym. Chem.* **2005**, *43* (22), 5520–5528 DOI: 10.1002/pola.21040.

(13) Dobrzynska, J. a; Joris, P.; Jiguet, S.; Renaud, P.; Gijs, M. a M. Polyimide Foam-like Microstructures: Technology and Mechanical Properties. *J. Micromechanics Microengineering* **2011**, *21* (10), 105016 DOI: 10.1088/0960-1317/21/10/105016.

(14) Raeis-Zadeh, M.; Kohl, P. A. High-Contrast, High-Sensitivity Aqueous Base-Developable Polynorbornene Dielectric. *J. Appl. Polym. Sci.* **2013**, *127* (6), 4366–

4373 DOI: 10.1002/app.37998.

(15) Raeis-zadeh, M.; Elce, E.; Knapp, B.; Kohl, P. A. Cross-Linking of Aqueous Base-Developable , Photosensitive Polynorbornene. **2011** DOI: 10.1002/app.

(16) Raeis-Zadeh, M.; Melendez, N. D.; Chen, Y.-C.; Kohl, P. A. Aqueous-Develop, Photosensitive Polynorbornene Dielectric: Optimization of Mechanical and Electrical Properties. *J. Electron. Mater.* **2011**, *40* (10), 2126–2138 DOI: 10.1007/s11664-011-1704-z.

(17) Mueller, B. K.; Elce, E.; Grillo, A. M.; Kohl, P. A. Positive-Tone, Aqueous-Developable, Polynorbornene Dielectric: Lithographic, and Dissolution Properties. *J. Appl. Polym. Sci.* **2013**, *127* (6), 4653–4661 DOI: 10.1002/app.38055.

(18) Schwartz, J. M.; Mueller, B. K.; Elce, E.; Pritchard, Z. D.; Li, H. W.; Grillo, A. M.; Lee, S. Y.; Kohl, P. A. Positive Tone, Polynorbornene Dielectric Crosslinking. *ECS J. Solid State Sci. Technol.* **2014**, *4* (1), N3008–N3014 DOI: 10.1149/2.0021501jss.

(19) Raeis-zadeh, M.; Elce, E.; Knapp, B.; Kohl, P. A. Cross-Linking of Aqueous Base-Developable , Photosensitive Polynorbornene. *J. Appl. Polym. Sci.* **2011**, *120*, 1916–1925 DOI: 10.1002/app.

(20) Rajarathinam, V.; Lightsey, C. H.; Osborn, T.; Knapp, B.; Elce, E.; Bidstrup Allen, S. A.; Kohl, P. a. Aqueous-Develop, Photosensitive Polynorbornene Dielectric: Properties and Characterization. *J. Electron. Mater.* **2009**, *38* (6), 778–786 DOI: 10.1007/s11664-009-0741-3.

(21) Chiniwalla, P.; Bai, Y.; Elce, E.; Shick, R.; Bidstrup Allen, S. A.; Kohl, P. A. Crosslinking and Decomposition Reactions of Epoxide- Functionalized Polynorbornene . II . Impact of Reactions on Mechanical Properties. *J. Appl. Polym. Sci.* **2004**, *91*, 1020–1029.

(22) Dammel, R. *Diazonaphthoquinone-Based Resists*, Fifth.; SPIE - The International Society for Optical Engineering: Bellingham, Washington, 1993.

(23) Waliraff, G. M.; Hinsberg, W. D.; Houle, F.; Opitz, J.; Hopper, D.; Hutchinson, J. M. Kinetics of Chemically Amplified Resists. *Proc. SPIE* **1995**, *2438*, 182–190.

(24) Ito, H.; Willson, C. G. Chemical Amplification in the Design of Dry Developing Resist Materials. *Polym. Eng. Sci.* **1983**, *23* (18), 1012–1018.

(25) *HD-8820 Aqueous Positive Polyimide*; 2005.

(26) *Cyclotene 4000 Series Advanced Electronic Resins (Photo BCB)*; 2005.

(27) Fan, B.; Trant, J. F.; Wong, A. D.; Gillies, E. R. Polyglyoxylates: A Versatile Class of Triggerable Self-Immolative Polymers from Readily Accessible Monomers. *J. Am. Chem. Soc.* **2014**, *136* (28), 10116–10123 DOI: 10.1021/ja504727u.

(28) Roth, M. E.; Green, O.; Gnaim, S.; Shabat, D. Dendritic, Oligomeric, and Polymeric Self-Immolative Molecular Amplification. *Chem. Rev.* **2015**, 1309–1352 DOI: 10.1021/acs.chemrev.5b00372.

(29) Phillips, S. T.; Robbins, J. S.; Dilauro, A. M.; Olah, M. G. Amplified Responses in

Materials Using Linear Polymers That Depolymerize from End-to-End When Exposed to Specific Stimuli. *J. Appl. Polym. Sci.* **2014**, *131* (19), 40992 DOI: 10.1002/app.40992.

(30) Phillips, S. T.; Dilauro, A. M. Continuous Head-to-Tail Depolymerization: An Emerging Concept for Imparting Amplified Responses to Stimuli-Responsive Materials. *ACS Macro Lett.* **2014**, *3*, 298–304.

(31) Park, C. W.; Kang, S.-K.; Hernandez, H. L.; Kaitz, J. A.; Wie, D. S.; Shin, J.; Lee, O. P.; Sottos, N. R.; Moore, J. S.; Rogers, J. A.; White, S. R. Thermally Triggered Degradation of Transient Electronic Devices. *Adv. Mater.* **2015**, *27* (25), 3783–3788 DOI: 10.1002/adma.201501180.

(32) DiLauro, A. M.; Phillips, S. T. End-Capped poly(4,5-Dichlorophthalaldehyde): A Stable Self-Immolative Poly(aldehyde) for Translating Specific Inputs into Amplified Outputs, Both in Solution and the Solid State. *Polym. Chem.* **2015**, *6*, 3252–3258 DOI: 10.1039/C5PY00190K.

(33) Hernandez, H. L.; Kang, S.-K.; Lee, O. P.; Hwang, S.-W.; Kaitz, J. A.; Inci, B.; Park, C. W.; Chung, S.; Sottos, N. R.; Moore, J. S.; Rogers, J. A.; White, S. R. Triggered Transience of Metastable Poly(phthalaldehyde) for Transient Electronics. *Adv. Mater.* **2014**, *26* (45), 7637–7642 DOI: 10.1002/adma.201403045.

(34) Uzunlar, E.; Schwartz, J.; Phillips, O.; Kohl, P. A. Decomposable and Template Polymers: Fundamentals and Applications. *J. Electron. Packag.* **2016**, *138* (2),

20802 DOI: 10.1115/1.4033000.

(35) Thompson, L. F.; Bowden, M. J. A New Family of Positive Electron Beam Resists—Poly(Olefin Sulfones). *J. Electrochem. Soc.* **1973**, *120* (12), 1722 DOI: 10.1149/1.2403352.

(36) Ito, H. Chemical Amplification Resists for Microlithography. *Adv. Polym. Sci.* **2005**, *172*, 37–245 DOI: 10.1007/b97574.

(37) Peterson, G. I.; Larsen, M. B.; Boydston, A. J. Controlled Depolymerization: Stimuli-Responsive Self-Immolative Polymers. *Macromolecules* **2012**, *45* (18), 7317–7328 DOI: 10.1021/ma300817v.

(38) Esser-Kahn, A. P.; Odom, S. A.; Sottos, N. R.; White, S. R.; Moore, J. S. Triggered Release from Polymer Capsules. *Macromolecules* **2011**, *44* (14), 5539–5553 DOI: 10.1021/ma201014n.

(39) Esser-Kahn, A. P.; Sottos, N. R.; White, S. R.; Moore, J. S. Programmable Microcapsules from Self-Immolative Polymers. *J. Am. Chem. Soc.* **2010**, *132* (30), 10266–10268 DOI: 10.1021/ja104812p.

(40) Sagi, A.; Weinstain, R.; Karton, N.; Shabat, D. Self-Immolative Polymers. *Angew. Chemie - Int. Ed.* **2008**, *47* (41), 7804–7806 DOI: 10.1002/anie.200802474.

(41) Peterson, G. I.; Church, D. C.; Yakelis, N. A.; Boydston, A. J. 1,2-Oxazine Linker As a Thermal Trigger for Self-Immolative Polymers. *Polymer (Guildf).* **2014**, *55* (23), 5980–5985 DOI: 10.1016/j.polymer.2014.09.048.

(42) Ma, L.; Baumgartner, R.; Zhang, Y.; Song, Z.; Cai, K.; Cheng, J. UV-Responsive Degradable Polymers Derived from 1-(4-Aminophenyl) Ethane-1,2-Diol. *J. Polym. Sci. Part A Polym. Chem.* **2015**, *53* (9), 1161–1168 DOI: 10.1002/pola.27550.

(43) Cheng, H.; Vepachedu, V. Recent Development of Transient Electronics. *Theor. Appl. Mech. Lett.* **2016**, *6* (1), 21–31 DOI: 10.1016/j.taml.2015.11.012.

(44) Hwang, S.; Rogers, J. A. A Physically Transient Form of Silicon Electronics. *Science (80-.).* **2013**, *337* (28), 1640–1644 DOI: 10.1126/science.1226325.

(45) Hwang, S.-W.; Kang, S.-K.; Huang, X.; Brenckle, M. A.; Omenetto, F. G.; Rogers, J. A. Materials for Programmed, Functional Transformation in Transient Electronic Systems. *Adv. Mater.* **2015**, *27* (1), 47–52 DOI: 10.1002/adma.201403051.

(46) Yin, L.; Cheng, H.; Mao, S.; Haasch, R.; Liu, Y.; Xie, X.; Hwang, S. W.; Jain, H.; Kang, S. K.; Su, Y.; Li, R.; Huang, Y.; Rogers, J. A. Dissolvable Metals for Transient Electronics. *Adv. Funct. Mater.* **2014**, *24* (5), 645–658 DOI: 10.1002/adfm.201301847.

(47) Hwang, S. W.; Kim, D. H.; Tao, H.; Kim, T. Il; Kim, S.; Yu, K. J.; Panilaitis, B.; Jeong, J. W.; Song, J. K.; Omenetto, F. G.; Rogers, J. A. Materials and Fabrication Processes for Transient and Bioresorbable High-Performance Electronics. *Adv. Funct. Mater.* **2013**, *23* (33), 4087–4093 DOI: 10.1002/adfm.201300127.

(48) Ali, S. N.; Ghafouri, S.; Yin, Z.; Froimowicz, P.; Begum, S.; Winnik, M. a. A

Comparative Thermogravimetric Study of Polymers Designed as Dry-Developing Photoresists. *Eur. Polym. J.* **2008**, *44* (12), 4129–4138 DOI: 10.1016/j.eurpolymj.2008.09.004.

(49) Uzunlar, E.; Schwartz, J. M.; Phillips, O.; Kohl, P. A. Decomposable and Template Polymers: Fundamentals and Applications. *J. Electron. Packag.* **2016**, No. c DOI: 10.1115/1.4033000.

(50) Odian, G. *Principles of Polymerization*, Fourth.; John Wiley & Sons: Hoboken, 2004.

(51) Bowden, M. J.; Thompson, L. F. Electron Irradiation of Poly(olefin Sulfones) Application to Electron Beam Resists. *J. Appl. Polym. Sci.* **1973**, *17*, 3211–3221.

(52) Bowden, M. J.; Thompson, L. F. Effect of Olefin Structure on the Vapor-Development of Poly (Olefin Sulfones) Under Electron Irradiation. *Polym. Eng. Sci.* **1977**, *17* (4), 269–273.

(53) Lee, O. P.; Lopez Hernandez, H.; Moore, J. S. Tunable Thermal Degradation of Poly(vinyl Butyl Carbonate Sulfone)s via Side-Chain Branching. *ACS Macro Lett.* **2015**, *4*, 665–668 DOI: 10.1021/acsmacrolett.5b00234.

(54) Phillips, O.; Schwartz, J. M.; Kohl, P. A. Thermal Decomposition of Poly(propylene Carbonate): End-Capping, Additives, and Solvent Effects. *Polym. Degrad. Stab.* **2016**, *125*, 129–139 DOI: 10.1016/j.polymdegradstab.2016.01.004.

(55) Vogl, O. Polymerization of Higher Aldehydes. III. Elastomeric Polyacetaldehyde.

J. Polym. Sci. Part A Polym. Chem. **1964**, *2*, 4591–4606.

(56) Kubisa, P.; Neeld, K.; Starr, J.; Vogl, O. Polymerization of Higher Aldehydes. *Polymer (Guildf).* **1980**, *21* (12), 1433–1447 DOI: 10.1016/0032-3861(80)90145-7.

(57) Vogl, O. Addition Polymers of Aldehydes. *J. Polym. Sci. Part A Polym. Chem.* **2000**, *38* (13), 2293–2299 DOI: 10.1002/1099-0518(20000701)38:13<2293::AID-POLA10>3.0.CO;2-M.

(58) Vogl, O. Polymerization of Higher Adlehydes. IV. Crystalline Isotactic Polyaldehydes: Anionic and Cationic Polymerization. *J. Polym. Sci. Part A Polym. Chem.* **1964**, *2*, 4607–4620.

(59) Vogl, O.; Bryant, W. Polymerization of Higher Aldehydes. VI. Mechanism of Aldehyde Polymerization. *J. Polym. Sci. Part A …* **1964**, *2* (May 1962), 4633–4645 DOI: 10.1002/pol.1964.100021030.

(60) DiLauro, A. M.; Robbins, J. S.; Phillips, S. T. Reproducible and Scalable Synthesis of End-Cap-Functionalized Depolymerizable Poly(phthalaldehydes). *Macromolecules* **2013**, *46* (8), 2963–2968 DOI: 10.1021/ma4001594.

(61) Tsuda, M.; Hata, M.; Nishida, R.; Oikawa, S. Acid-Catalyzed Degradation Mechanism of Poly (Phthalaldehyde): Unzipping Reaction of Chemical. *J. Polym. Sci. Part A Polym. Chem.* **1997**, *35*, 77–89.

(62) Kaitz, J. A.; Diesendruck, C. E.; Moore, J. S. Dynamic Covalent Macrocyclic

Poly(phthalaldehyde)s: Scrambling Cyclic Homopolymer Mixtures Produces Multi-Block and Random Cyclic Copolymers. *Macromolecules* **2013**, *46* (20), 8121–8128 DOI: 10.1021/ma401744k.

(63) Kaitz, J. A.; Diesendruck, C. E.; Moore, J. S. End Group Characterization of Poly(phthalaldehyde): Surprising Discovery of a Reversible, Cationic Macrocyclization Mechanism. *J. Am. Chem. Soc.* **2013**, *135* (34), 12755–12761 DOI: 10.1021/ja405628g.

(64) Yin, L.; Bozler, C.; Harburg, D. V.; Omenetto, F.; Rogers, J. A. Materials and Fabrication Sequences for Water Soluble Silicon Integrated Circuits at the 90 Nm Node. *Appl. Phys. Lett.* **2015**, *106* (1), 14105 DOI: 10.1063/1.4905321.

(65) Hong, M.; Chen, E. Y.-X. Towards Truly Sustainable Polymers: A Metal-Free Recyclable Polyester from Biorenewable Non-Strained γ-Butyrolactone. *Angew. Chemie - Int. Ed.* **2016**, *55* (13), 4188–4193 DOI: 10.1002/anie.201601092.

(66) Maex, K.; Baklanov, M. R.; Shamiryan, D.; Lacopi, F.; Brongersma, S. H.; Yanovitskaya, Z. S. Low Dielectric Constant Materials for Microelectronics. *J. Appl. Phys.* **2003**, *93* (11), 8793 DOI: 10.1063/1.1567460.

(67) Oliver, W. C.; Pharr, G. M. Measurement of Hardness and Elastic Modulus by Instrumented Indentation: Advances in Understanding and Refinements to Methodology. *J. Mater. Res.* **2011**, *19* (1), 3–20 DOI: 10.1557/jmr.2004.19.1.3.

(68) ASTM International. Standard Test Methods for AC Loss Characteristics and Permittivity (Dielectric Constant) of Solid Electrical Insulation 1. *D150 - 11*

2012, No. C, 1–20 DOI: 10.1520/D0150-11.2.

(69) Ammann, C.; Meier, P.; Merbach, A. A Simple Multinuclear NMR Thermometer. *J. Magn. Reson.* **1982**, *46* (2), 319–321 DOI: 10.1016/0022-2364(82)90147-0.

(70) Dainton, F. S.; Ivin, K. J. Reversibility of the Propagation Reaction in Polymerization Processes and Its Manifestation in the Phenomenon of a "Ceiling Temperature." *Nature* **1948**, *162*, 705–707 DOI: 10.1038/162705a0.

(71) Dainton, F. S.; Ivin, K. J. Changes of Entropy and Heat Content during Polymerization. *Trans. Faraday Soc.* **1949**, *162*, 705.

(72) Aso, C.; Tagami, S. Polymerization of Aromatic Aldehydes. III. The Cyclopolymerization of Phthalaldehyde and the Structure of the Polymer. *Macromolecules* **1969**, *3* (3), 414–419.

(73) Mueller, B. K. Photo-Definable Dielectrics with Improved Lithographic, Mechanical, and Electrical Properties, Georgia Institute of Technology, 2015.

(74) Koshiba, M.; Murata, M.; Matsui, M.; Harita, Y. Thermally Induced and Base Catalyzed Reactions of Naphthoquinone Diazides. *Adv. Resist Technol. Process. V* **1988**, *920*, 364–371.

(75) De Winter, J.; Dove, A. P.; Knoll, A.; Gerbaux, P.; Dubois, P.; Coulembier, O. Control over Molar Mass, Dispersity, End-Groups and Kinetics in Cyclopolymerization of Ortho-Phthalaldehyde: Adapted Choice of a Phosphazene Organocatalyst. *Polym. Chem.* **2014**, *5* (3), 706 DOI: 10.1039/c3py01307c.

(76) Kaitz, J. A.; Diesendruck, C. E.; Moore, J. S. Divergent Macrocyclization Mechanisms in the Cationic Initiated Polymerization of Ethyl Glyoxylate. *Macromolecules* **2014**, *47* (11), 3603–3607 DOI: 10.1021/ma500674c.

(77) Aso, C.; Tagami, S.; Kunitake, T. Polymerization of Aromatic Aldehydes. IV. Cationic Copolymerization of Phthalaldehyde Isomers and Styrene. *J. Polym. Sci. Part A-1* **1970**, *8*, 1323–1336.

(78) Aso, C.; Tagami, S.; Kunitake, T. Polymerization of Aromatic Aldehydes. II. Cationic Cyclopolymerization of Phthalaldehyde. *J. Polym. Sci. Part A-1* **1969**, *7*, 497–511 DOI: 10.1002/pol.1969.150070208.

(79) Hilt, G.; Pünner, F.; Möbus, J.; Naseri, V.; Bohn, M. A. A Lewis Acidity Scale in Relation to Rate Constants of Lewis Acid Catalyzed Organic Reactions. *European J. Org. Chem.* **2011**, No. 30, 5962–5966 DOI: 10.1002/ejoc.201101029.

(80) Laszlo, P.; Teston, M. Determination of the Acidity of Lewis Acids. *J. Am. Chem. Soc.* **1990**, *112* (24), 8750–8754 DOI: 10.1021/ja00180a017.

(81) Satchell, D. P. N.; Satchell, R. S. Quantitative Aspects of the Lewis Acidity of Covalent Metal Halides and Their Organo Derivatives. *Chem. Rev.* **1969**, *69* (3), 251–278 DOI: 10.1021/cr60259a001.

(82) Corey, E. J.; Rohde, J. J.; Fischer, A.; Azimioara, M. D. A Hypothesis for Conformational Restriction in Complexes of Formyl Compounds with Boron Lewis Acids. Experimental Evidence for Formyl CH--O and CH--F Hydrogen Bonds. *Tetrahedron Lett.* **1997**, *38* (1), 33–36 DOI: 10.1016/S0040-

4039(96)02248-4.

(83) Evans, A. G.; Meadows, G. W. The Polymerization of Isobutene by Boron Trifluoride. *Trans. Faraday Soc.* **1950**, *46*, 327–331.

(84) Kennedy, J. P.; Huang, S. Y.; Feinberg, S. C. Cationic Polymerization with Boron Halides. III. BCl3 Coinitiator for Olefin Polymerization. *J. Polym. Sci.* **1977**, *15*, 2801–2819.

(85) Gajewski, J. J.; Ngernmeesri, P. Equilibrium Constants between Boron Trifluoride Etherate and Carbonyl Compounds in Chloroform Solution. *Org. Lett.* **2000**, *2* (18), 2813–2815.

(86) Maria, P. C.; Gal, J.-F. A Lewis Basicity Scale for Nonprotogenic Solvents: Enthalpies of Complex Formation with Boron Trifluoride in Dichloromethane. *J. Phys. Chem.* **1985**, *89* (7), 1296–1304 DOI: 10.1021/j100253a048.

(87) Craig, B. Y. R. A.; Richards, R. E. Hydrogen and Fluorine Nuclear Magnetic Resonances in Some Adducts of Boron Trifluoride. *Trans. Faraday Soc.* **1963**, *59*, 1962–1971.

(88) Yuan, C.; Yan, D. Influence of Termination and Transfer on Molecular Weight Distribution of Polymers, 8. Spontaneous Transfer. *Makromoleculare Chemie* **1987**, *188*, 341–348.

(89) Yuan, C.; Yan, D. Influence of Termination and Transfer on Molecular Weight Distribution of Polymers : 9. Chain Transfer to Monomer and Spontaneous

Transfer. *Polym. J.* **1988**, *29* (5), 924–928.

(90) van Scheppingen, W.; Dorrestijn, E.; Arends, I.; Mulder, P.; Korth, H.-G. Carbon-Oxygen Bond Strength in Diphenyl Ether and Phenyl Vinyl Ether: An Experimental and Computational Study. *J. Phys. Chem. A* **1997**, *101* (97), 5405–5411 DOI: 10.1021/jp9704325.

(91) Strahan, J. R. Advanced Organic Materials for Lithographic Applications, University of Texas at Austin, 2010.

(92) Yin, L.; Farimani, A. B.; Min, K.; Vishal, N.; Lam, J.; Lee, Y. K.; Aluru, N. R.; Rogers, J. A. Mechanisms for Hydrolysis of Silicon Nanomembranes as Used in Bioresorbable Electronics. *Adv. Mater.* **2015**, *27* (11), 1857–1864 DOI: 10.1002/adma.201404579.

(93) McBride, R. A.; Gillies, E. R. Kinetics of Self-Immolative Degradation in a Linear Polymeric System: Demonstrating the Effect of Chain Length. *Macromolecules* **2013**, *46* (13), 5157–5166 DOI: 10.1021/ma4009753.

(94) Kaitz, J. A.; Moore, S. Copolymerization of O ‐ Phthalaldehyde and Ethyl Glyoxylate: Cyclic Macromolecules with Alternating Sequence and Tunable Thermal Properties. *Macromolecules* **2014**.

(95) Kaitz, J. A.; Moore, S. Functional Phthalaldehyde Polymers by Copolymerization with Substituted Benzaldehydes. *Macromolecules* **2013**, *46* (3), 608–612.

(96) Hashimoto, K.; Sumitomo, H. Equilibrium Cyclotrimerization of N-

Butyraldehyde. *J. Polym. Sci.* **1977**, *15* (7), 1609–1618.

(97) Schwartz, J. M.; Phillips, O.; Engler, A.; Sutlief, A.; Lee, J.; Kohl, P. A. Stable, High-Molecular-Weight Poly(phthalaldehyde). *J. Polym. Sci. Part A Polym. Chem.* **2017**, *55* (7), 1166–1172 DOI: 10.1002/pola.28473.

(98) Schwartz, J. M.; Engler, A.; Phillips, O.; Lee, J.; Kohl, P. A. Determination of Ceiling Temperature and Thermodynamic Properties of Low Ceiling Temperature Polyaldehydes.

(99) Freund, B.; Cantow, H.-J. Synthesis and Anionic Polymerization of 2-Isopropenylquinoline. *Polym. Bull.* **1985**, *14*, 73–77.

(100) Snow, R. D.; Frey, F. E. The Reaction of Sulfur Dioxide with Olefins: The Ceiling Temperature Phenomenon. **1943**, *2312* (2), 2–3.

(101) McCormick, H. W. Ceiling Temperature of Alpha-Methylstyrene. *J. Polym. Sci.* **1957**, *25* (111), 488–490 DOI: 10.1002/pol.1957.1202511112.

(102) Kostler, S.; Zechner, B.; Trathnigg, B.; Fasl, H.; Kern, W.; Ribitsch, V. Amphiphilic Block Copolymers Containing Thermally Degradable Poly(phthalaldehyde) Blocks. *J. Polym. Sci. Part A Polym. Chem.* **2009**, *47*, 1499–1509.

(103) Aitken, R. A.; Hauduc, C.; McLennan, R. S.; Slawin, A. M. Z.; Wilson, H. S. Novel Ether and Thioether Macrocycles from Phthalaldehyde. *Tetrahedron Lett.* **2015**, *56* (15), 1937–1940 DOI: 10.1016/j.tetlet.2015.02.003.

(104) Hong, M.; Chen, E. Y.-X. Completely Recyclable Biopolymers with Linear and Cyclic Topologies via Ring-Opening Polymerization of Gamma-Butyrolactone. *Nat. Chem.* **2016**, *8* (1), 42–49 DOI: 10.1038/nchem.2391.

(105) Sirard, S. M.; Kalinovski, I.; Hahn, J. Systems and Methods for Drying High Aspect Ratio Structures Without Collapse Using Sacrificial Bracing Material That Is Removed Using Hydrogen-Rich Plasma. 14/507,080, 2016.